Fakultät für Medizin
Deutsches Zentrum für Neurodegenerative Erkrankungen (DZNE) in der Helmholtz-Gemeinschaft

The role of Fragile X Mental Retardation Protein in Parkinson's disease

Yi Tan

Vollständiger Abdruck der von der Fakultät für Medizin der Technischen Universität München zur Erlangung des akademischen Grades eines
Doktors der Naturwissenschaften (Dr. rer. nat.)
genehmigten Dissertation.

Vorsitzender: Prof. Dr. Mikael Simons

Prüfer der Dissertation:
1: Prof. Dr. Stefan Lichtenthaler
2: Prof. Dr. Harald Luksch

Die Dissertation wurde am 05.02.2020 bei der Fakultät für Medizin der Technischen Universität München eingereicht und durch die Fakultät für Medizin am 12.05.2020 angenommen.

Affidavit

I hereby declare that the dissertation titled
The role of Fragile X Mental Retardation Protein in Parkinson's disease
prepared under the guidance and supervision of Univ.-Prof. Dr. Günter U. Höglinger at the Chair for Translational Neurodegeneration, Technical University or Munich (TUM) in cooperation with Deutsches Zentrum für Neurodegenerative Erkrankungen (DZNE) Munich in der Helmholtz-Gemeinschaft
and submitted to the degree-awarding institution of: The Faculty of Medicine
of TUM is my own, original work undertaken in partial fulfillment of the requirements for the doctoral degree. I have made no use of sources, materials or assistance other than those specified in § 6 (6) and (7), clause 2.
[X] I have not employed the services of an organization that provides dissertation supervisors in return for payment or that fulfills, in whole or in part, the obligations incumbent on me in connection with my dissertation.
[ ] I have not submitted the dissertation, either in the present or a similar form, as part of another examination process.
[ ] The complete dissertation was published in _____
The degree-awarding institution:

_____
has approved prior publication of the dissertation.
[X] I have not yet been awarded the desired doctoral degree nor have I failed the last possible attempt to obtain the desired degree in a previous doctoral program.
[ ] I have already applied for admission to a doctoral program at the school or college of _____
at (university) _____
by submitting a dissertation on the topic _____
with the result: _____
I am familiar with the publicly available Regulations of the Award of Doctoral Degrees of TUM, in particular § 28 (Invalidation of doctoral degree) and § 29 (Revocation of doctoral degree). I am aware of the consequences of filling a false affidavit.
[X] I agree, [ ] I do not agree
that my personal data is stored in the TUM alumni database.

Munich, 20.12.2019, Tanyi

Table of contents

Abstract

Parkinson's disease (PD) is the most common neurodegenerative movement disorder characterized by the progressive loss of dopamine (DA)-producing neurons in the substantia nigra pars compacta (SNc). A neuropathological hallmark of PD is the gradual appearance of neuronal protein aggregates termed Lewy bodies (LBs). The main component of these aggregates is the protein α-Synuclein (α-Syn). Although the exact mechanism of α-Syn-mediated cell death remains elusive, recent research suggests that α-Syn-induced alterations in neuronal excitability precede cell death in PD. The fragile X mental retardation protein (FMRP) controls the expression and function of numerous neuronal genes related to neuronal excitability and synaptic function. Therefore, we investigated the role of FMRP in α-Syn-associated pathological changes in cell culture and animal models of PD as well as in post-mortem human brain tissue from PD patients. We found the abundance of FMRP to be decreased in cultured human DA neurons and in SNc DA neurons of mice over-expressing α-Syn. Reminiscent of fragile X syndrome (FXS) neurons, DA neurons overexpressing α-Syn exhibited an increased membrane abundance of the N-type calcium channel α1 subunit $Ca_V2.2$ and a large increase in N-type calcium currents as measured by patch-clamp electrophysiology. Similar to FXS, α-Syn overexpression increased the phosphorylation of extracellular signal-regulated kinase 1/2 (ERK1/2), eukaryotic translation initiation factor 4E (eIF4E) and S6, the expression of Matrix Metalloproteinase 9 (MMP9) and the overall cellular protein synthesis. Similar to cultured neurons and to mouse brain, FMRP expression was lost in SNc DA neurons of PD patients where it disappeared early in the disease course and prior to the appearance of LBs. Different from FXS, fragile X mental retardation 1 (*FMR1*) did not exhibit a hyper-methylation-induced transcriptional silencing in cultured neurons over-expressing α-Syn but appeared to be regulated through a mechanism involving protein kinase C (PKC) and cyclic adenosine monophosphate (cAMP) response element-binding protein (CREB)-driven transcription. *Fmr1* knockout (*FMR1* KO) mice were protected from reduced striatal DA release when injected with

α-Syn-expressing adeno-associated viruses (AAV) into the SN, suggesting a protective effect of FMRP loss in PD. In summary, our results reveal a new role of FMRP in PD and will support the examination of FMRP-regulated genes in PD disease progression.

List of figures

List of tables

List of symbols and abbreviations

4V	Fourth ventricle
6-OHDA	6-Hydroxydopamine
α-Syn	α-Synuclein
ATX	ω-Agatoxin
Aβ	Amyloid-β
AAV	Adeno-associated viruses
AD	Alzheimer's disease
ADP	afterdepolarization
AHP	After-hyperpolarization
AP	Action potential
$APt_{1/2}$	Half-maximal AP amplitude duration time
Aq	Aquaeduct
BCA	Bicinchoninic acid
cAMP	Cyclic adenosine monophosphate
CE	Coefficient of error
ChAT	Choline acetyltransferase
CNRQ	Comparative normalized relative quantity
CREB	cAMP response element-binding
CYT	Cytosol
CT	Threshold cycle
DA	Dopamine
DLB	Dementia with Lewy bodies
DMV	Dorsal motor nucleus of the vagus nerve
DPT	Days post transduction
ECS	Extracellular solution
eIF4E	Eukaryotic translation initiation factor 4E
4E-BPs	eIF4E binding proteins
ERK	Extracellular signal-regulated kinase
Egp	External globus pallidus
FMR1	fragile X mental retardation 1
FMRP	Fragile X Mental Retardation Protein
FXS	Fragile X syndrome
FXTAS	Fragile X-associated tremor/ataxia syndrome
GBA	Glucosylceramidase beta
GWAS	Genome-wide association studies
HBS	Hepes-buffered saline
HCN	Hyperpolarization-activated and cyclic nucleotide-gated
H&E	Hematoxylin-eosin
HM	Heavy intracellular membranes
Igp	Internal globus pallidus
iLBD	Incidental Lewy body disease

ICC	Immunocytochemistry
IHC	Immunohistochemistry
LBP	Lewy body pathology
lc	Locus coeruleus
LDH	Lactate dehydrogenase
LM	Light plasma membranes
LRRK2	Leucine-rich repeat kinase 2
LTD	Long-time depression
LUC	Luciferase
LUHMES	Lund Human Mesencephalic
MAPK	Mitogen-activated protein kinase
MAPT	Microtubule-associated protein tau
mGluR	Metabotropic glutamate receptor
MPP^+	1-Methyl-4-phenylpyridinium
MNKs	MAP kinase interacting protein kinases
MOI	Multiplicity of infection
MPTP	1-Methyl-4-phenyl-1,2,3,6-tetrahydropyridine
MSA	Multiple system atrophy
mTORC1	Mechanistic target of rapamycin complex 1
nbM	Nucleus basalis of Meynert
NL	Nuclear lysate
NLS	Nuclear localization signal
NM	Nuclear membrane
NP	Nuclear pellet
OB	Olfactory bulb
OCTX	ω-Conotoxin GIVA
PCR	Polymerase chain reaction
KCl	Potassium chloride
PD	Parkinson’s disease
PFFs	Preformed fibrils
PKC	Protein kinase C
PSP	Progressive supranuclear palsy
Pu	Putamen
qRT-PCR	Quantitative real-time PCR
REM	Rapid eye movement
rn	Raphe nuclei
Rn	Red nucleus
RSD	REM sleep disorder
ROI	Region of interest
SDS	Sodium dodecylsulfate
siRNAs	Small interfering RNAs
SN	Substantia nigra

SNCA	Synuclein Alpha
SNpc	Substantia nigra pars compacta
SNP	Single nucleotide polymorphisms
TEA	Tetraethyl ammonium
TH	Tyrosine hydroxylase
TH2	Tryptophan hydroxylase 2
TTX	Tetrodotoxin
UPS	Ubiquitin/proteasome system
VEH	Vehicle
VGCC	Voltage-gated calcium channels
VTA	Ventral tegmental area
WB	Western blot

1 Introduction

1.1 Parkinson's disease

Parkinson's disease (PD), initially named "the shaking palsy" by James Parkinson two hundred years ago (Parkinson, 1817), is one of the most prevalent neurodegenerative diseases with an incidence of 2–3% among the population above 65 years of age (Kalia & Lang, 2015). In PD, dopaminergic neurons in the substantia nigra pars compacta (SNc) undergo a progressive cell death (Del Rey et al., 2018; Fyfe, 2017; Postuma & Berg, 2016). This results in a reduced striatal dopamine (DA) release and, as a consequence, in an inhibition of cortical motor programs, causing the typical parkinsonian motor features, including muscular rigidity, tremor, freezing gait and impaired movement execution (Calabresi, Picconi, Tozzi, Ghiglieri, & Di Filippo, 2014; Kones, 2010; Rodriguez-Sabate et al., 2017). Beyond the evident motor deficiency, PD patients exhibit multiple non-motor symptoms, such as hyposmia, constipation, and cognitive decline (Phillipson, 2017; Tibar et al., 2018), thus demonstrating the additional affection of other brain regions. Moreover, the associated non-motor symptoms frequently appear years ahead of the motor dysfunction and characterize the early stages of the disease (Berg et al., 2014; Postuma & Berg, 2016; Ray Chaudhuri et al., 2016; Tibar et al., 2018). Although tremendous efforts have been made so far, the definitive diagnosis remains challenging during the early stages (De Pablo-Fernandez, Lees, Holton, & Warner, 2019). Until today, the ultimate cause of PD remains elusive (Phillipson, 2017). Existing research supports the theory that environmental and genetic risk factors both contribute to the development of the disease (Del Tredici & Braak, 2016; Pan-Montojo et al., 2012). The diagnostic criterion for PD is the appearance of Lewy pathology and the degeneration of SNpc neurons (Goedert, Spillantini, Del Tredici, & Braak, 2013; Hawkes, Del Tredici, & Braak, 2010). Previous studies have identified misfolded α-Synuclein (α-Syn) and lipids as the main component of Lewy bodies (Auluck, Caraveo, & Lindquist, 2010; Doria, Maugest, Moreau, Lizard, & Vejux, 2016; Marin et al., 2017; Tan et al., 2019), in conjunction with Lewy neurites termed Lewy pathology (Prymaczok, Riek, & Gerez,

2016; Volpicelli-Daley, Luk, & Lee, 2014). Due to the neuroanatomical spreading pattern of Lewy pathology in many cases from the brainstem to the cortex, Braak et al. developed a staging with six different disease stages (Braak et al., 2003; Del Tredici & Braak, 2016). Although there is currently no cure for PD, disease-modifying drugs likely require an early diagnosis and treatment intervention (Ray Chaudhuri et al., 2016; Tibar et al., 2018). Therefore, studying the early molecular events and looking for potential targets during such an early prodromal stage will make a noteworthy contribution to the diagnosis and cure of the disease.

1.1.1 Clinical characterization and genetic risks

In general, the clinical features of PD can be divided into two main sub-groups: classical motor features and non-motor features (Brys, Nunes, & Fuentes, 2017; Stacy, 2011). This system of classification offers a unique perspective on the pathogenic progression of PD, as it was able to indicate a prolonged prodromal stage, sometimes up to a decade, before the appearance of gradually worsening motor features (**Figure 1**).

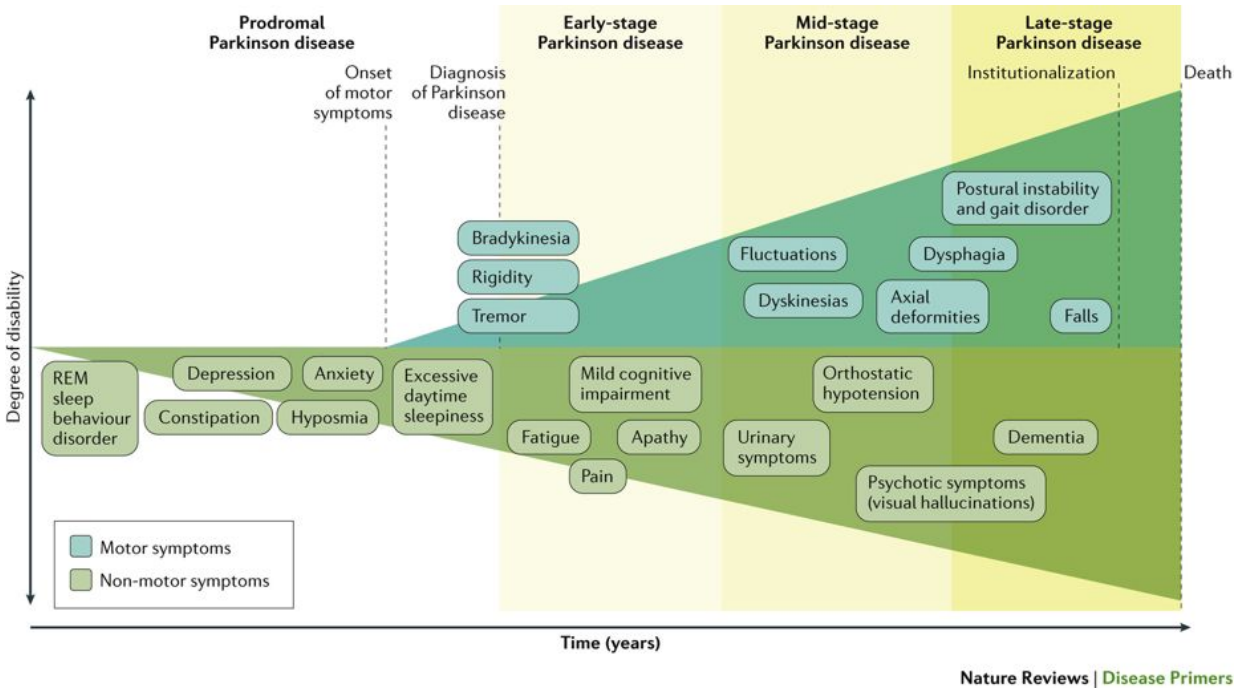

Figure 1 Progression of PD and clinical features during different stages (from Poewe et al., 2017). PD usually begins with a prodromal stage in which patients only develop non-motor features like depression. The appearance of motor features during the early stage assists in the PD diagnosis. However, the accurate diagnosis is often made years later than the onset of non-motor features and more additional non-motor features appear during the early stage. The disability is getting worse over time and during the mid-stage, patients will develop dyskinesias accompanied by psychotic features. In the late stage, frequent falls and other postural instability are prevalent. Meanwhile, patients also suffer from severe cognitive deficiency. REM= rapid eye movement.

Classical motor features of PD include rigidity, tremor, bradykinesia, and postural instability (Berg et al., 2014; Del Rey et al., 2018). In fact, there might be only one or two features present in a given patient, especially during the early disease stages. Tremor sometimes is not obvious or even absent in PD, people thereby further categorize motor features into three subtypes: tremor-dominant, non-tremor-dominant, and mixed. Clinical statistics reveal that the non-tremor-dominant disease variant is usually developing more rapidly than tremor-dominant patients do, and also has a higher tendency to associate with a severe movement disability later on (Fyfe, 2017; G. M. Halliday et al., 1996).

Non-motor features are miscellaneous, including enteric nervous system symptoms like constipation or hypotension; brainstem symptoms, including REM sleep disorder (RBD), depression, or anxiety; basal ganglia symptom like rigidity or bradykinesia; and cortical symptom including cognitive decline and dementia (Kurtis, Rajah, Delgado, & Dafsari, 2017; Tibar et al., 2018).

Up to 90% of all PD cases are sporadic. Current theories suggest that the interplay between environment and genetic risk factors contributes to the progression of the disease (Kones, 2010; Pan-Montojo et al., 2012; M. Zhang et al., 2017). For instance, 1-methyl-4-phenyl-1,2,3,6-tetrahydropyridine (MPTP) has been shown to induce parkinsonism (Dauer & Przedborski, 2003; Patil, Jain, Ghumatkar, Tambe, & Sathaye, 2014). From post-mortem brain examination of MPTP-intoxicated patients; however, no Lewy bodies were identified as well as in the MPTP-induced mouse and primate models (Gibb & Lees, 1988; G. Halliday et al., 2009; Jiang & Dickson, 2018). Therefore, more attention was focused on the genetic risk factors when A53T synuclein alpha (*SNCA)* was identified as an autosomal-dominant mutation for PD at the end of the last century (Puschmann et al., 2009). Subsequent research, in succession, discovered more and more pathogenic *SNCA* genetic variants including A30P, E46K, H50Q, G51N, as well as gene duplications and triplications (Campelo & Silva, 2017). Other than *SNCA*, there are 21 additional genetic loci that have been identified to be associated with PD (**Table 1**). Glucosylceramidase beta (*GBA*) and microtubule-associated protein tau gene (*MAPT*) have been recently demonstrated as candidates through large genome-wide association studies (GWAS) (Lill, 2016). Different from PD-causative mutants, genetic variants in *GBA* only contribute to higher susceptibility in PD, whereas the strongest relative mutations at GWAS level, like *MAPT*, usually correlate with an earlier age-at-onset. Meanwhile, there are still several PD-associated loci under debate due to a limited amount of original research, like *TMEM230* (Giri et al., 2017).

Locus	Gene	Inheritance	Onset	Location	Variants	Function
PARK1/4	*SNCA*	Dominant Risk factor	EO	4q21.3-q22	5 point mutations, multiplications Rep1 risk variant in the promoter	Synaptic vesicles trafficking
PARK2	*PARKIN*	Recessive	EO	6q25.2-q27	>250 point mutation, ins/de and exon rearrangements	Mitophagy
PARK3	Unknown	Dominant	LO	2p13	?	?
PARK5	*UCHL1*	Dominant	LO	4p13	1 missense variant in one sibling pair	Proteasome
PARK6	*PINK1*	Recessive	EO	1p36.12	>100 point mutations, ins/del and exon rearrangements	Mitophagy
PARK7	*DJ-1*	Recessive	EO	1p36.23	>20 point mutations and deletions	Mitophagy
PARK8	*LRRK2*	Dominant Risk factor	LO	12q12	7 point mutations Risk variants p.R1628P and p.G2385R	Autophagy?
PARK9	*ATP13A2*	Recessive	EO	1p36	>20 point mutations	Lysosomes
PARK10	Unknown	Risk factor	?	1p32	?	?
PARK11	*GIGYF2*	Recessive	EO	2q36-7	7 missense variants	Insulin-like growth factors (IGFs) signaling
PARK12	Unknown	Risk factor	?	Xq21-q22	?	?
PARK13	*HTRA2*	Dominant	?	2p13.1	1 missense variant	Mitophagy,
PARK14	*PLA2G6*	Recessive	EO	22q13.1	>18 missense variants	Lipids metabolism
PARK15	*FBXO7*	Recessive	EO	22q12.3	4 point mutations	Mitophagy
PARK16	Unknown	Risk factor	?	1q32	?	?
PARK17	*VPS35*	Dominant	LO	16q12	2 point mutations	Endosomes
PARK18	*EIF4G1*	Dominant	LO	3q27.1	1 missense variant	Protein translation
PARK19	*DNAJC6*	Recessive	EO	1p31.3	9 missense variants	Endosomes
PARK20	*SYNJ1*	Recessive	EC	21q22.11	3 missense variants	Endosomes
PARK21	*DNAJC13*	Dominant	LO	3q22.1	1 missense variant	Endosomes
PARK22	*CHCHD2*	Dominant	LO/EO	7p11.2	1 missense variant, 1 truncation	Mitochondria-mediated apoptosis and metabolism?
PARK23	*VPS13C*	Recessive	EO	15q22.2	2 missense variants,l truncation	Mitophagy
–	*GBA*	AD, AR in GD Risk factor	LO	lq22	>10 missense variants	Lysosomes
–	*MAPT*	Sporadic Risk factor		17q21.31	H1 haplotype increase PD risk and disease severity	Microtubules

EO, early onset; LO, late onset.

Table 1 Causative gene for PD (from Del Rey et al., 2018).

1.1.2 Lewy body pathology, synucleinopathies and the Braak staging hypothesis

Existing research recognized Lewy body pathology (LBP), including the appearance of Lewy bodies and Lewy neurites, as a specific neuropathological hallmark in PD (Berg et al., 2014; Braak et al., 2003). Lewy bodies are intracellular inclusions containing insoluble, misfolded and unbranched α-Syn aggregates (DelleDonne et al., 2008). Aggregated α-Syn has a β-sheet structure with highly packed repetitive and hyperphosphorylated α-Syn molecules at Ser129 (Delic et al., 2018; Karampetsou et al., 2017). The hyperphosphorylation is mainly regulated by G-protein-coupled receptor kinases (Arawaka et al., 2006). Interestingly, based on

hematoxylin-eosin (H&E) staining, two distinct forms of LBs can be distinguished (Covell et al., 2017; Kuusisto, Parkkinen, & Alafuzoff, 2003); one was found in the brainstem with an eosinophilic, argyrophilic core and strong peripheral pale halo, the other one was discovered in both the limbic system and cortex with irregular formation, weak halo, and robust α-Syn immunoreactivity. Lewy neurites can be generally divided into spheriform and linear patterns (Kuusisto et al., 2003). When vestigial Lewy neurites wrap extracellular amyloid-β (Aβ) aggregates in some Alzheimer's disease (AD) cases, it forms a specific deposit termed Lewy plaque (Adamowicz et al., 2017; Orr, Wordehoff, Hoyer, & Tamamis, 2016). Thus far, LBs have been broadly demonstrated as a pathogenic indicator for PD; however, whether the presence of LBs induces cell death still remains unclear. According to some studies, it is certain that cells can survive for many years despite the presence of intracellular Lewy bodies (Beyer, Domingo-Sabat, & Ariza, 2009). On the other hand, LBs can be found anywhere in the whole neuraxis and developing numbers of LBs (Sorrentino et al., 2017), in most cases, reflect the progression and severity of the disease.

Abnormal α-Syn not only accumulates in neurons but also in oligodendrocytes termed Papp-Lantos bodies which are the typical hallmark of multiple system atrophy (MSA) (Jellinger & Lantos, 2010; Peng et al., 2018), another synucleinopathy with distinct clinical traits. Together with LBP, the α-Syn aggregation-induced pathological lesion was named synucleinopathies (Alegre-Abarrategui et al., 2019; Candelise et al., 2019; El-Agnaf et al., 2017). From previous research, the Papp-Lantos body was shown to contain ubiquitin, tau, leucine-rich repeat kinase 2 (*LRRK2*), and many other proteins, but with α-Syn remaining the main component. Besides, it was also infrequently identified in progressive supranuclear palsy (PSP) cases and other neurodegenerative diseases (Jellinger, 2009). With different clinical presentations, MSA patients can be classified into parkinsonism- (over 80%) and cerebellar-predominant (Peelaerts, Bousset, Baekelandt, & Melki, 2018). The former sometimes was initially misdiagnosed with PD, but MSA

patients later will develop additional symptoms and exhibit a weak response to levodopa treatment, which in a way could help to distinguish it from PD (Schrag et al., 2010)

As described earlier, PD is a progressive neurodegenerative disorder with constantly worsening motor symptoms. By examining post mortem brain tissue from PD patients at different disease stages, Braak et al. (Braak et al., 2003) found LBs to appear in a predictable pattern. In the first stage, LBs mainly accumulated in the olfactory bulb or lower brainstem. In accord, Braak stage 1 is characterized by non-motor symptoms like loss of olfaction. In stage 2, LBs were observed in the raphe nuclei, medulla oblongata, and locus coeruleus, whereas patients exhibited more non-motor symptoms. Once Lewy bodies can be identified in the SN or nucleus basalis Meynert, this indicates the disease moving to stage 3 or higher. Usually, the motor dysfunction remains unnoticeable during stage 3 and starts to be evident from stage 4 when LBs reach the temporal cortex. In stage 5, LBs appear in the neocortex and significant dopaminergic neurodegeneration can be observed. The patients also display obvious cognitive dysfunction in this stage. Finally, the LBs will “spread” to the whole neocortex and reach the primary sensory area in stage 6. The symptoms also become the most serious during the last stage (**Figure 2**). As has been noted, the pathology exhibits a strong spreading pattern following the disease progression which was well supported by presenting of LBs in the grafted tissue (Kordower, Chu, Hauser, Freeman, & Olanow, 2008; J. Y. Li et al., 2008).

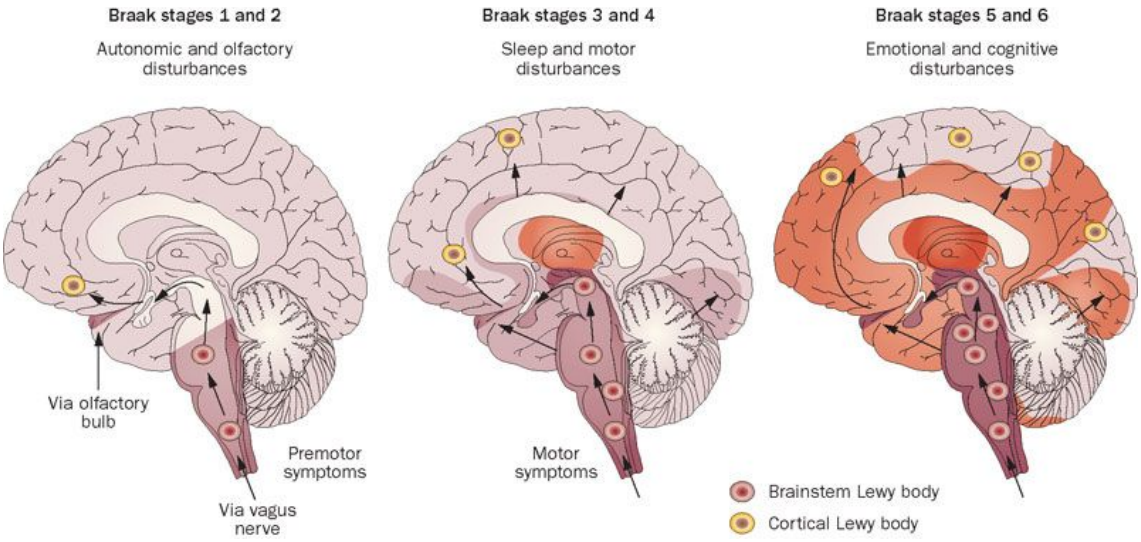

Figure 2 Braak staging hypothesis (from Doty, 2012).

1.1.3 The role of α-Syn in PD and incidental Lewy body disease

Spillantini (Spillantini et al., 1997) demonstrated α-Syn as the main component of LBs. α-Syn was initially identified by Maroteaux (Maroteaux, Campanelli, & Scheller, 1988) and isolated from synaptic vesicles and the nuclear envelope in cholinergic neurons of *Torpedo californica*. It has three homologues: β-synuclein, γ-synuclein, and synoretnin, all of them with frequent KTKEGV repeat sequences (Lashuel, Overk, Oueslati, & Masliah, 2013; Rodriguez et al., 2015). Interestingly, although all the family members are highly homologous, only α-Syn has the propensity for aggregation (Auluck et al., 2010). Data from several sources suggested a 12 amino acid region in the hydrophobic domain of α-Syn, which was absent in other homologues, to be responsible for α-Syn's ability to oligomerize and aggregate (Giasson, Murray, Trojanowski, & Lee, 2001). On the other hand, there was research that demonstrated the existence of SDS-non-resistant α-Syn oligomers of ~ 60 kDa in size in both control and LBD patients (Bartels, Choi, & Selkoe, 2011). Different from monomers, native tetramers do not puncture the lipid membrane and display a limited tendency to form aggregates (Nuber et al., 2018; W. Wang et al., 2011). Debate continues about whether α-Syn oligomers exist under physiological conditions or whether different conformations exist in different cellular

compartments. Independent from these experiments, SDS-resistant α-Syn oligomers, in particular dimers, have been frequently detected from different models under oxidative stress condition or after treatment with cytochrome c/hydrogen peroxide (Grassi et al., 2018; Hashimoto, Hsu, et al., 1999; Hashimoto, Takeda, Hsu, Takenouchi, & Masliah, 1999). Therefore, studying the function and distribution of α-Syn oligomers may contribute to a better understanding of PD pathology.

So far, the actual function of α-Syn is still under the mask. Current research indicates α-Syn monomer to be involved in synaptic function, lipid metabolism, and epigenetic modification (Adamczyk & Strosznajder, 2006; Auluck et al., 2010; Soldner et al., 2016). The α-Syn oligomers, fibrils, and aggregates have been reported to harm neurons by inducing mitochondrial dysfunction, impairing vesicle trafficking, and protein degradation (Phillipson, 2017). Meanwhile, α-Syn fibrils were shown to exhibit prion-like features, in accord with Braak's staged progression (Hasegawa, Nonaka, & Masuda-Suzukake, 2016).

Although LBs contain a large amount of α-Syn fibrils, the accumulation mechanism under physiological condition has not yet been comprehensively investigated due to the limitation of appropriate model systems. LBs seem to be restricted to humans and are not even present in our primate relatives (Visanji et al., 2016). However, a consistent mechanism of α-Syn accumulation and aggregation in different models still can be recapitulated. First, increased production of α-Syn, caused by *SNCA* gene triplication or single nucleotide polymorphisms (SNPs) of the SNCA gene, leads to an accumulation of α-Syn (Oliveira et al., 2015). Current knowledge based on in vitro protein kinetic assays can well explain the formation of oligomers and fibrils in a long run from sufficient monomer α-Syn (Narkiewicz, Giachin, & Legname, 2014; Ponzini et al., 2019). Second, factors such as mutations and oxidative stress can induce α-Syn accumulation through seeding from a small seed concentration (Lazaro et al., 2016; W. Wang et al., 2016). Of note, different mutations under distinct conditions exhibit identical patterns of

aggregation. For example, A30P α-Syn expedites the process of α-Syn oligomerization in vitro but induces fibrillation in vivo (Lemkau et al., 2012; J. Li, Uversky, & Fink, 2001). Third, impaired protein degradation, autophagy dysfunction for instance, is also able to accelerate protein aggregation (Melo, Copray, & Ferrari, 2018; Moors et al., 2017). Reduced protein degradation leads to an increased level of α-Syn or misfolded α-Syn (Cuervo, Stefanis, Fredenburg, Lansbury, & Sulzer, 2004). Meanwhile, previous studies suggest that misfolded protein elimination deficiency is associated with sporadic PD and DLB (Candelise et al., 2019). Although different forms of α-Syn were monitored in vitro and in vivo, it remained unclear whether they are toxic or not. A systematic study that examined the effect of α-Syn conformation on toxicity in vivo was reported by Peelaerts et al. (Peelaerts et al., 2015). They demonstrated that fibrils are more toxic than oligomers and ribbons, also distinct strains resulted in a different pathology pattern. The incidental Lewy body disease (iLBD) refers to cases without clinical symptoms of PD, but with the appearance of LBs and LNs in the brain (DelleDonne et al., 2008). Nearly one-third of people above 65 have iLBD. The iLBD has hitherto received scant attention by scholars' due to vague clinical symptoms. Current preliminary researches suggest iLBD is likely the preclinical phage of DLB and PD (Bloch, Probst, Bissig, Adams, & Tolnay, 2006).

1.1.4 Voltage-gated calcium channels in PD

Voltage-gated calcium channels (VGCCs) are membrane resident calcium-conducting ion channels that flux calcium in response to membrane depolarization. VGCCs control many functions including gene expression, neurotransmitters release, cell excitability, etc. (Buraei & Yang, 2013; Dolphin, 2009). According to their electrophysiological and pharmacological characterization, VGCCs are generally grouped into Ca_V1, Ca_V2 and Ca_V3 (**Table 2**). Ca_V1 and Ca_V3 family are L-type and T-type, respectively. Ca_V2 contains P/Q-type ($Ca_V2.1$), N-type ($Ca_V2.2$), and T-type ($Ca_V2.3$) (Dai, Hall, & Hell, 2009). Perturbed calcium homeostasis due to

the activation of different VGCCs has been reported in different PD models (Duda, Potschke, & Liss, 2016; Hurley & Dexter, 2012). Chan et al. found that isradipine, which is an L-type calcium channel blocker, can rescue the SNc neurons by changing aged pacemaking to the juvenile form in the MPTP-induced mouse PD model (Chan et al., 2007). The protective effect of L-type calcium channel blockers in different PD models is well supported by other researches (Guzman et al., 2018; Liss & Striessnig, 2019) and isradipine was recently a potential drug for early PD patients in clinical trial phase III. α-Syn overexpressed in SH-SY5Y cells induced a cobalt-non-sensitive calcium channel activation (Danzer et al., 2007), indicating that the N-type calcium channel is not involved. Conversely, Adamczyk (Adamczyk & Strosznajder, 2006) reported omega-conotoxin GVIA, which is also an N-type calcium channel blocker, to block calcium influx induced by extracellular α-Syn in rat brain synaptosomes.

Channel	Current	Associated subunits	Expression detected	General Cellular functions
Cav1.1 (CACNA1S)	L	α2δ, β, γ	Brain, Leukemia	Excitation-contraction coupling
Cav1.2 (CACNA1C)	L	α2δ, β, γ	Colorectal, Gastric, Pancreas, Sarcoma, Leukemia, Brain, Breast, Uterus, Skin, Prostate	Excitation-contraction coupling
Cav1.3 (CACNA1D)	L	α2δ, β, γ	Prostate, Breast, Colorectal, Bladder, Gastric, Lung, Brain, Uterus, Esophagus	Excitation-contraction coupling
Cav1.4 (CACNA1F)	L	α2δ, β, γ	Testis	Excitation-contraction coupling
Cav2.1 (CACNA1A)	P/Q	α2δ, β, possibly γ	Leukemia, Ovarian, Sarcoma, Brain, Uterus, Ovarian, Lung, Cervix,	Neurotransmitter release; dendritic Ca2+ transients; hormone release
Cav2.2 (CACNA1B)	N	α2δ/β1, β3, β4, possibly γ	Prostate, Breast	Neurotransmitter release; dendritic Ca2+ transients; hormone release
Cav2.3 (CACNA1E)	R	α2δ, β, possibly γ	Esophagus, Uterus	Repetitive firing; dendritic calcium transients
Cav3.1 (CACNA1G)	T	None	Sarcoma, Colorectal, Uterus, Lung, Prostate, Breast	Pacemaking; repetitive firing
Cav3.2 (CACNA1H)	T	None	Renal, Sarcoma, Gastric	Pacemaking; repetitive firing
Cav3.3 (CACNA1I)	T	None	Breast, Sarcoma, Esophagus	Pacemaking; repetitive firing

Table 2 Different voltage-gated calcium channels (from C. Y. Wang, Lai, Phan, Sun, & Lin, 2015).

Existing research recognizes the critical role of α-Syn in regulating calcium homeostasis. In turn, deregulated intracellular calcium can induce α-Syn oligomerization and aggregation which further accelerates the disease progression (Nath, Goodwin, Engelborghs, & Pountney, 2011;

Zaichick, McGrath, & Caraveo, 2017). A study by Follett et al. showed that pre-incubation with BAPTA-AM can significantly reduce α-Syn aggregation in both HEK293T and SHSY-5Y cells (Follett, Darlow, Wong, Goodwin, & Pountney, 2013). Likewise, an increased intracellular calcium level by applying thapsigargin or the calcium ionophore A23187 resulted in the formation of α-Syn plaques (Nath et al., 2011).

1.2 Fragile X syndrome

Fragile X syndrome (FXS) is an inherited mental disease due to the absence of the fragile X mental retardation protein (FMRP) (Budimirovic & Kaufmann, 2011). FMRP is coded from the fragile X mental retardation 1 (*FMR1*) gene on the X chromosome (De Rubeis & Bagni, 2011). In line, male patients usually have more severe symptoms than female patients (Alisch et al., 2013). In FXS patients, there are more than 200 CGG repeats (full mutation) in the 5′ untranslated region of *FMR1*. These induce hypermethylation of *FMR1* followed by transcriptional silencing (Jalnapurkar, Cochran, & Frazier, 2019). FMRP acts as a transcriptional regulator, controls the expression of many synaptic proteins like Arc and STEP (H. Y. Lee et al., 2011; Richter, Bassell, & Klann, 2015), and plays a critical role in the synaptic maturation (Oostra & Willemsen, 2003). The deficiency of FMRP leads to nervous system dysfunction and abnormal synapse formation (Sunamura, Iwashita, Enomoto, Kadoshima, & Isono, 2018). Healthy people normally harbor 5-40 times CGG repeats. Individuals with 55 to 200 CGG repeats, termed *FMR1* premutation, have a risk to develop what is called the fragile X-associated tremor/ataxia syndrome (FXTAS) (R. J. Hagerman & Hagerman, 2016). Different from FXS, FXTAS patients usually retain general intelligence and typical symptoms like tremor and/or ataxia only occur in the middle age (D. A. Hall et al., 2005). Instead of silenced gene expression of *FMR1* in FXS, the transcription of the *FMR1* gene in FXTAS is increased and therefore produces excess *FMR1* mRNA (D. A. Hall, Howard, Hagerman, & Leehey, 2009). However, the FMRP level is either normal or moderately decreased in FXTAS (P. J. Hagerman & Hagerman, 2015). Thus, the cause of FXTAS is rather due to elevated RNA gain of function toxicity. In addition, pathogenic intranuclear inclusions, which are tau and α-Syn negative, are frequently observed in both neurons and glial cells throughout FXTAS patients' brain (Boivin, Willemsen, Hukema, & Sellier, 2018). Although there is currently no cure for FXS and FXTAS, normalizing the over-activated mGluR5-mediated FXS pathophysiology showing great potential in ameliorating FXS behaviors in mouse model. In 2018, a new emerging CRISPR-Gold technic

has shown that controlling the numbers of affected striatum mGluR5 neurons can improve abnormal behaviors of *FMR1* knockout (*FMR1* KO) mice (B. Lee et al., 2018).

1.2.1 Clinical characterization and pathogenesis

Intellectual disability is the most prominent clinical feature of FXS and includes impaired short-term memory, delayed development of speech, and inattention (Bagni, Tassone, Neri, & Hagerman, 2012). Apart from intellectual disability, FXS patients also exhibit morphological abnormalities after puberty, including a long face with an arched palate, big ears, soft skin, unusually hyperextensible fingers, flat feet as well as macroorchidism (Contractor, Klyachko, & Portera-Cailliau, 2015). Associated symptoms include autism-like behavior, social anxiety, and hypersensitivity (Tranfaglia, 2011). Unlike FXS, FXTAS patients exhibit predominantly motor symptoms and therefore are often misdiagnosed as PD at the beginning (Sellier et al., 2017). Individuals with FXTAS usually present with action tremor, rigidity, ataxia, slow movement, and diminished sensation (Niu et al., 2014). In addition, some patients suffer from immune system problems (R. J. Hagerman & Hagerman, 2016). Similar to FXS, the number of CGG repeats correlates with the severity of the disease (Oostra & Willemsen, 2003).

The “fragile locus” constriction in FXS was identified from the long arm of the X chromosome by Lubs in 1969 (Lubs, 1969). Under the healthy condition, FMRP is abundant in the human brain and can selectively bind to a large number of mRNAs. Studies have suggested that up to 4% of RNA transcripts in the brain interact with FMRP (Bhakar, Dolen, & Bear, 2012; Miyashiro et al., 2003). Through physical binding, FMRP is able to cargo newly synthesized mRNAs out of the nucleus and suppress their translation (Garber, Smith, Reines, & Warren, 2006; Stefani, Fraser, Darnell, & Darnell, 2004). Most of these mRNAs exist in dendrites and translated proteins are predominantly associated with the synaptic function (Feng et al., 1997; Higashimori et al., 2013). As a result, mRNA translation and protein synthesis are increased in FXS and accompanied by abnormal dendritic spine morphology in FXS human neurons and

neurons from *FMR1* KO mice (De Rubeis & Bagni, 2011; Kazdoba, Leach, Silverman, & Crawley, 2014). The abnormal development and structure of synapses lead to impaired synaptic plasticity, learning and memory (K. Zhang et al., 2017). This is likely the basis of the early intellectual disability in FXS children. Moreover, FMRP loss can amplify neuronal long-time depression (LTD) through the metabotropic glutamate receptor (mGluR) cascade (Osterweil, Krueger, Reinhold, & Bear, 2010). FMRP loss likely impairs DA release, which may contribute to typical features in FXS, such as hyperactivity (H. Wang et al., 2008).

In the case of FXTAS, much uncertainty still remains about the RNA gain of function toxicity. In view of published work so far, previous studies support the hypothesis that excess *FMR1* mRNAs competitively bind to some RNA-binding proteins and derail the actual function of those proteins (Sellier et al., 2017). The subsequent protein aggregation forms inclusions (Greco et al., 2002), and exerts neuronal toxicity to induce cell death (Jeon et al., 2012). In addition, mitochondrial deficiency or inflammation may also have a detrimental effect on disease progression (Liu et al., 2018; Shen et al., 2019).

1.2.2 Regulation of fragile X mental retardation protein and protein-related pathways

In the mouse brain, neurons start to express FMRP in the early stages of gestation (Arsenault et al., 2016; Kazdoba et al., 2014). Later on, FMRP expression is restricted to the brain (Zhang et al., 2015). In neuronal cells, FMRP mainly exists in the perikaryon, bound to ribosomes or polyribosomes, as well as in neurites (Liu et al., 2018). Others spot at nucleopore or in the nucleolus (Lai, Sakkas, & Huang, 2006). Although in situ hybridization and immunofluorescent studies have recognized the distribution and localization of FMRP (Dictenberg, Swanger, Antar, Singer, & Bassell, 2008; Feng et al., 1997), no systematic studies have been performed to investigate the regulation of protein expression and shuttling mechanism of FMRP between nucleus and cytoplasm. According to the promoter sequences, Hansen et al. (H. Wang et al., 2012) speculated that the phosphorylation of cyclic AMP-

responsive element-binding protein (CREB), as a transcriptional factor, might be a key intermediate step involved in the translation of FMRP. Full-length FMRP contains a nuclear localization signal (NLS) domain (Kim, Bellini, & Ceman, 2009), however, the binding sequence of classical NLS receptor, importin alpha, is absent in its NLS domain. Therefore, the translocation mechanism of FMRP remains unclear.

Two canonical pathways under mGluRs, mechanistic target of rapamycin complex 1 (mTORC1) and mitogen-activated protein kinase/extracellular signal-regulated kinase (MAPK/ERK), are hyperactivated in both FXS patients and *FMR1* KO mice (**Figure 3**) (Sharma et al., 2010; Zhao, Chuang, Bianchi, & Wong, 2011). In *FMR1* KO mice, inhibitory pharmacologic treatments targeting these pathways, like metformin, exhibit a protective effect with rescued abnormal spine morphology and alleviated behavior deficits (Gantois et al., 2017). The mTOR is a highly conserved kinase among different species, and involved in almost all the aspects of cellular processes, including cell survival, growth, proliferation, protein degradation, lipid synthesis, et al. (Niere & Raab-Graham, 2017; Zhu, Chen, Mays, Stoica, & Costa-Mattioli, 2018). Unlike mTORC2, which is a rapamycin-insensitive mTOR complex, mTORC1 mainly regulates phosphorylation of eukaryotic translation initiation factor 4E (eIF4E) binding proteins (4E-BPs) and p70 S6 kinase 1 (S6K1) (Marat et al., 2017; Niere & Raab-Graham, 2017). As a consequence of mTORC1 activation, eIF4E-eIF4G translation initiation complex is assembled and protein synthesis is boosted therewith (Napoli et al., 2008). Additional knockout of S6K1 in *FMR1* KO mice exhibits recovered social behavior, dendritic morphology, and function (Bhattacharya et al., 2012). Moreover, treatment of temsirolimus, a mTORC1 inhibitor, improves mice cognitive function which is impaired in *FMR1* KO mice (H. Wang, Pati, Pozzo-Miller, & Doering, 2015). The MAPK/ERK pathway, as the name suggests, is mainly related to cell proliferation in response to extracellular mitogens (Y. Li et al., 2016). Therefore, it has been well studied in cancer research. ERK also acts on eIF4E, but through MAP kinase interacting protein

kinases (MNKs) (Waskiewicz, Flynn, Proud, & Cooper, 1997; Waskiewicz et al., 1999). Normalizing ERK signal by lovastatin has ameliorated movement activity in FXS patients and has shown corrected protein synthesis in vivo (Caku, Pellerin, Bouvier, Riou, & Corbin, 2014; Osterweil et al., 2013). Once again, genetically deletion of MMP9, which is frequently implicated in FXS as excessive production of eIF4E phosphorylation, prevents the formation of immature spine morphology (Sidhu, Dansie, Hickmott, Ethell, & Ethell, 2014).

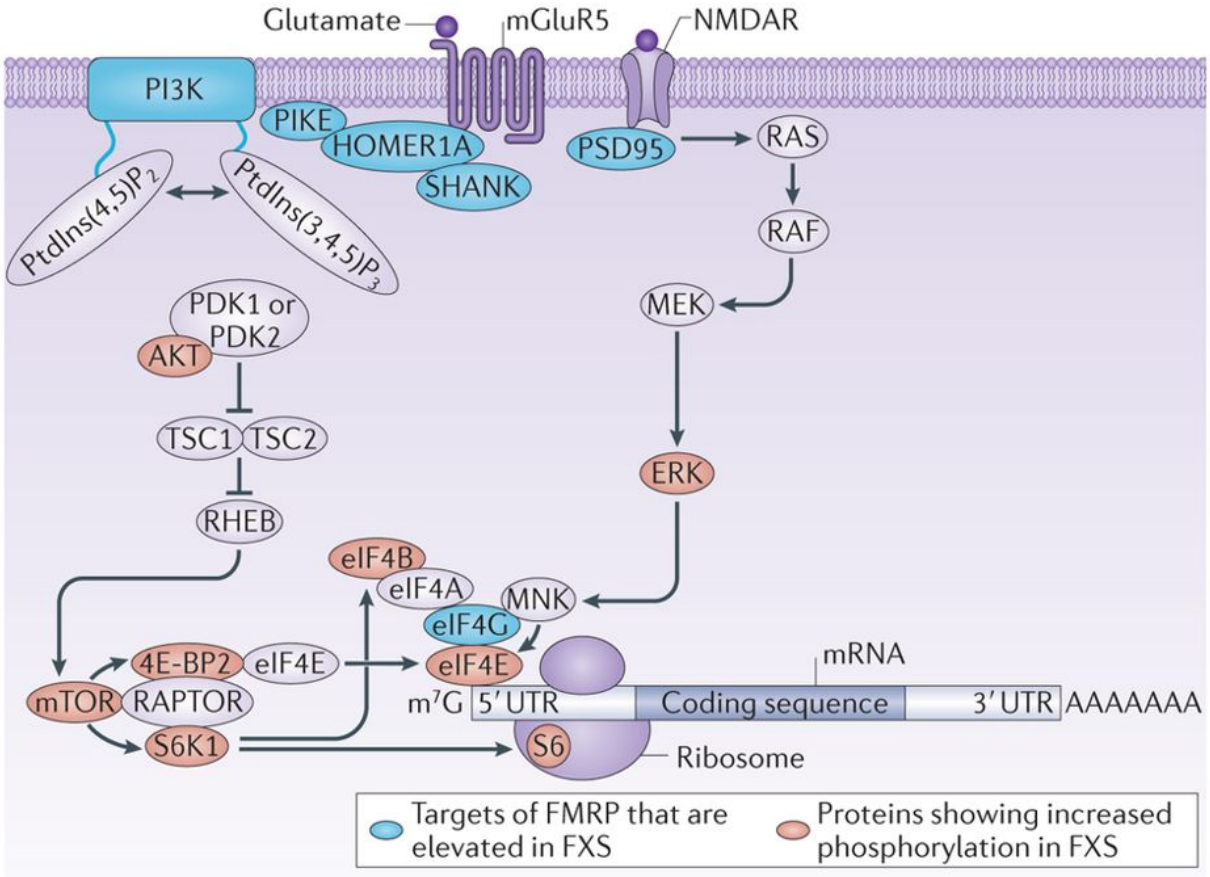

Figure 3 FMRP related protein translation initiation pathways (from Richter et al., 2015).

1.2.3 Commonalities with PD

FXS patients do not exhibit a PD-like movement disorder. Hall et al. reported a 60-year-old male FXS patient, with 540 and 447 CGG repeats in two alleles, displaying a prominent cognitive decline and parkinsonism (D. Hall, Pickler, Riley, Tassone, & Hagerman, 2010). In

FXTAS, which is normally diagnosed at a later age, parkinsonism has been commonly reported (Cilia et al., 2009). Interestingly, almost all typical PD symptoms, including both non-motor and motor, have been found in FXTAS patients (Fay-Karmon & Hassin-Baer, 2019). FXTAS cases sometimes have concomitant LBP in the brain. Meanwhile, nearly one-fifth of the FXTAS patients have also shown impaired nigrostriatal projection and related DA deficiency (D. A. Hall, Jennings, Seibyl, Tassone, & Marek, 2010).

1.3 Aim of the study

1) Neuronal calcium homeostasis contributes to neurodegeneration in PD (Duda et al., 2016). The effect of α-Syn on neuronal calcium channels has not been well studied. Therefore, we aimed to investigate the effect of α-Syn on VGCCs in cultured dopaminergic neurons.

2) Activated N-type calcium channels were recognized in this dissertation to be related to α-Syn overexpression in LUHMES cells. Although one publication reported a physical direct interaction between FMRP and N-type calcium channel (Ferron, Nieto-Rostro, Cassidy, & Dolphin, 2014), much uncertainty still exists about the relationship between N-type calcium channels and FMRP. Thus, we attempted to ascertain the role of FMRP in regulating N-type calcium channels and other downstream proteins in PD models.

3) FMRP has been reported in a number of FXS studies involving in regulating synaptic function and protein synthesis. However, the role of FMRP has hitherto received scant attention in PD research. Our third aim of this study was to assess the FMRP expression in different pathological stages and regions of PD patients' brains.

2 Materials and methods

2.1 Materials

2.1.1 Antibodies

Antibody	Cat. No.	Dilution (WB)	Dilution (ICC/IHC)	Supplier
FMRP	4317S	1:1000	1:50	Cell Signaling
FMRP 5C2	834701		1:100	Biolegend
FMRP 4G9	NBP1-42567		1:100	Novus Biologicals
Alpha-synuclein 15G7	ab195561		1:50	Abcam
Alpha-synuclein	2642S	1:1000		Cell Signaling
Alpha-synuclein C20	sc-7011-R	1:1000		Santa Cruz
Beta-actin	4967S	1:10000		Cell Signaling
CACNA1B	PA5-21440	1:1000	1:100	Thermo Fisher
CACNA1B	ACC-002	1:1000	1:100	Alomone Labs
CACAN1B	Sc-377489		1:200	Santa Cruz
S6 Ribosomal Protein 5G10	2217S	1:1000		Cell Signaling
Phospho-S6 Ribosomal Protein Ser240/244	2215S	1:1000		Cell Signaling
Phospho-eIF4E Ser209	9741S	1:1000		Cell Signaling
eIF4E	9742S	1:1000		Cell Signaling
MMP-9	PA5-16851	1:1000		Thermo Fisher
MMP-9 D6O3H	13667S	1:1000		Cell Signaling
EEA1	610456	1:1000		BD Transduction Laboratories
HDAC2(3F3)	5113	1:1000		Cell Signaling
GAPDH(14C10)	3683S	1:1000		Cell Signaling
CREB 48H2	9197S	1:1000		Cell Signaling
Phospho-CREB Ser133 87G3	9198S	1:1000		Cell Signaling
Phospho-CREB Ser133	MA5-11192	1:1000		Thermo Fisher
Tyrosine Hydroxylase	AB152		1:500	Millipore
Tyrosine Hydroxylase	PA1-4679,		1:100	Thermo Fisher
Na^+-K^+-ATPase	3010S	1:1000		Cell Signaling
NMDAR1	48066	1:1000		BD Pharmingen
Pan-Cadherin	4068	1:1000		Cell Signaling
Puromycin	MABE343	1:1000		Millipore
Tryptophan Hydroxylase 2	ABN60		1:200	Millipore

Choline Acetyltransferase	Ab178850		1:500	Abcam
LC3B (D11)	3868S	1:1000		Cell Signaling
Goat anti-Mouse IgG H&L Alexa Fluor® 488	ab150117		1:500	Abcam
Peroxidase Labeled Goat anti-Rabbit IgG H&L	PI-1000	1:10000		Vector
Peroxidase Labeled Goat anti-Mouse IgG H+L	PI-2000	1:10000		Vector
Biotynl Tyramide	6241			Tocris
Cy®3-Streptavidin	434315		1:300	Invitrogen
Cy®5-Streptavidin	434316		1:300	Invitrogen
Donkey anti-Rabbit IgG H+L Alexa Fluor® 594	A21207		1:500	Life Technologies
Goat anti-Rabbit IgG H&L Alexa Fluor® 488	A11008		1:500	Invitrogen
Donkey anti-Rabbit IgG H+L Alexa Fluor® 680	A10043		1:500	Life Technologies
Goat anti-Rat IgG H&L Alexa Fluor® 568	A11077		1:500	Invitrogen
Horse anti-Mouse Biotinylated IgG	BA-2000		1:2000	Vectastain
Goat anti-Mouse Biotin-SP-conjugated IgG H+L	115-065-068		1:2000	Jackson ImmunoResearch

Table 3 Antibodies used for WB, VIP, Co-Immunoprecipitation, and immunofluorescent staining.

2.1.2 PCR Primers

Gene	Primer Name	Sequence 5' to 3'
FMR1	Forward Primer	CCAACAAACCTGCCACAAAAG
	Reverse Primer	GCACACATTTGCCGTAAGTCTT
POLR2A	Forward Primer	GCGGAATGGAAGCACGTTAAT
	Reverse Primer	CCCAGCACAAAACACTCCTC
RPL22	Forward Primer	CACGAAGGAGGAGTGACTGG
	Reverse Primer	TGTGGCACACCACTGACATT
TBP	Forward Primer	AAAGAACGCTGTACTCAGTGTG
	Reverse Primer	CCCCGGTTGAGGGCTTTTA

Table 4 qRT-PCR primer sequences for FMR1 and housekeeping genes.

Gene	Primer Name	Sequence 5' to 3'
FMR1	Forward Primer	ATAGGATCCGGCCACCATGGAGGAGCTGGT
	Reverse Primer	GACTGCAGAATTCTTAGGGTACTCCATTCACCAGC
Backbone	Forward Primer	GTAAGAATTCGATATCAAGCTTATCGAT
	Reverse Primer	ATACTCGAGGATCCAATTCTTTGCCAAAATGATG

Table 5 Primer sequences for FMR1 plasmid cloning.

2.1.3 Human brain samples

Case #	Braak Stage	Age at Disease Onset (yrs)	Clinical Symptoms	Age at Death (yrs)	Sex	Tissue Fixation Time (days)
1	5	unknown	PD, D, Dep	82	f	83
2	6	51	PD, D	73	m	96
3	6	unknown	PD	86	f	71
4	3	n.a.	-	54	m	83
5	3	unknown	PD	58	m	103
6	4	80	D	86	f	111
7	6	65	PD	82	m	42
8	6	49	PD, D	69	m	68
9	6	65 (D), 73 (PD)	PD, D	77	m	112
10	6	54 (PD), 69 (D)	PD, D	74	m	100
11	6	73	PD	82	f	113
12	2	n.a.	-	60	m	14
13	1	unknown	Dys	66	m	41
22	1	unknown	RLS	90	f	377
23	1	unknown	RLS	95	f	352
24	1	n.a.	-	65	f	14
14	0	n.a.	-	70	m	68
15	0	n.a.	-	60	f	47
16	0	n.a.	-	59	f	110
18	0	n.a.	-	60	m	30
19	0	n.a.	-	82	m	63
20	0	n.a.	-	73	f	111
21	0	n.a.	-	66	f	90

Table 6 Information on PD and control brain tissue donors. All the brain slices were provided by the Munich Brain Bank, Department of Neuropathology, Ludwig Maximilian University Munich. The selected 24 cases were staged according to the presence of LBs in the dorsal motor nucleus of the vagus nerve (DMV), locus coeruleus, the SN and the cortex. The table shows the respective Braak stage, the disease onset age, symptoms, sex, death age, and fixation time for each case. PD: Parkinson's disease; D: Dementia; Dep: Depression; Dys: Dystonia; RLS: Restless Legs Syndrome, -: no neurological or psychiatric symptoms; n.a. = not applicable.

Case #	Age at Death	Sex	Neuropathological Diagnosis	Tissue Fixation Time (days)
30	73	f	PSP	4
31	62	f	PSP	<89
32	67	m	PSP	<30
33	81	m	PSP	<112
34	71	m	PSP	6
35	62	m	PSP	<66
36	62	f	PSP	<56
37	76	m	PSP	<106
38	74	m	PSP	9
39	71	m	PSP	<59
40	68	f	MSA	60
41	64	m	MSA	59
42	71	m	MSA	56
43	76	f	MSA	55
44	64	f	MSA	62
45	63	m	MSA	67
46	62	m	MSA	62
47	77	f	MSA	103
48	37	m	MSA	18

Table 7 Information on PSP and MSA brain tissue donors. All the brain slices were provided by the Munich Brain Bank, Department of Neuropathology, Ludwig Maximilian University Munich. The selected 24 cases were staged according to the presence of LBs in the dorsal motor nucleus of the vagus nerve (DMV), locus coeruleus, the SN and the cortex. The table shows the age, sex fixation time of all brain tissues. PSP: Progressive supranuclear palsy; MSA: Multiple System Atrophy.

2.2 Molecular biology

2.2.1 Plasmid cloning

AAV5-α-Syn and AAV5-GFP (both from BioFocus DPI, Saffron Walden, England) were described elsewhere (Hollerhage et al., 2014). The AAV5-FMRP vector plasmid was generated by cloning the mouse *Fmr1* gene from the plasmid pCMV-EGFP-FMR1 (a gift from D. Edbauer, German Center for Neurodegenerative Research, https://benchling.com/s/seq-gP4TDhOSjnm4IdV0NSkf) into the open reading frame of the AAV expression plasmid pAAV-CAG-GFP (Addgene # 37825, https://benchling.com/s/seq-LGOlDvNxKaeEecH6vPzA) by using *BamH1* and *EcoR1* restriction sites. The primer sequences used for cloning and amplification are specified in **Table 5**. The resulting plasmid was packed into an AAV5 at the viral vector core facility at the Technical University Munich (https://benchling.com/s/seq-UmUs71yDNZ8jb9SUuy4P).

2.2.2 Nucleic acids and polymerase chain reaction

RNA was extracted from cultured neurons by using the NucleoSpin™ RNA Kit (Macherey-Nagel, Düren, Germany). For quantitative real-time polymerase chain reaction (qRT-PCR), 1 µg RNA was converted into cDNA using the iScript™ single cDNA Synthesis Reaction Kit (Bio-Rad, Hercules, USA). The qRT-PCRs reactions were performed using SYBR Green™ Select qPCR Supermix (Life Technologies, Carlsbad, USA). All primers used for qRT-PCR were designed using OLIGO™ Primer analysis software (Vers. 6.41; Molecular Biology Insights) and are listed in **Table 4**. The qRT-PCR analysis was performed on a Step One Plus instrument (Thermo Fisher Scientific, Waltham, USA). Initial incubation at 10 min at 95 °C was followed by 40 cycles of 15 sec at 95 °C and 60 sec at 60 °C. The threshold cycle (CT) values were set within the exponential phase of the PCR. Data were normalized to three housekeeping genes: *POLR2A*, *RPL22* and *TBP* and the comparative normalized relative quantity (CNRQ) was used to calculate fold expression (qBase, Biogazelle, Zwijnaarde, Belgium). Gene regulation was statistically evaluated by two-tailed Student's t-test on the assumption of equal variances.

2.2.3 Small interfering RNA transfection

Small interfering RNAs (siRNAs) (Silencer Select siRNAs™, Thermo Fisher Scientific) targeting *FMR1* (# 4392420) or control siRNAs (# 4390843) were mixed with Lipofectamine RNAiMax™ in Optimum medium (Thermo Fisher Scientific) according to the manufacturer recommendations. The siRNAs were applied 24 h post-transduction with the AAVs at a final concentration of 10 nM and the cells were incubated with the siRNAs for the following 3 days until day 6 in vitro, which is when the cells were harvested for Western blot or used for electrophysiology.

2.2.4 Methylation sequencing

To detect the methylation status of FMRP in cultured neurons, the cells were differentiated and transduced with α-Syn- or GFP-expressing viruses as described above. On day 4 post-transduction, the cells were washed once and detached in PBS. After spinning down (300 x g for 5 min at 4°C), the pellet was collected and stored at -80°C. For DNA extraction, the QiaAmp™ DNA Mini Kit was used according to the manufacturer`s protocol (Qiagen, Hilden, Germany). The Infinium Human Methylation EPIC BeadChip™ (Illumina Inc., San Diego, USA) was used for methylation analysis. 200 ng of bisulfite-converted DNA was hybridized to the arrays according to the manufacturer´s instructions. Array data were evaluated, preprocessed and normalized using the ChAMP pipeline (V.2.8.1) (Morris et al., 2014; Tian et al., 2017) with minor modifications. Specifically, raw array data were uploaded to the ChAMP pipeline using the minfi option (Aryee et al., 2014). Probes with less than three measured beads or a detection P-value > 0.01, as well as probes interrogating CpGs that fall on or near to a SNP, were removed based on recommendations by Zhou et al. (Zhou, Laird, & Shen, 2017). Similarly, probes aligning to multiple locations as defined by Nordlund et al. were removed from the analysis (Nordlund et al., 2013). All samples had more than 99.3 % of valid probes; therefore no samples were removed from the analysis based on the quality of the data. Differences between probes due to InfI and InfII probe usage as well as between samples were normalized using BMIQ

(Teschendorff et al., 2013). Differential methylation was determined using the champ.dmp function using linear regression analysis based on the limma package (Smyth, 2004) adjusting P-values for multiple testing with Benjamini-Hochberg correction. Differentially methylated CpGs were considered significant at adjusted P-values < 0.05.

2.3 Cell biology

2.3.1 Cell culture

Proliferating LUHMES (Lund human mesencephalic) cells were maintained on Nunc™ Delta Surface tissue culture flasks (Thermo Fisher Scientific) coated with 100 µg/ml poly-L-lysine (Sigma-Aldrich, St. Louis, USA). The proliferation medium consisted of DMEM/F-12 (Sigma-Aldrich) with 1% N2 supplement (Life Technologies) and 0.04 µg/ml basic fibroblast growth factor (Peprotech). In order to differentiate the cells, they were cultured on Nunc™ Delta Surface multi-well tissue culture vessels (Thermo Fisher Scientific) in differentiation medium consisting of DMEM/F-12 supplemented with 1% N2, 1 µg/ml tetracycline, 0.5 µg/ml dibutyryl cyclic AMP (all Sigma-Aldrich), and 2 ng/mL glial cell-derived neurotrophic factor (R&D Systems, Minneapolis, USA). Unless stated otherwise, the cells were seeded at a density of 125,000 cells/cm^2 to achieve a final confluence of ~ 50%. Before plating the cells for differentiation, the tissue culture vessels were coated with 0.1 mg/mL poly-L-lysine (Sigma-Aldrich) at 4 °C overnight, washed three times with phosphate-buffered saline and coated again with 5 µg/ml bovine fibronectin (Sigma-Aldrich) at 37°C overnight. Proliferating and differentiated LUHMES cells were cultured at 37 °C with 5% CO_2 and water-saturated air. Unless otherwise stated, cells were differentiated for 6 days in differentiation medium into post-mitotic neurons with a dopaminergic phenotype (Bruch et al., 2017; Scholz et al., 2011). In order to achieve viral overexpression of α-Syn, GFP or FMRP, AAV5-α-Syn, AAV5-GFP or AAV5-FMRP were added 24 h after plating the cells in differentiation medium at an MOI (multiplicity of infection) of 2.15 as described previously (Hollerhage et al., 2014). After the virus application, the cells were incubated for another 24 h and rinsed thereafter three times with PBS before the fresh differentiation medium was added and the cells incubated for another 4 days before being used for experimentation. Rotenone (Sigma) was dissolved in DMSO; the cells were treated for 24 h with increasing concentrations of rotenone as described elsewhere (Bruch, Xu, De Andrade, & Hoglinger, 2014) and cell death was measured against DMSO by quantifying medium LDH. For

C1 (20μM) and Go6983 (5μM) treatment (both from Tocris, Wiesbaden-Nordenstadt, Germany), both compounds were dissolved in DMSO and the cells were incubated after virus washing.

2.3.2 Quantification of cell death by LDH release

Cell death in cultured dopaminergic neurons was quantified as described before (Hollerhage et al., 2014). In brief, lactate dehydrogenase (LDH) released into the culture medium was measured using the CytotoxOne Membrane Integrity Assay (Promega, Madison, USA) according to the manufacturer's instructions with a Fluostar Omega fluorescence reader (BMG Labtech, Ortenberg, Germany).

2.3.3 Subcellular fractionation

The protocol to separate distinct cellular compartments has been applied as described (Alisch et al., 2013) with minor modifications (**Figure 4**). In brief, differentiated LUHMES cells (at day 6 post-transduction) were trypsinized for 5 min., centrifuged at 1,200 x g for 7 min. and the cell pellet homogenized by using a pre-chilled Dounce homogenizer in a detergent-free lysis buffer containing the following: 10 mM Tris/HCl (pH 7.4), 10 mM NaCl, 0.5 mM $MgCl_2$, and EDTA-free protease inhibitor cocktail (Roche, Rotkreuz, Switzerland). The homogenates were centrifuged at 1,200 x g for 5 min. The pellets (P1) were re-suspended in 250 mM sucrose solution containing 10 mM $MgCl_2$ and centrifuged through an 880 mM sucrose cushion containing 0.5 mM $MgCl_2$ at 1,200 x g for 10 min in order to obtain the crude nuclear fraction. The supernatants (S1) were centrifuged at 1,200 x g for 5 min to obtain the crude cytosolic fraction (S2). This fraction was further subjected to a 16,000 x g centrifugation step for 10 min to isolate the heavy membrane pellet (S3) and the post-nuclear supernatants. The post-nuclear supernatants were then centrifuged for 90 min at 130,000 x g. The resulting supernatants contained the cytosolic fraction (S4); the pellets contained the light membrane fraction and polysomes (P4). The nuclei (P5) were resuspended and homogenized in the detergent-free lysis buffer by pipetting up and down and centrifuged through a cushion of 880 mM sucrose

containing 0.5 mM $MgCl_2$ at 2000 x g for 20 min to isolate the nucleolar pellets (P6) and post-nucleolar supernatant (S6). The post-nucleolar supernatants were finally centrifuged for 90 min at 130,000 x g. The resulting pellets contained the nuclear membranes and the supernatants of the nucleoplasmic fractions. All fractionation steps were carried out at 4 °C. The protein concentration of all fractions was determined by bicinchoninic acid (BCA) assay. The samples were mixed with loading buffer containing 10% beta-mercaptoethanol and 4x Laemmli sample buffer (Bio-Rad). In total, 14 µg of protein of each fraction was subjected to WB.

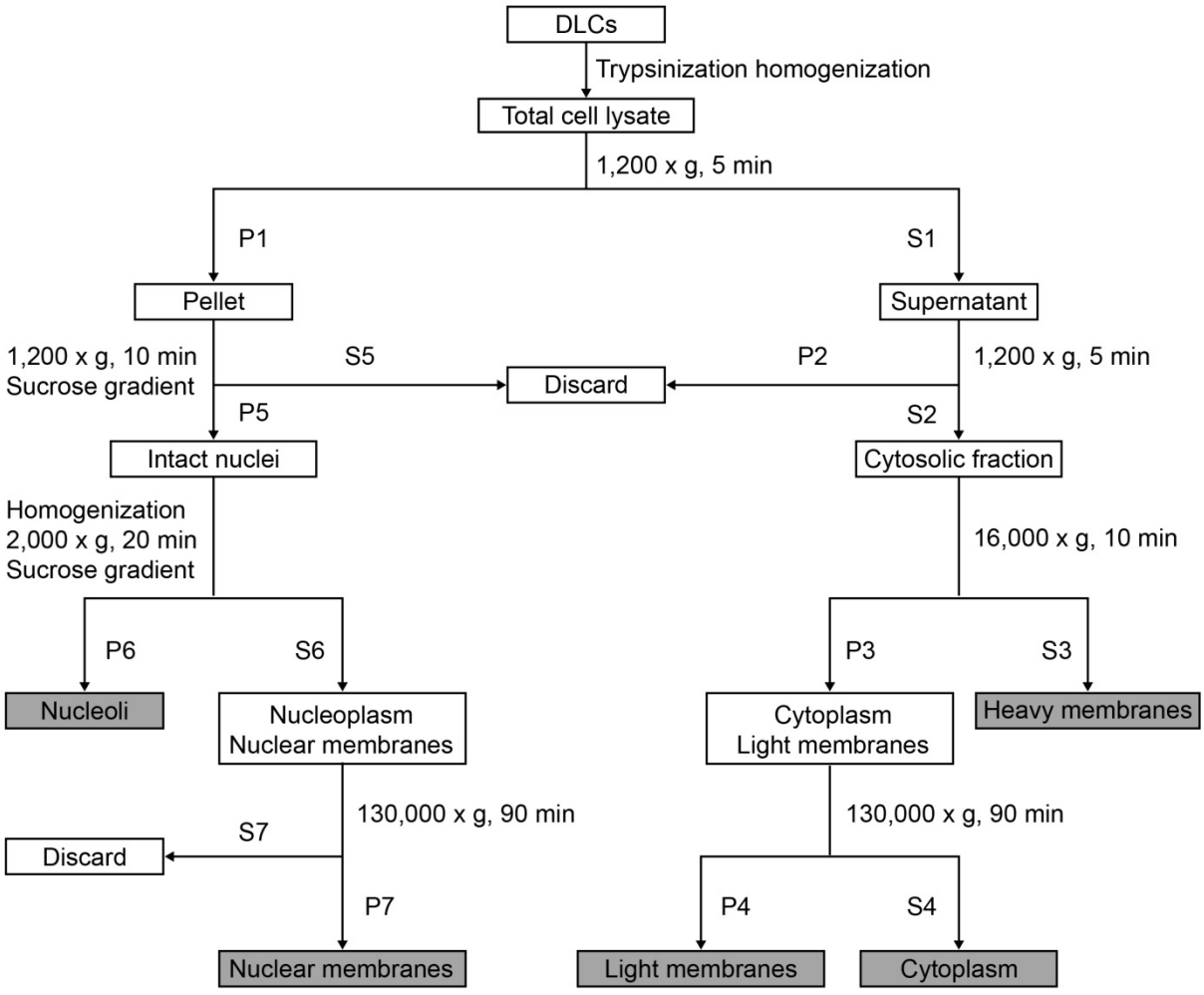

Figure 4 Schematic for subcellular fractionation of cultured human DA neurons.

2.3.4 Cell surface protein biotinylation

In order to label cell surface proteins, cultured neurons were rinsed twice with PBS and incubated with PBS containing 1 mg/ml Sulfo-NHS-SS-Biotin™ (Thermo Fisher Scientific) for 30 min. at room temperature. Excess biotin was quenched by washing with PBS containing 200 mM glycine. Cells were lysed in RIPA buffer (Sigma) including protease inhibitors for 30 min on ice and the lysates clarified by centrifugation (14,000 x g, 30 min, and 4 °C). Biotinylated proteins were precipitated by adding streptavidin-agarose beads (Thermo Fisher Scientific) and incubated 1 h at 4 °C. The streptavidin-agarose beads were washed three times and incubated for 1 h at 37 °C with 100 mM dithiothreitol and 4 x Laemmli sample buffer. Eluted proteins were separated by SDS–PAGE and subjected to Western blot.

2.3.5 Calcium imaging

Cells were plated onto 25 mm coverslips instead. Absolute cytosolic Ca^{2+} levels in cells were determined using the Ca^{2+}-sensitive fluorescent indicator Fura-2 AM (Molecular Probes / Invitrogen, Waltham, USA) and a Leica Live-Cell fluorescence microscope equipped with Fura-2 filters. Cells were loaded with Fura-2 in sterile-filtered Hepes-buffered saline (HBS: 20 mM Hepes, 150 mM NaCl, 5 mM KCl, 1 mM $CaCl_2$, 1 mM $MgCl_2$, 10 mM glucose, pH 7.4) containing 2.5 µM Fura-2 AM for 30 min at 37°C, 5% CO_2. The Fura-2-containing medium was replaced with fresh HBS without Fura-2 and incubated additionally for 30 min. The fluorescence was measured on the microscope using excitation wavelengths at 340 and 380 nm and emission at 510 nm. The ratio of the fluorescence signal at 510 nm upon excitation at 340 nm and excitation at 380 nm (FL_ex340/ FL_ex380) gives a relative Ca^{2+} estimate independent of cell morphology. The cytosolic Ca^{2+} levels in single cells were measured by placing a region of interest (ROI) outside the nucleus.

2.4 Protein biochemistry

2.4.1 Immunochemistry

2.4.1.1 Immunocytochemistry (ICC)

For immunocytochemistry (ICC), cultured neurons were fixed for 15 min. at room temperature in 4% paraformaldehyde, washed once for 10 min. in PBS and permeabilized for 1 min. with 0.125 % Triton X-100 in PBS. Unspecific antibody binding was blocked by 1% bovine serum albumin in PBS for 1 h followed by incubation with the respective primary antibody at 4 °C overnight. Unbound antibodies were removed by washing with PBS and the cells were incubated with Alexa Fluor-conjugated secondary antibodies for 1 h at room temperature. Unbound secondary antibodies were removed by washing in PBS and the cells were air-dried, covered with fluorescence mounting medium (Dako, Jena, Germany) and sealed under the cover glass.

2.4.1.2 Immunohistochemistry (IHC)

For immunohistochemistry (IHC) of mouse brain slices, the animals were anesthetized with a combination of midazolam, medetomidine, and fentanyl, and perfused transcardially with PBS for 2.5 min. and 4% paraformaldehyde for 10 min. The brains were quickly removed, immersed in 4% paraformaldehyde for 24 h at 4°C and in 30 % sucrose for another 24 h at 4°C. The post-fixed brains were frozen over liquid nitrogen, cut into 60 µm thick coronal sections with a cryotome (Leica, Wetzlar, Germany) and the free-floating sections were transferred into PBS. The tissue sections were blocked with 1% bovine serum albumin in PBS for 1 h and incubated with the respective primary antibody overnight at 4 °C. The brain slices were then washed 3 x 5 min. with PBS and incubated with fluorescent secondary antibodies for 1 h at room temperature and mounted in fluorescence mounting medium (Dako).

Human brain samples were obtained at autopsy with approval from Ludwig Maximilian University ethics commission from the Munich Brain Bank (Department of Neuropathology, Ludwig Maximilian University, Munich, Germany) and in accordance with the anatomical tissue

procurement guidelines. Human SNc sections were deparaffinized in xylene and rehydrated in graded alcohol series. The slices were incubated in 10 µg/ml proteinase K (Qiagen) in TE buffer (pH = 7.5) for 10 min at 37 °C in a humidified chamber. The sections were subsequently permeabilized by 0.125% Triton X-100 for 10 min. at room temperature and blocked in 5% normal serum (Vector Laboratories, Burlingame, USA) for 1 h at room temperature. Tissue sections were rinsed multiple times in PBS and incubated with anti-FMRP primary antibody (Novus Biologicals, Centennial, USA) overnight at 4 °C. Tissue sections were washed with PBS and incubated with anti-mouse biotinylated secondary antibodies (Vector Laboratories) for 2 h at room temperature. Sections were then washed with PBS and incubated with AB solution (ABC kit, Vector) for 1 h Biotinylated tyramide (10 µM), containing 0.005 % H_2O_2 was used for 20 min for signal amplification as described (G. Wang, Achim, Hamilton, Wiley, & Soontornniyomkij, 1999). FMRP immunoreactivity was visualized by Cy3-conjugated streptavidin (Invitrogen). After washing, sections were air-dried and mounted with a quick-hardening mounting medium (Fluka, Buchs, Switzerland). All mages were captured using a Leica SP5 confocal microscope and analyzed using Fiji software (http://fiji.sc/Fiji). Two pictures per case were used for analysis. One set of macros was created for semi-automated fluorescence analysis. In brief, the grey channel was selected manually for identifying the region of interest (ROI) of neuromelanin-positive cells, and then the red channel was selected manually to quantify the mean fluorescent intensity of FMRP from the same ROI. Meanwhile, the background fluorescent intensity of FMRP was acquired manually and subtract from cell fluorescent intensity for normalization. All antibodies used for ICC and IHC are listed in **Table 3**.

2.4.2 Western blot

For total protein lysates, cultured neurons were lysed in RIPA buffer incl. a protease and phosphatase inhibitor cocktail (Complete™ Protease Inhibitor Cocktail, PhosStop™ Phosphatase Inhibitor Cocktail, both Roche). The lysates were incubated for 30 min. on ice and

centrifuged at 5,000 x g for 15 min. at 4 °C, and the supernatant retrieved. The membrane protein fraction from cultured cells was isolated by using the Mem-PER™ Plus Membrane Protein Extraction Kit (Pierce Protein Biology, Waltham, USA) according to the manufacturer's instructions. Protein concentrations were determined using the BCA method (Thermo Fisher Scientific) and a spectrophotometer (NanoDrop™, Thermo Fisher Scientific). After adjusting protein concentrations, total and membrane protein lysates were heated to 75 °C for 15 min. in Laemmli sample buffer containing 10 % beta-mercaptoethanol. SDS-PAGE was performed by using Mini-Protean TGX™ Gels (Bio-Rad Laboratories) and a Tris-glycine-based running buffer. The protein was blotted onto polyvinylidene difluoride (PVDF) membranes (Bio-Rad) at 150 mA for 60 - 120 min on ice. The membranes were blocked with 5 % dry milk in TBST wash buffer (Tris-buffered saline containing 0.05 % Tween) for 1 h and incubated at 4 °C overnight under gentle shaking with the primary antibody in TBST / 5 % BSA (Cell Signaling Technology, Danvers, USA). The membranes were washed and incubated with the respective HRP-conjugated secondary antibody (Vector Labs) in TBST / 5 % milk for 1 h, followed by further washing and exposure to Clarity™ Western blot ECL Substrate (Bio-Rad) or ECL Prime™ (GE Healthcare, Chicago, USA). Chemiluminescence was detected with the LI-COR Odyssey Fc Imaging system and analyzed by Image Studio software (Licor, Lincoln, USA). Western blot images were further processed by ImageJ and the optical densities of target proteins were scaled to the respective loading controls for statistical analysis. Therefore, a normalized experimental signal (measured experimental signal/lane normalization factor) was used, where the lane normalization factor was calculated from the ratio between the measured signals of a housekeeping protein for each lane divided by the highest measured signal of housekeeping protein on the blot. All antibodies used for Western blot are listed in **Table 3**.

2.4.3 Puromycin incorporation

Overall protein synthesis was quantified as described previously (Schmidt, Clavarino, Ceppi, & Pierre, 2009). In brief, puromycin (10µg/ml) was added to the medium 30 min. prior to cell harvesting. Standard western-blot was then developed with the puromycin antibody.

2.4.4 Co-Immunoprecipitation

The FMRP antibody was immobilized on beads as recommended by the manufacturer (Pierce). Immobilized antibody beads were incubated in modified high salt cell lysates containing the following: 10 mM Hepes (pH = 7.4), 200 mM NaCl, 30 mM EDTA, 0.5% Triton X-100, 1 x Protease Inhibitor (Roche), and 1 x PhosStop Phosphatase Inhibitor Cocktail Tablets (Roche) at 4 °C overnight. Washing and elution steps were carried out as described in the protocol from the kit. The eluted sample was resolved by SDS-PAGE and analyzed by Western blotting.

2.4.5 Generation of α-Syn preformed fibrils and Silver Staining

Preformed fibrils (PFFs) were generated from monomeric α-Syn. Therefore, 50 µM α-Syn was dissolved in 50 mM Tris-HCl (pH = 7.0), 100 mM NaCl and 0.02% NaN_3. The solution was agitated on a shaker (500 rpm) for 6 days at 37 °C, aliquoted, snap-frozen and stored at -80°C until used. For silver staining, PFFs were diluted in Tris buffer and centrifuged at 100,000 x g for 1 h at 4°C and the Tris soluble fraction obtained from the supernatant. The pellet was resuspended in 5% SDS buffer and centrifuged again at 100,000 x g for 30 min at 25°C and the SDS soluble fraction obtained from the supernatant. The pellet was again resuspended in 8 M Urea in 5% SDS buffer to obtain the Urea soluble fraction. 5 µg of protein of each fraction was loaded on a Bis-Tris 4- 12% gradient gel and stained with silver according to the manufacturer's instructions (Pierce).

2.4.6 Thioflavin T Assay

Aggregation reaction samples were taken at DIV 0 and DIV 6, and mixed with a ThT solution with a final concentration of 25 μM thioflavine T (ThT; Sigma-Aldrich). Fluorescence was measured with a FLUOstar Omega plate reader.

2.5 Electrophysiology

2.5.1 Patch-clamp

Whole-cell patch-clamp electrophysiology in differentiated LUHMES cells was performed on a BX51 upright microscope (Olympus, Shinjuku, Japan). Experiments were performed at room temperature. Cells were grown in differentiation medium for 6-8 days on coverslips at a density of 75,000/cm^2. The coverslips were transferred to the recording chamber and immersed with extracellular solution (ECS) containing the following (in mM): 140 NaCl, 2.4 KCl, 10 Hepes, 10 glucose, 4 $CaCl_2$ and 4 $MgCl_2$, 320 mOsmol/L, pH 7.4); Patch electrodes were fabricated from filamented, thin-wall borosilicate glass (Sutter Instruments, Novato, USA) pulled on a P1000 pipette puller (Sutter). Pipette resistance was typically 3 - 6 MΩ when filled with the recording solution. The recording internal solution (pipette solution) consisted of (in mM): 40 KCl, 10 Hepes, 10 EGTA, 1 $MgCl_2$, 5 NaCl, 90 K-Gluconate, 15 creatine phosphate, and 5 U/ml phosphocreatine kinase, 315–320 mOsmol/L, pH 7.3. Somatic whole-cell patch-clamp recordings were obtained via an EPC-10 USB amplifier (Heka, Lambrecht/Pfalz, Germany) interfaced to a PC running PatchMaster (Heka). The signal was filtered at 1-4 kHz and digitized at 5–20 kHz and the data analyzed by Igor Pro (WaveMetrics, Lake Oswego, USA). For current-clamp recordings, the amplifier bridge circuit was adjusted to compensate for electrode resistance and monitored continuously throughout the experiment.

The following compounds were used in conjunction with electrophysiological measurements: isradipin, SNX-428, ω-agatoxin (ATX), ML-218, ω-conotoxin GIVA (OCTX), tetrodotoxin (TTX), tetraethyl ammonium (TEA) (all from Tocris) and diluted in ECS. NS309 (Sigma) was diluted in DMSO, cobalt (II) chloride (Sigma) was diluted in ECS.

2.5.2 Fast-scan cyclic voltammetry

Following isoflurane anesthesia, brains from mice were removed and coronal brain slices (400 µm) including the dorsal striatum were prepared in carbogen-bubbled, cold high-sucrose solution (in mM: Sucrose 194, NaCl 30, KCl 4.5, $MgCl_2$ 1, $NaHCO_3$ 26, NaH_2PO_4 1.2, Glucose

10), as described previously (Sgobio et al., 2014). Slices from the left hemisphere were stored separately from the right hemisphere and kept at 32 ˚C for 30 min and then at room temperature before the recording session in oxygenated ECS containing the following (in mM): NaCl 126, KCl 2.5, NaH_2PO_4 1.2, $CaCl_2$ 2.4, $MgCl_2$ 1.2, $NaHCO_3$ 25, glucose 11, Hepes 20, L-ascorbic acid 0.4. For voltammetry recordings, the slices were transferred into a recording chamber and perfused at a rate of 1.5 ml/min with ECS at 32 °C. Cylindrical carbon-fiber microelectrodes (75 – 125 µm exposed fiber) were prepared with T650 fibers (Goodfellow, Huntingdon, UK) and inserted into a glass pipette containing a 2 M KCl solution. The sensitivity of carbon-fiber electrodes was calculated exposing them to different standard concentrations of DA (1, 5 and 10 µM) before and after the recording sessions. The carbon-fiber electrode was held at - 0.4 V. Every 100 ms, the potential was ramped to + 1.2 V and back at 400 V / s. DA release was evoked every 3 min. by a rectangular stimulus (400 µA, 1.2 ms, monophasic) generated by a DS3 Constant Current Stimulator (Digitimer, Welwyn Garden, UK) and delivered by a bipolar electrode placed in the corpus callosum. Data were collected using the DEMON software (Yorgason, Espana, & Jones, 2011). Ten cyclic voltammograms of charging currents were recorded as background before stimulation, and the average was subtracted from data collected during and after stimulation. DA peak amplitude responses were obtained from nine to twelve recordings across the rostro caudal extent of the dorsolateral striatum in each hemisphere and averaged for every single mouse. Input / output function (I/O) curves were generated by plotting the peak amplitude of DA release as a function of the stimulus current over a range of increasing stimulus intensities.

2.6 Animal related methods

2.6.1 Animal surgery

All animal procedures were performed according to the EU Council Directive 2010/63/EU, the Guide for the Care and Use of Laboratory Animals (National Research Council 2011), and the guidelines of the local institutional committee. The experiments were approved by the local authority. Overexpression of α-Syn and LUC was achieved by stereotaxic injection of α-Syn- or LUC-expressing adeno-associated viruses (AAVs). Premade AAV5-α-Syn and AAV5-LUC viruses, which express α-Syn or LUC under the CBA promoter, were obtained from the viral vector core facility at the University of North Carolina, USA through the Michael J. Fox Foundation (Perez-Villalba et al., 2018; Volpicelli-Daley, Kirik, Stoyka, Standaert, & Harms, 2016). Either C57BL/6J or *Fmr1* KO mice (B6.129P2-Fmr1tm1Cgr/J, Stock No.: 003025) were purchased from The Jackson Laboratory and housed under standard conditions with access to food and water ad libitum. 8-10 wks. old female animals were anesthetized with midazolam, medetomidine and fentanyl, and given eye ointment. Thereafter, the mice were placed in a stereotaxic head frame (Stoelting) and the dorsal scull was disinfected with a povidone iodine scrub. Analgesics consisting of buprenorphine (0.1 mg/kg) and carprofen (4 mg/kg) were injected. The skin was opened by a 1 cm long midline incision and a 2-mm wide borehole was drilled on either side. Subsequently, 2 x 10^{12} viral particles of AAV5-α-Syn, AAV5-LUC or AAV5-FMPR in 2 µl PBS were injected at a rate of 0.2 µl/min with a 33-gauge needle on a Hamilton syringe at the following coordinates relative to bregma: anterior -3.16 mm, lateral +1.50 mm, ventral -4.50 mm. The needle was left in place for an additional 5 min before being retracted. Subsequent to surgery, the mice were returned to their home cages, housed singly, allowed unrestricted movement and access to food and water ad libitum, and put on an analgesic regimen of buprenorphine (0.1 mg/kg) and carprofen (4 mg/kg) for 3 days. Thereafter, the animals were housed under standard housing conditions with 1 mice/cage until sacrifice.

2.6.2 Stereological cell counting

A series of 60 µm thick, coronal midbrain sections were stained with tyrosine hydroxylase (TH) as described above. Every fourth section between - 2.92 mm and - 3.88 mm relative to bregma was used for stereological analysis. The slices were examined and pictures taken under a 10 x objective of an inverted microscope (Leica). The number of TH-positive neurons in each SNc was quantified using the optical fractionator function of Stereo Investigator™ 8, an unbiased stereological procedure (MicroBrightField Inc., Williston, USA). The sampling scheme was designed to maintain a coefficient of error (CE) of less than 10 %.

2.7 Statistical analysis

Prism 7 (GraphPad Software) was used for statistical analysis and for creating line and bar graphs. Two datasets were compared by t-tests. When there were more than two datasets with two variables, data were generally compared by two-way ANOVAs with Tukey's or Dunnett's post hoc test, unless indicated otherwise. Assays with one variable were compared by oneway ANOVAs with Tukey's or LSD post hoc test. Data are shown as mean ± standard error of the mean (SEM). $P < 0.05$ was considered to be significant.

3 Results

Most of the following results have been published recently in *Acta Neuropathologica* (Tan et al., 2019). The authorization letter for using the published figures and tables is attached below in the authorization section. The first author of the manuscript mentioned above (Yi Tan) participated in almost all the following work individually or together with collaborators under the supervision of Dr. Thomas Köglsperger and Prof. Günter U. Höglinger. Dr. Thomas Köglsperger contributed the cell electrophysiology characterization data as the preliminary driving force of the project.

3.1 α-Syn Overexpression activates N-type calcium channel in transduced Lund Human Mesencephalic (LUHMES) cells

α-Syn-mediated neurodegeneration is associated with a deregulated calcium homeostasis. (Rcom-H'cheo-Gauthier, Goodwin, & Pountney, 2014). In order to investigate the effect of α-Syn on neuronal calcium channels, we began by characterizing suitable cell culture model systems to study DA neuron physiology in vitro. The immortalized LUHMES cell line exhibits a neuronal phenotype upon differentiation (Scholz et al., 2011). Moreover, differentiated LUHMES cells exhibit a dose-dependent neuronal death in response to viral α-Syn overexpression (Fussi et al., 2018; Hollerhage et al., 2014). Collectively, these studies suggested them as a potential model for electrophysiological examination of DA neurons.

3.1.1 Electrophysiological characteristics of LUHMES cells

The first step in this section was to measure the action potential (AP) after 6 days of differentiation. **Figure 5** and **6** indicate typical spontaneous and induced APs in differentiated LUHMES cells.

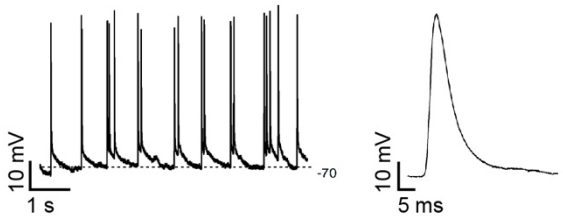

Figure 5 Spontaneous APs in differentiated LUHMES cells. After differentiation, LUHMES cells displayed spontaneous APs under current clamp.

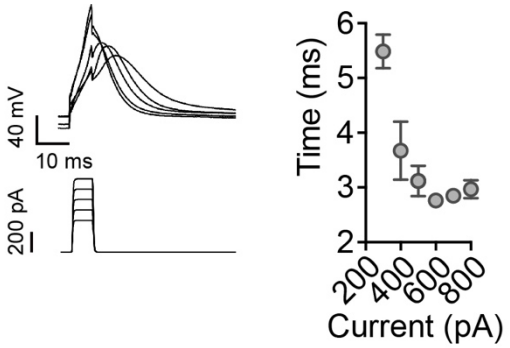

Figure 6 Induced APs in differentiated LUHMES cells. GFP-transduced LUHMES cells exhibited typical induced APs after current injection (left). The half-maximal AP amplitude duration time ($APt_{1/2}$) related to different current injection (right) (n=15). Data are shown as means ± SEM.

The second major electrophysiological feature was a prominent hyperpolarization-activated inward current presented in **Figure 7**.

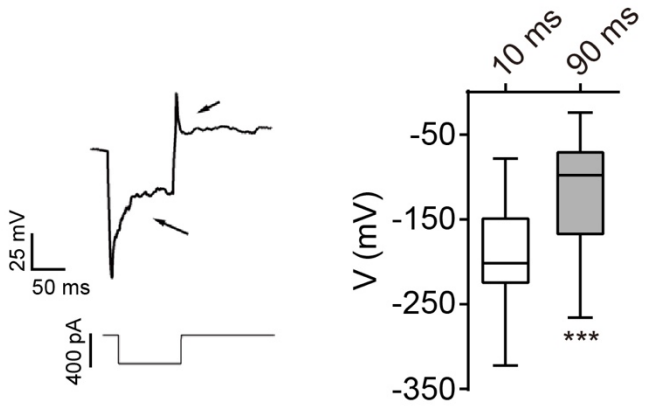

Figure 7 Differentiated LUHMES cells display a prominent hyperpolarization-activated inward current. After 100 ms-hyperpolarizing current injection, the membrane potential was becoming significantly positive at 90 ms than at 10 ms, indicating a hyperpolarization-activated inward

current in LUHMES cells upon differentiation (n=10). For comparison of the means, two-tailed unpaired t-test was used. ***P < 0.001. Data are shown as means ± SEM.

Additionally, we observed an SK-type potassium channel induced outward current in **Figure 8** and SK-type channel-mediated after hyperpolarization (AHP) which can be blocked by apamin and enhanced by the SK channel activator NS309 in **Figure 9**.

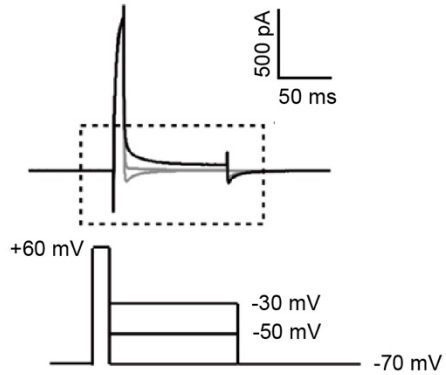

Figure 8 Differentiated LUHMES cells exhibit SK-type channel induced outward current. Differentiated LUHMES cells exhibited SK-channel-mediated outward currents in response to a tail current protocol.

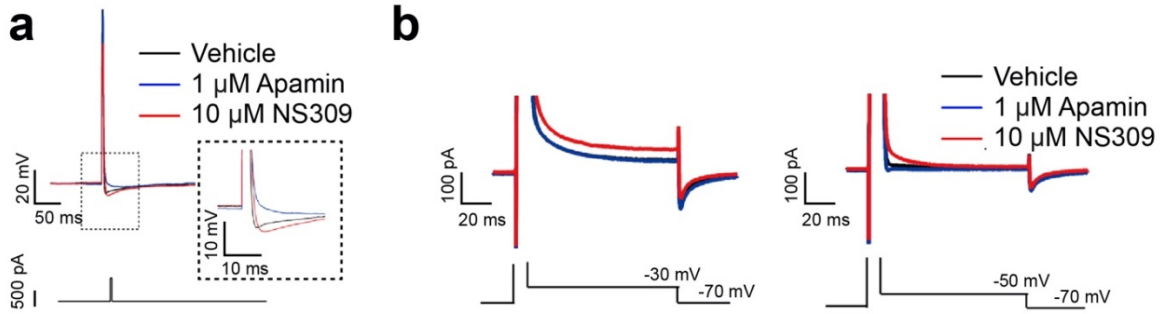

Figure 9 After-hyperpolarization (AHP) induced by SK-type channel was blocked by apamin or elevated by SK-channel activator NS309. (**a**) After current injection, cells exhibited an AHP which can be elevated by the SK-channel activator NS309 (10 µM) and blocked by SK-channel blocker apamin (1 µM) (n = 15). (**b**) Under voltage clamp, cells showed an enhanced outward current by NS309 and a reduced current in response to apamin (n=15).

Together, the evidence above suggests that LUHMES cells exhibit typical electrophysiological features of A9 SNpc neurons, making them a suitable model for further

investigation. Prior to commencing the study of neuronal excitability and calcium influx, we inspected the ion channel activity under voltage clamp. As shown in **Figure 10**, rectangular voltage steps in LUHMES cells led to fast-inactivating Na^+ inward currents and sustained K^+ outward currents which can be respectively blocked by TTX, and TEA with Cesium internal solution.

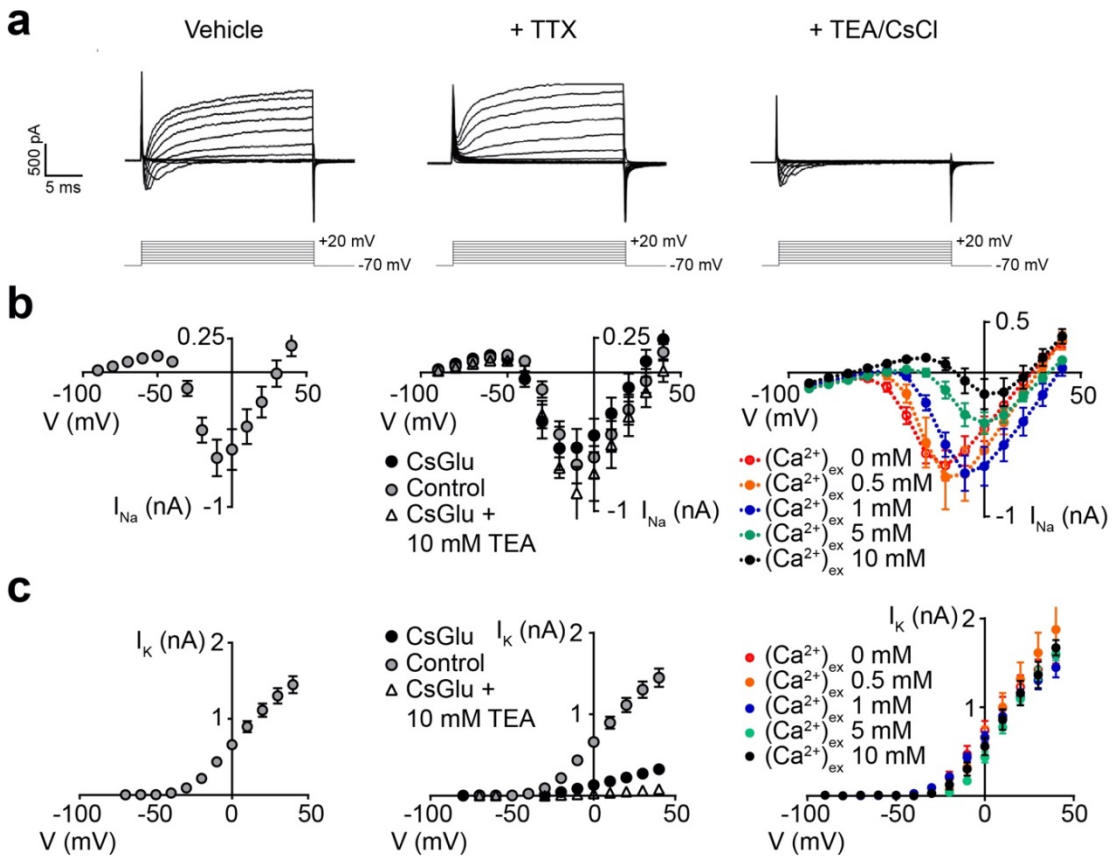

Figure 10 Fast-inactivating Na^+ inward currents and sustained K^+ outward currents in differentiated LUHMES cells which can be blocked, respectively, by tetrodotoxin (TTX) and tetraethyl ammonium (TEA). (**a**) Traces indicating LUHMES cells to have voltage-activated fast-inactivating inward Na^+ and sustained K^+ channels (left) which can be blocked by TTX (1 µM) (middle) and TEA (10 mM) with cesium-based internal pipette solution(right). (**b**) I-V graphs illustrating voltage-activated inward currents in LUHMES cells that can be modulated by the extracellular calcium concentration, thus indicating that the inward currents are driven by Na^+ channels. (**c**) I-V graphs illustrating voltage-activated K^+ outward currents which are efficiently blocked by TEA (n=25). Data are shown as means ± SEM. $(Ca^{2+})_{ex}$ = extracellular calcium concentration.

3.1.2 α-Syn transduced LUHMES cells exhibit activated calcium channel currents

After these initial electrophysiological experiments, cells were transduced with α-Syn adenovirus or GFP adenovirus at the same multiplicity of infection (MOI = 2.15). By comparing cells under these two different conditions, we found that APs in α-Syn transduced cells were followed by a prominent afterdepolarization (ADP) that was absent in GFP transduced neurons (**Figure 11**).

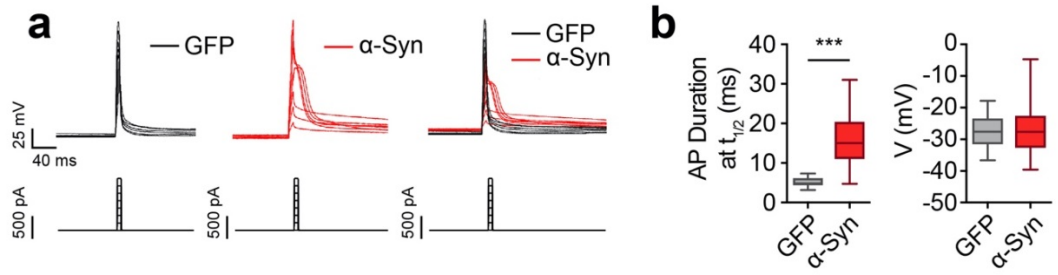

Figure 11 Induced APs in GFP or α-Syn transduced LUHMES cells. (**a**) Induced APs in α-Syn transduced LUHMES cells displayed a brief ADP which was missing in GFP transduced cells. (**b**) Quantification of $APt_{1/2}$ in GFP and α-Syn transduced LUHMES (left) and the corresponding voltage when the $APt_{1/2}$ was calculated (right) (n=15). For comparison of the means, two-tailed unpaired t-test was used in (**b**). ***P < 0.001. Data are shown as means ± SEM.

Moreover, unlike the GFP transduced cells, **Figure 12** indicates an additional slow-inactivating inward current after the fast Na^+ inward current in α-Syn transduced cells.

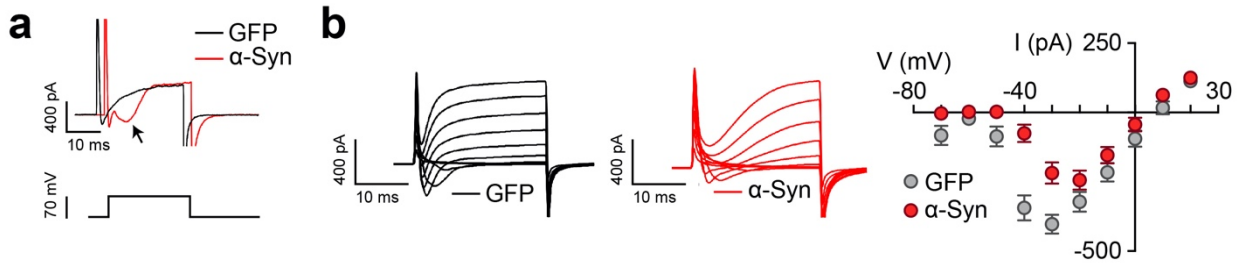

Figure 12 α-Syn transduced cells show additional slow-inactivating Na^+ inward current. (**a**) Rectangular voltage steps led to a brief membrane depolarization with an additional non-sodium inward current in α-Syn transduced LUHMES cells. (**b**) Averaged current traces (n = 10) of both α-Syn and GFP transduced LUHMES under rectangular voltage step, and corresponding I-V graph. Data are shown as means ± SEM.

To better understand the regulations of these conductances, cultured cells were treated with 1 µM TTX and 10 mM TEA for blocking Na^+ and K^+ channels. In addition, potassium chloride has been replaced with cesium chloride in the pipette solution. As can be seen from **Figure 13**, it is apparent that APs in α-Syn transduced cells showed a long plateau phase which is otherwise missing in GFP transduced cells.

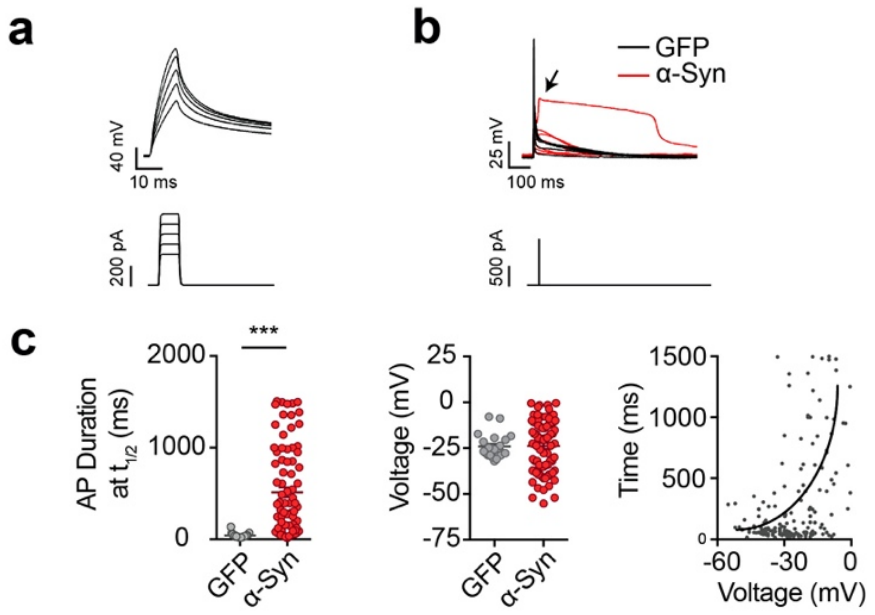

Figure 13 α-Syn transduced LUHMES cells present sustained induced Aps. (**a**) Rectangular current puls injection led to a capacitive membrane potential deflection in LUHMES cells treated with TTX, TEA and cesium-based internal solution. (**b**) Different from GFP transduced cells, α-Syn transduced cells exhibited sustained APs with a long plateau phase after current injection under the same condition as in (**a**). (**c**) Quantification of $APt_{1/2}$ (left), VAP (middle) and the duration of the APs (right) (n = 20). For comparison of the means, a two-tailed unpaired t-test was used. ***P < 0.001. Data are shown as means ± SEM.

When using voltage-clamp, α-Syn transduced cells, in particular, displayed high-voltage activated inward currents as displayed in **Figure 14,** which were consistent with previous current-clamp studies.

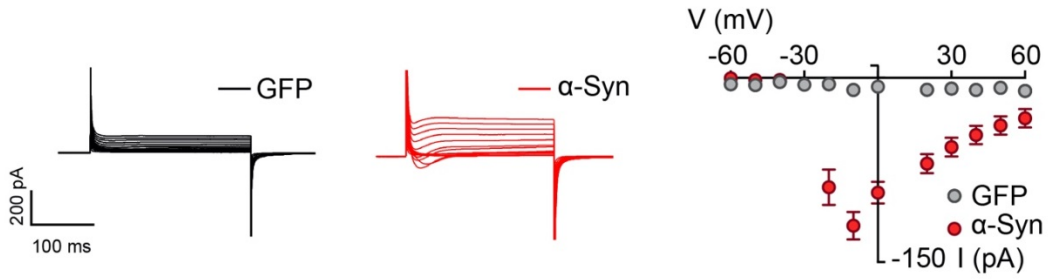

Figure 14 α-Syn transduced cells display activated inward currents. When blocking both Na^+ and K^+ channels, α-Syn transduced cells exhibited an additional voltage activated inward currents. Corresponding I/V graph with leak current compensation (n = 15). α-Syn transduced cells also exhibited increased leak current. Data are shown as means ± SEM.

3.1.3 α-Syn overexpression enhances N-type calcium channel-mediated calcium currents

Finally, we aimed to identify the specific type of calcium channels activated in the α-Syn transduced cells. By applying different VGCC-specific antagonists, our data revealed that activated inward currents were efficiently blocked by N-type calcium channel specific antagonists, including cobalt-II-chloride and ω-conotoxin GIVA, at 500 µM and 100 nM, respectively. No significant reduction in currents was found when applying other VGCC-specific antagonists (**Figure 15**).

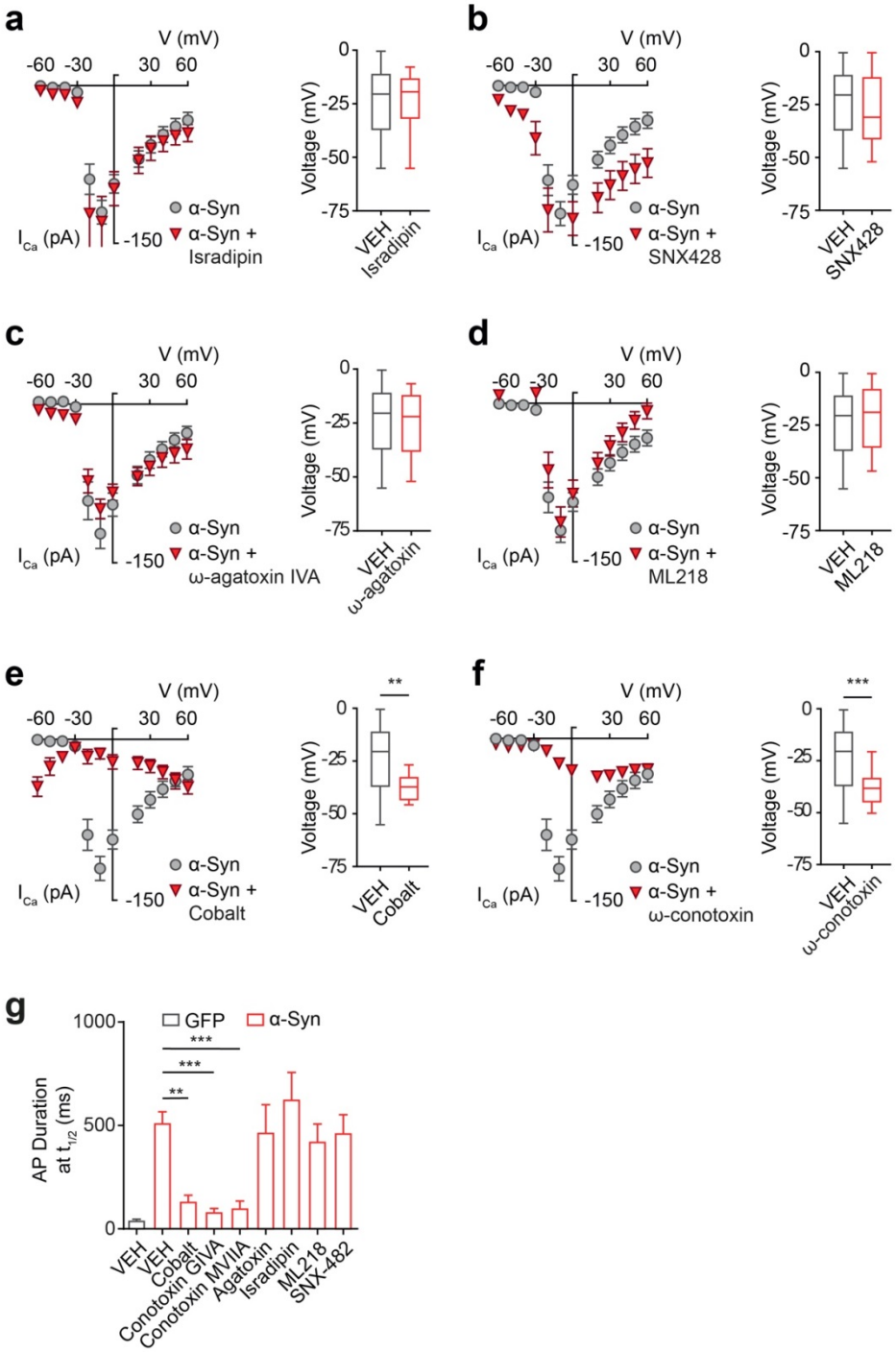

Figure 15 α-Syn transduced LUHMES cells show elevated N-type calcium currents. (**a-f**) I/V graphs of α-Syn transduced LUHMES cells and cells after the treatment with different calcium channel antagonists (in brackets, the blocked channel type is specified) (n=15/condition), including isradipine (L-type), SNX 428 (R-type), ω-agatoxin (P-type), ML-218 (T-type), cobalt-II-chloride (VGCCs), conotoxin GIVA (N-type). (**g**) Quantification of $APt_{1/2}$ for different conditions suggesting cobalt-II-chloride, ω-conotoxin GIVA and MVIIA can inhibit activated inward currents in α-Syn transduced LUHMES cells. Data were analyzed by one-way ANOVA followed by

Tukey's post hoc test in (**g**). ***P < 0.001, **P < 0.01. Box and whiskers representing min to max values ± SEM.

To confirm the electrophysiology results, Fura-2-based calcium imaging was applied. Compared to the GFP transduced cells, α-Syn overexpression aggravated the calcium influx in response to 30 mM potassium chloride (KCl) excitation (**Figure 16**). Pre-incubation with ω-conotoxin in α-Syn transduced cells normalized the calcium influx to the GFP control level.

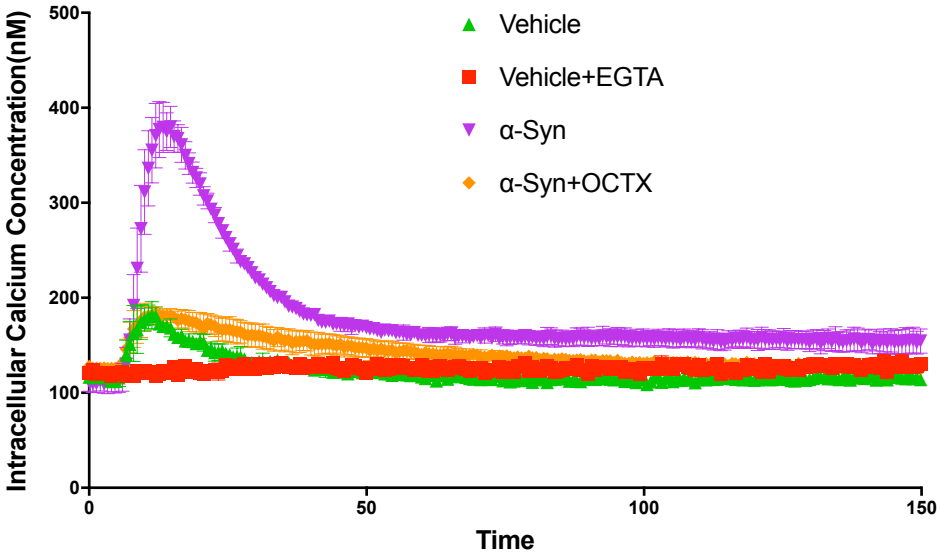

Figure 16 Inhibition of calcium influx by ω-conotoxin GIVA (OCTX) demonstrate the activation of N-type calcium channel in α-Syn transduced LUHMES cells. GFP transduced cells exhibited a small amount of calcium influx after depolarization with 30 mM KCl. The average traces returned to base level at 50 s. An elevated calcium influx was observed in α-Syn transduced cells under the same condition. Treatment with ω-conotoxin abolished the activated N-type calcium channel-mediated calcium influx (n=6). Data are shown as means ± SEM. OCTX: ω-conotoxin GIVA.

Overall, the results in this chapter indicate that α-Syn overexpression in LUHMES cells leads to enhanced N-type calcium channel-mediated inward calcium currents.

3.2 Overexpression of α-Syn leads to a decrease expression of FMRP in transduced LUHMES cells

As described in the previous chapter, it is clear that α-Syn overexpression activates the N-type calcium channel, but what remains unclear is how α-Syn regulates N-type calcium channel activity. N-type calcium channels localize predominantly in the presynaptic membrane where neurotransmission and synaptogenesis are extraordinarily active. Results from earlier research suggest a consistent and solid association between synaptogenesis and synaptic protein synthesis (Dictenberg et al., 2008). The regulation of synaptic protein synthesis has been shown to be related to several signaling pathways (Hafner, Donlin-Asp, Leitch, Herzog, & Schuman, 2019; Niere & Raab-Graham, 2017; Zhang et al., 2015). Among these pathways, the postsynaptic FMRP-controlled pathway appears to be closely linked with calcium channels (Castagnola et al., 2018; Danesi et al., 2018). In particular, previous data has demonstrated that the N-type calcium channels have a direct interaction with FMRP and that FMRP acts as a negative regulator of N-type calcium channels. Therefore, it is intriguing to examine whether FMRP is affected by α-Syn overexpression.

3.2.1 WB result displays reduced FMRP intensity in α-Syn transduced LUHMES cells

In order to test the conceivable hypothesis that α-Syn regulates N-type calcium channels through FMRP, we investigated FMRP abundance in α-Syn transduced LUHMES cells 6 days post transduction (DPT). As demonstrated in **Figure 17** and **Figure 18**, FMRP shows a clear trend of reduction in response to the overexpression of wildtype, mutant A53T and A30P α-Syn as compared to GFP transduced neurons. Conversely, treatment of α-Syn preformed fibrils (PFFs) did not result in an additional effect on FMRP (**Figure 19** and **Figure 20**).

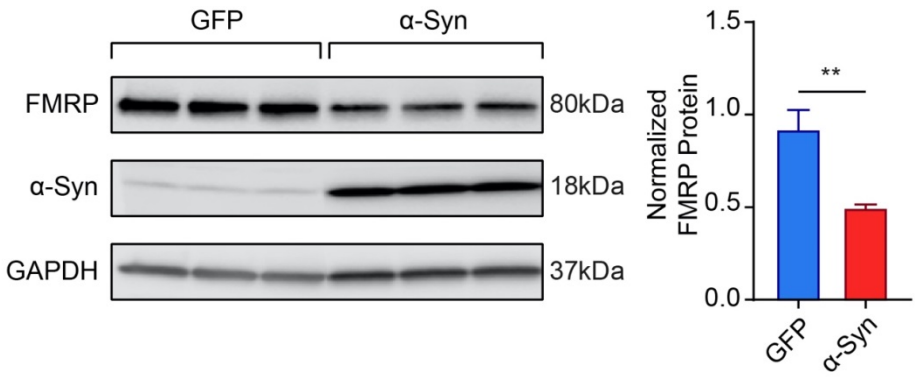

Figure 17 α-Syn transduced LUHMES cells show downregulated FMRP. WB result and quantification (n = 9) demonstrating a significant reduction of FMRP in α-Syn transduced LUHMES cells, as compared to GFP transduced cells. For comparison of the means, two-tailed unpaired t-test was used. **P < 0.01. Data are shown as means ± SEM.

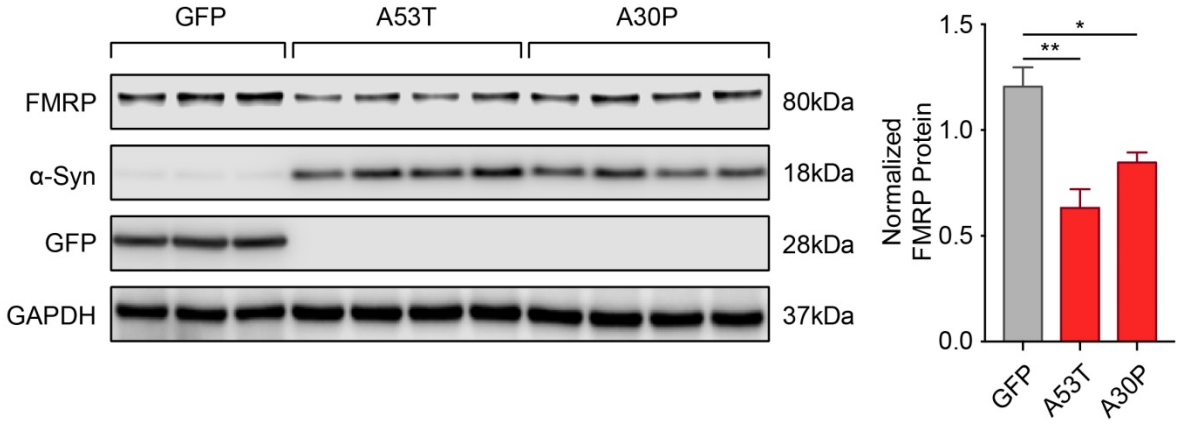

Figure 18 Overexpression of mutant α-Syn (A53T, A30P) decrease FMRP expression. WB result and quantification (n = 4) demonstrating a significant reduction of FMRP in A53T and A30P α-Syn transduced LUHMES cells, as compared to GFP transduced cells. For comparison of the means, two-tailed unpaired t-test was used. **P < 0.01, *P < 0.05. Data are shown as means ± SEM.

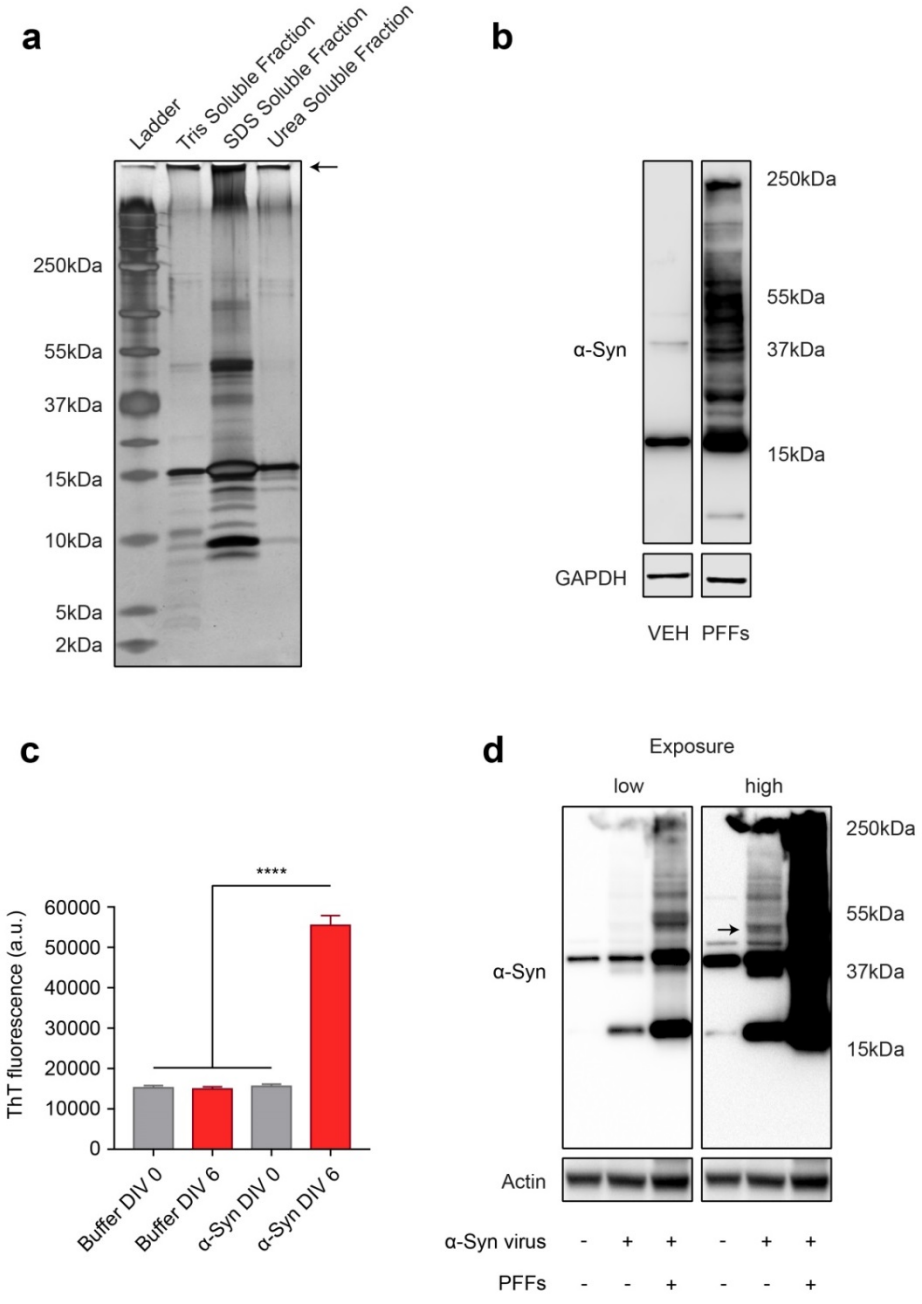

Figure 19 Characterization of α-Syn preformed fibrils. (**a**) Representative silver staining shows different α-Syn molecular fractions in PFF-treated neurons after elution by Tris, sodium dodecylsulfate (SDS) and urea. By using different solvents, different α-Syn fractions at different molecular weight emerged; the insoluble fraction is indicated as arrow. (**b**) WB result shows the existence of α-Syn at different molecular weights after the treatment of α-Syn PFFs (150 nM, 4 days). (**c**) Increased Thioflavin T fluorescence indicates the generation of beta sheet-rich fibrillary material after the treatment with α-Syn PFFs (n = 12). (**d**) α-Syn overexpression leads

to the generation of a well-defined 37 kDa oligomeric α-Syn fractions (middle lane). Treatment of PFFs additionally increased the amount of all α-Syn species in LUHMES cells. For comparison of the means, one-way ANOVA with Tukey's post hoc test was used in (**c**). ****P < 0.0001. Data are shown as means ± SEM.

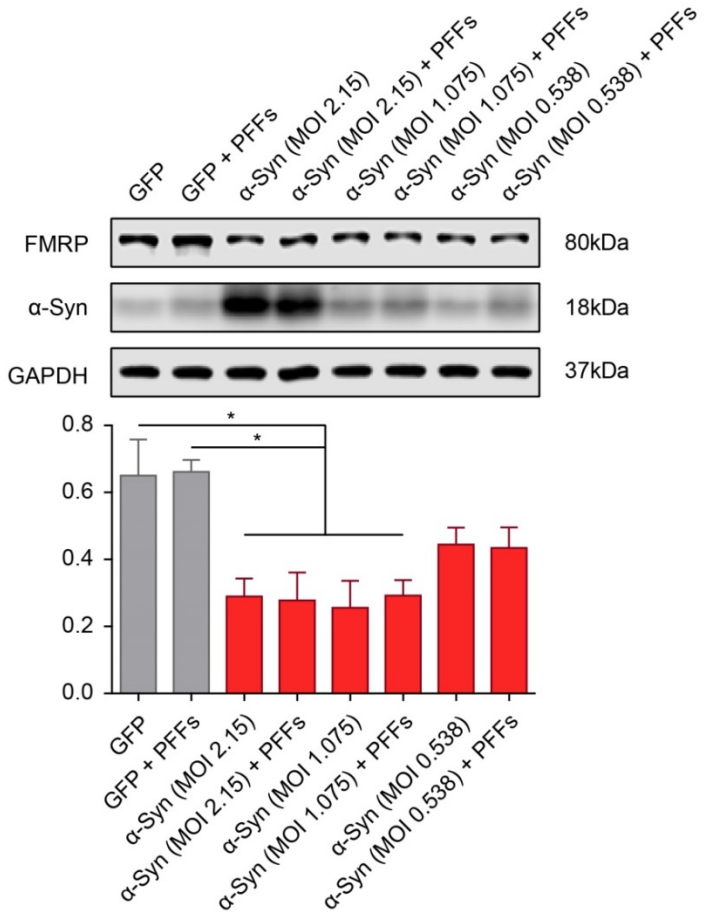

Figure 20 α-Syn PFFs co-application doesn't further decrease FMRP expression. WB and bar graph showing the FMRP expression after α-Syn PFFs co-application in LUHMES cells. α-Syn overexpression leads to the downregulation of FMRP in a dose-dependent manner (MOI: multiplicity of infection). High MOI (2.15) had a stronger effect on FMRP expression than low MOI (0.538). α-Syn PFFs so-application (150 nM) had no additional effect on FMRP expression (n = 3). For comparison of the means, one-way ANOVA with Tukey's post hoc test was used. *P < 0.05. Data are shown as means ± SEM.

3.2.2 Immunofluorescent result shows decreased FMRP abundance in α-Syn transduced LUHMES cells

Further immunofluorescent staining confirmed the reduced fluorescent FMRP intensity in α-Syn transduced cells (**Figure 21**). Among the α-Syn positive neurons, cells with a weak α-Syn

signal (arrowhead) also exhibited a higher FMRP intensity than cells with strong α-Syn intensity (arrow), thus demonstrating a negative correlation between FMRP and α-Syn.

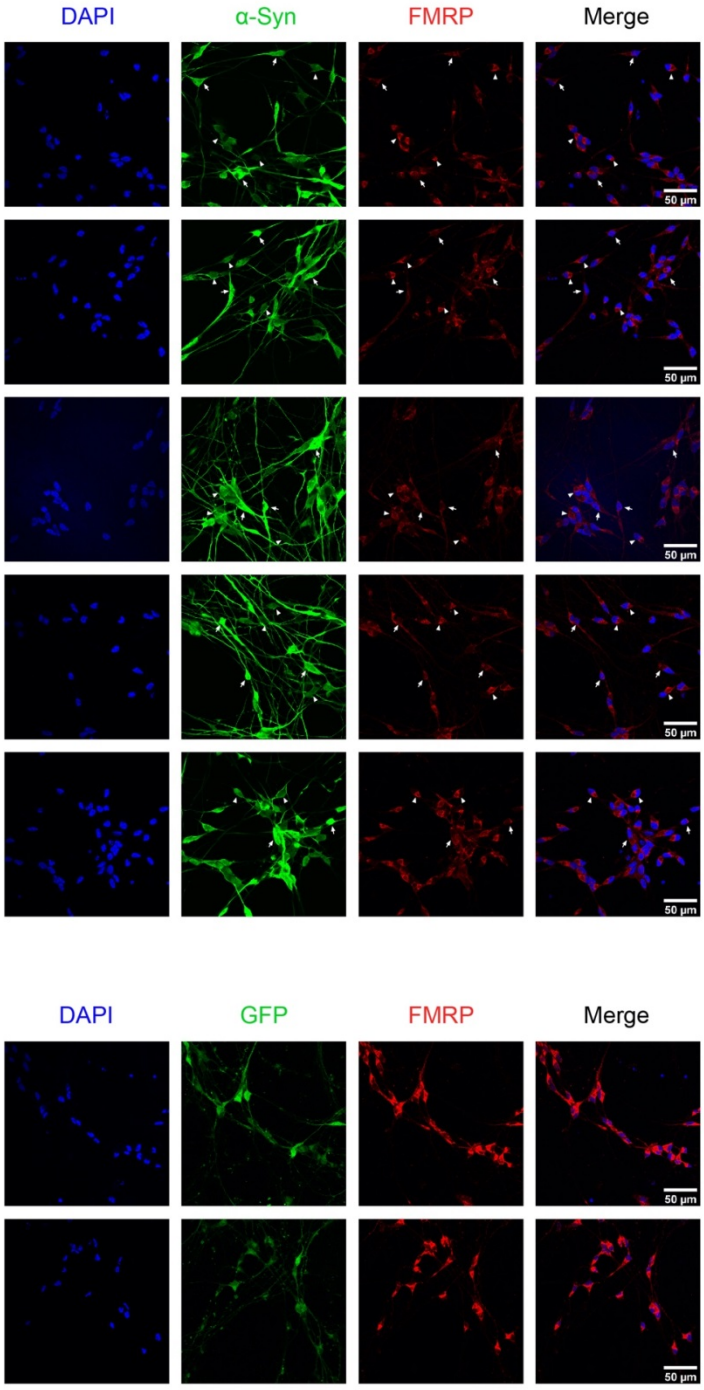

Figure 21 FMRP signal is significantly decreased in α-Syn transduced cells. Immunostaining results demonstrating a reduced FMRP intensity in α-Syn transduced neurons as compared to GFP transduced cells. In α-Syn transduced neurons, cells expressing a higher amount of α-Syn (arrow) also exhibited a lower FMRP intensity than cells expressing less α-Syn (arrowheads).

3.2.3 FMRP decreases in both cytoplasmatic and nuclear compartments in response to α-Syn transduction in LUHMES cells.

When we investigated the distribution of FMRP in LUHMES cells, we found that FMRP localizes to the perinuclear region, which is consistent with its role as a mRNA binding protein (**Figure 22**)(Richter et al., 2015), while punctate FMRP-positive structures in the nucleus potentially indicates its presence in Cajal bodies (Dury et al., 2013). In α-Syn transduced cells, we found FMRP to be diminished in both compartments.

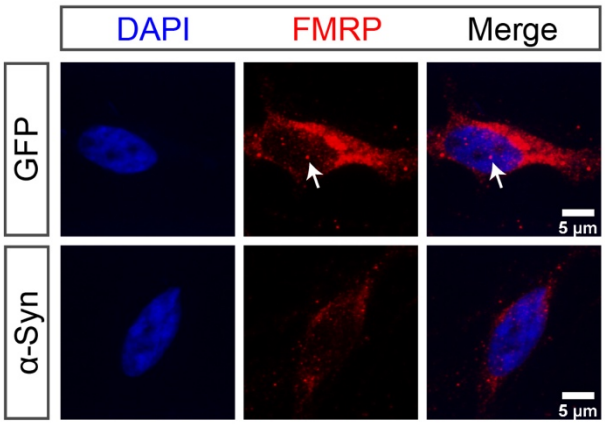

Figure 22 High magnification of FMRP signal in α-Syn or GFP transduced cells. High resolution FMRP immunostaining images of GFP and α-Syn transduced cells at 6 DPT showing the absence of perinuclear (arrow) FMRP-positive structures and an overall reduction of FMRP intensity in α-Syn transduced LUHMES cells.

To further characterize the distribution of FMRP in LUHMES cells, we separated different compartments of LUHMES cells through biochemical fractionation (**Figure 4**, method section 2.3.3). Our WB results (**Figure 23**) suggest that α-Syn transduced cells exhibit a reduced FMRP signal in the light and heavy membrane fraction, and the nuclear lysate, thus confirming the downregulation of FMRP in both compartments after α-Syn overexpression.

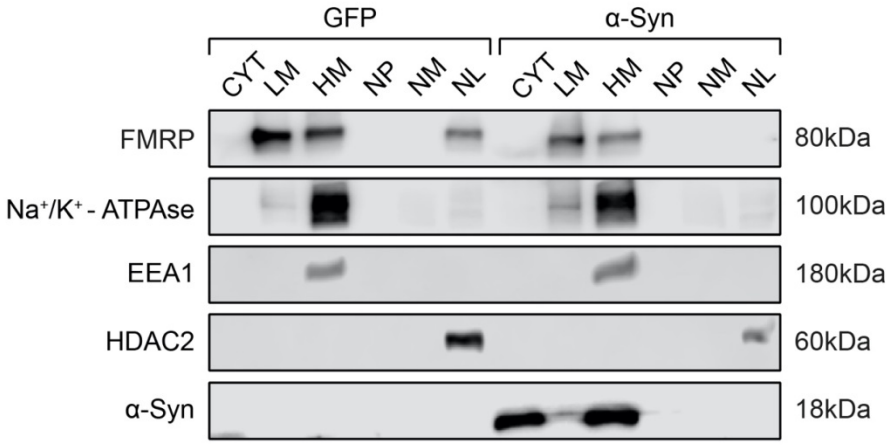

Figure 23 FMRP in the light membrane, heavy membrane, and nuclear lysate were less in α-Syn transduced cells. WB results of separated cellular compartments indicating that FMRP mainly located in light plasma membranes (LM), heavy intracellular membranes (HM), and the nuclear lysate (NL). Meanwhile, the α-Syn transduced cells showed a decreased intensity in all the existing fractions. CYT=cytosol, NP=nuclear pellet, NM=nuclear membrane.

3.2.4 FMRP shows persistent downregulation after α-Syn transduction in LUHMES cells

We next set out to investigate the effect of α-Syn overexpression on FMRP over time; therefore, we tested the abundance of FMRP in α-Syn-transduced neurons after different periods of time. It is apparent from **Figure 24** that GFP did not change the expression of FMRP, whereas a constant downregulation of FMRP was observed in α-Syn transduced cells as early as day 2 after transduction.

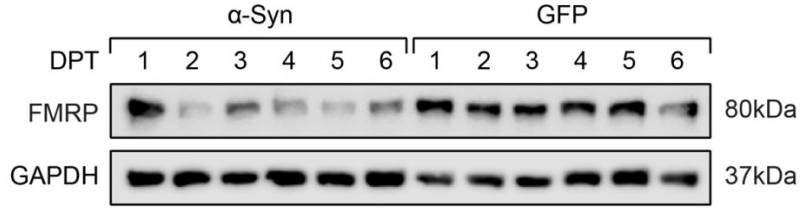

Figure 24 α-Syn overexpression leads to constant downregulation of FMRP. WB of FMRP in LUHMES cells from 1-6 DPT with α-Syn showing that FMRP started to decrease at 2 DPT.

3.2.5 The effect of different neurotoxins on the expression of FMRP

Another unanswered question concerns the effect of cell death on FMRP since the results from **Figure 25** illustrates an increased cell death on day 6 after α-Syn transduction. We, therefore, assessed the FMRP level in response to treatment with the mitochondrial complex-I

inhibitor rotenone. Treatment with the complex-I inhibitor rotenone is a widely used model in PD research (Ebrahimi, Oryan, Izadpanah, & Hassanzadeh, 2017; Pacelli et al., 2015). By treating cultured neurons with rotenone for 48 hours (0-1μM), FMRP remained unchanged (**Figure 26**), even though measuring LDH release (**Figure 27**) confirmed the increase in cell death in response to rotenone treatment.

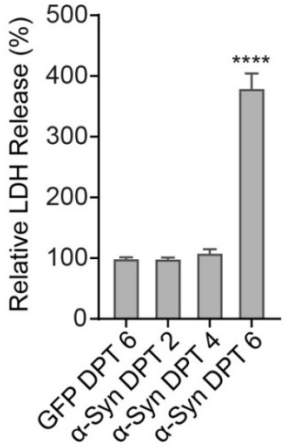

Figure 25 α-Syn induces cell apoptosis after 6 DPT. Bar graph of LDH result showing that α-Syn-induced neuronal cell death is absence before 4 DPT and significantly increases at 6 DPT (n=4). For comparison of the means, one-way ANOVA with Tukey's post hoc test was used. ****P < 0.0001. Data are shown as means ± SEM.

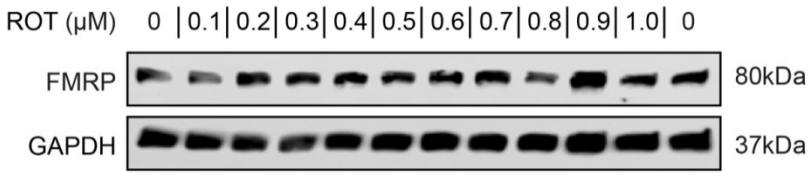

Figure 26 Expression of FMRP remains steady in response to rotenone-induced cell apoptosis. WB result demonstrating that treatment with rotenone from 0-1μM for 24 h doesn't affect FMRP expression.

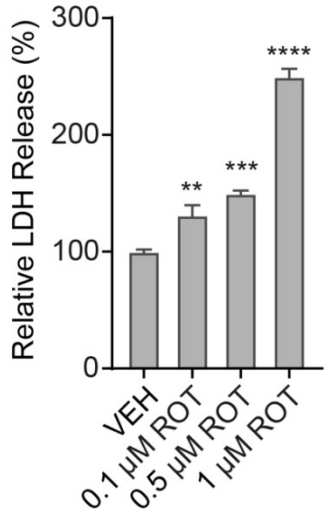

Figure 27 Rotenone-induced cell apoptosis. Bar graph of LDH results demonstrating that rotenone induces a dose-dependent cell apoptosis (n=4). For comparison of the means, one-way ANOVA with Tukey's post hoc test was used. ****P < 0.0001, ***P < 0.001, **P < 0.01. Data are shown as means ± SEM.

In addition, application of the 10 µM PD-associated toxins 1-Methyl-4-phenylpyridinium (MPP^+) for 24 h (**Figure 28**) or substrate starvation (**Figure 29**) did not decrease the expression of FMRP. Interestingly, treatment with 20 µM 6-hydroxydopamine (6-OHDA) for 24 h decreased FMRP by ~30% (**Figure 28**). Further research is required to explore the relation between FMRP and DA. As α-Syn overexpression-induced cell death is associated with the ubiquitin/proteasome system (UPS) pathway and autophagy (Winslow et al., 2010), we also investigate the influence of the treatment with 100 nM of the autophagy inhibitors bafilomycin A1 (6 h), 1µM UPS-inhibitor MG132 (6 h) and 50 µM chloroquine (24 h) on FMRP. WB results indicate that these three compounds did not have a further effect on the expression of FMRP in LUHMES cells (**Figure 30**).

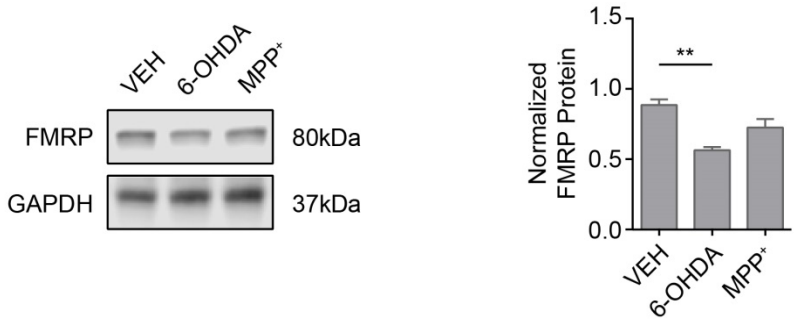

Figure 28 6-Hydroxydopamine (6-OHDA), but not MPP^+, decreases the FMRP expression. WB and bar graph show the application of 10 µM 6-OHDA (24 h) significantly decreased FMRP expression, while application of 50 µM MPP^+ (24 h) did not statistical significantly affect FMRP expression (n = 3). For comparison of the means, one-way ANOVA with Tukey's post hoc test was used. **P < 0.01. Data are shown as means ± SEM.

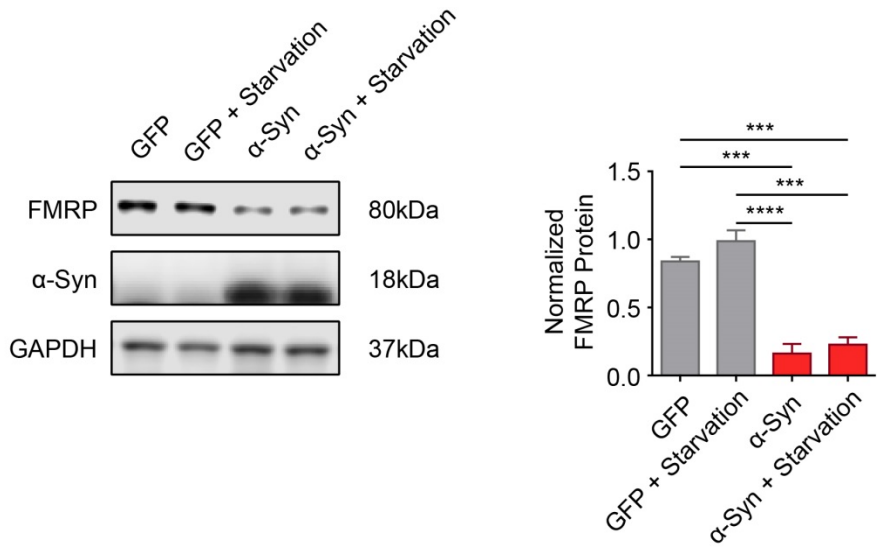

Figure 29 Starvation has no effect on FMRP expression. WB and bar graph demonstrating that substrate starvation does not affect FMRP expression. LUHMES cells were cultured in pure DMEM without glucose and other additives (N2 Supplement, cAMP or GDNF) (n = 3). For comparison of the means, one-way ANOVA with Tukey's post hoc test was used. ****P < 0.0001, ***P < 0.001. Data are shown as means ± SEM.

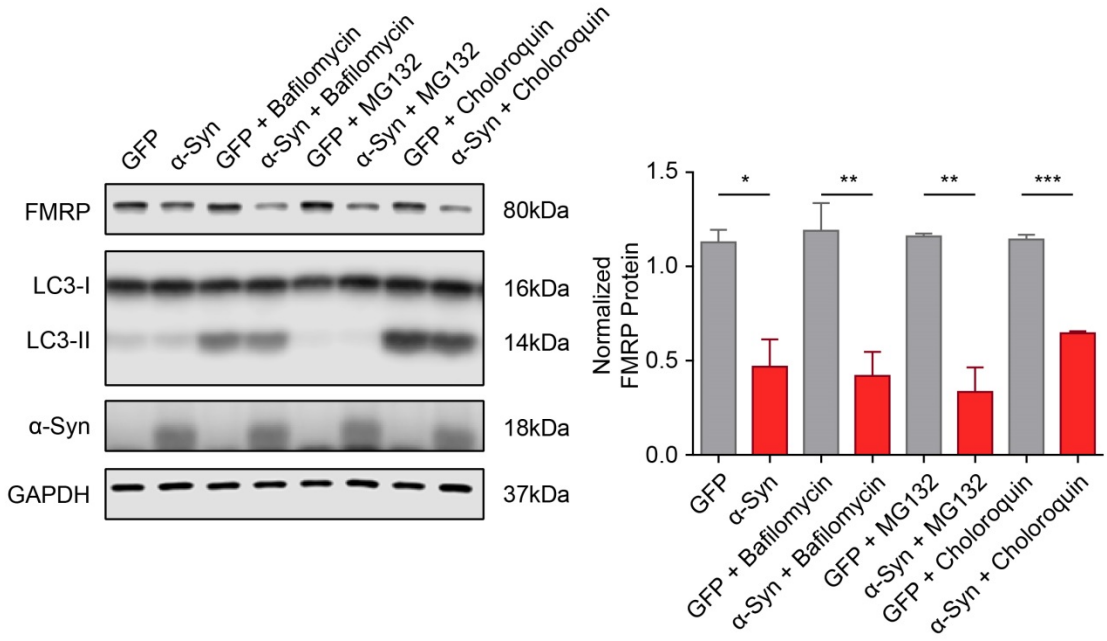

Figure 30 FMRP expression is independent of ubiquitin/proteasome system (UPS) and autophagy. Western blot and bar graph demonstrating that treatment with 1 µM MG132 (6 h), 100 nM bafilomycin A1 (6 h) and 50 µM chloroquine (24 h) did not produce any further effect on FMRP. Increased LC3-II after application of Bafilomycin A1 and chloroquine demonstrating the inhibition of autophagy (n = 3). For comparison of the means, one-way ANOVA with Tukey's post hoc test was used. ***P < 0.001, **P < 0.01, *P < 0.05. Data are shown as means ± SEM.

Taken together, the results in this chapter suggest that wildtype, A53T and A30P mutations α-Syn overexpression induces FMRP downregulation in dopaminergic LUHMES neurons independent from α-Syn-induced cell apoptosis. Moreover, FMRP expression was independent from starvation, UPS, autophagy and MPP^+-induced neurotoxin, whereas treatment of 6-OHDA resulted in a decreased abundance of FMRP in LUHMES cells.

3.3 α-Syn regulates N-type calcium channel activity by modulating FMRP

The results of the previous chapter demonstrate that α-Syn overexpression induces a downregulation of FMRP. We therefore further tested, if α-Syn activates N-type calcium channels through decreasing the FMRP protein abundance.

3.3.1 α-Syn overexpression enhances the membrane proportion of N-type calcium channels

First, we investigated the membrane abundance of the N-type calcium channel pore-forming subunit alpha 1B in response to α-Syn overexpression via two different approaches, namely by using a detergent-based membrane protein extraction and by surface protein biotinylation. **Figure 31** illustrates that the proportion of membrane-resident $Ca_V2.2$ was increased with both approaches in response to α-Syn overexpression. In accord with a role for FMRP, we found that co-expression of FMRP normalized the increase $Ca_V2.2$ membrane abundance. Given the unchanged total amount, our results thus support a regulation of membrane N-type calcium channels by FMRP (Ferron et al., 2014).

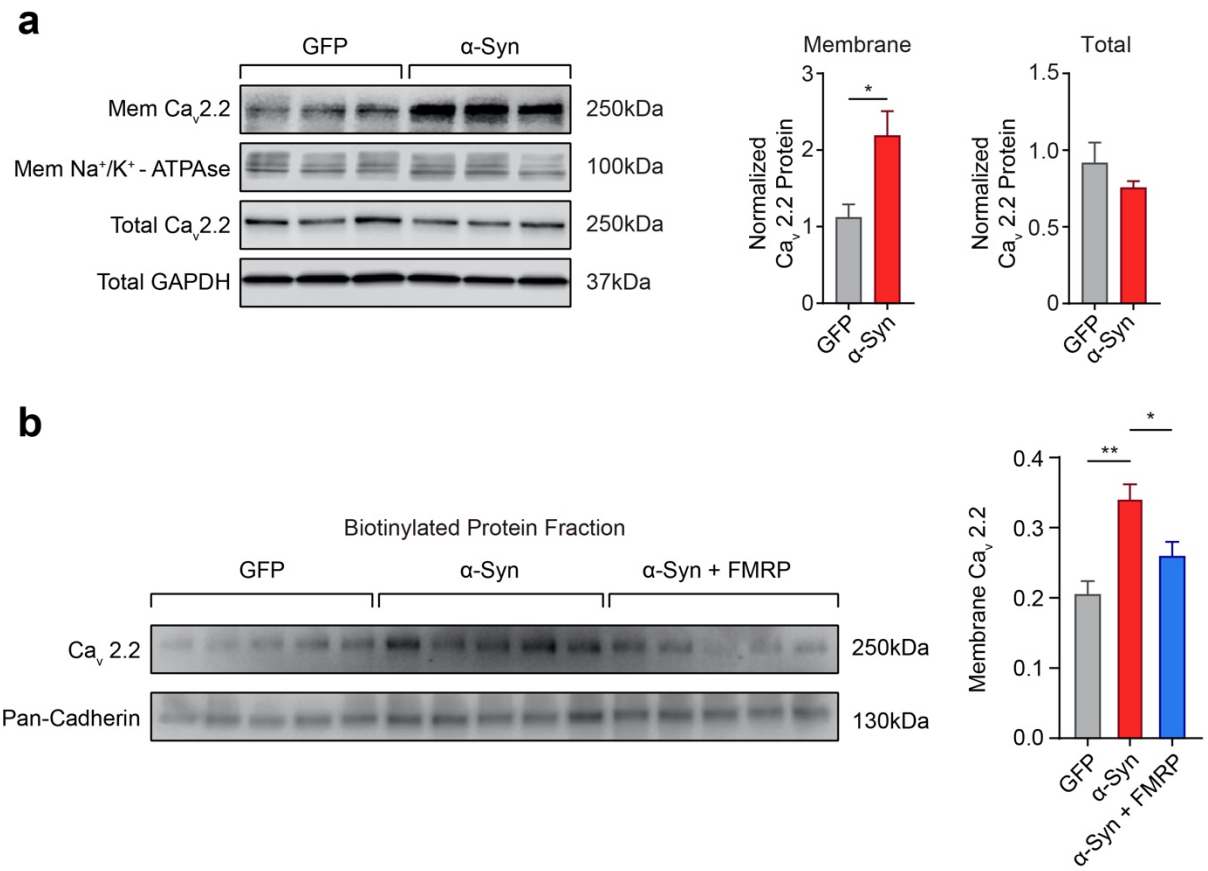

Figure 31 α-Syn transduced cells exhibit increased membrane N-type calcium channel. (**a**) WB and quantification of separated membrane proteins by the membrane protein extraction kit (Thermo fisher) illustrating that α-Syn transduced cells have a higher membrane N-type calcium channel density as compared with GFP transduced cells at 6 DPT. Na^+/K^+ - ATPase was used as control for membrane protein. Total cell lysate WB and quantification illustrating that α-Syn overexpression doesn't affect the total N-type calcium abundnace (n=6). (**b**) Alternative biotinylated membrane protein extraction confirmed that membrane biotinylated N-type calcium channels were increased in the α-Syn transduced cells. NMDAR1 and Pan-Cadherin was used as control for normalization and quantification. Co-overexpression FMRP in α-Syn transduced cells normalized the increased surface membrane N-type calcium channel (n=5). For comparison of the means, two-tailed unpaired t-test was used (**a**) and one-way ANOVA with Tukey's post hoc test was used in (b). **P < 0.01, *P < 0.05. Data are shown as means ± SEM.

3.3.2 α-Syn overexpression does not raise the mRNA level of N-type calcium channels

To systematically assess the regulation of N-type calcium channels under α-Syn overexpression, we examined the mRNA of *CACNA1B,* which is the coding gene for subunit

alpha 1B. The results suggested a slight decrease of CACNA1B after α-Syn overexpression (**Figure 32**).

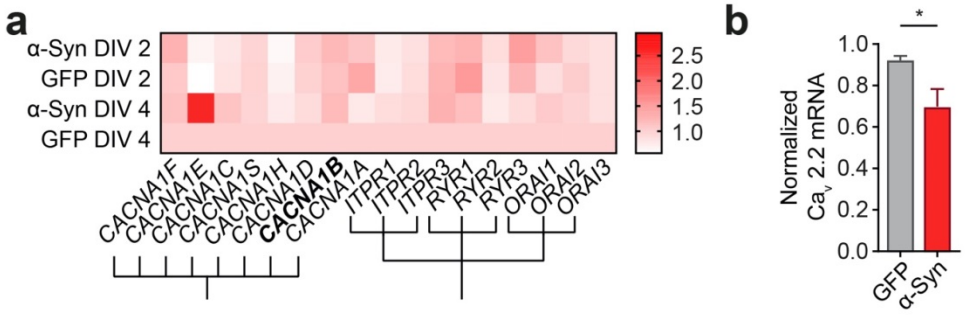

Figure 32 Gene array and qRT-PCR indicate a moderate downregulation of CACNA1B mRNA in α-Syn transduced cells. (**a**) Heat map of voltage- and ligand-activated calcium channel mRNA level measured through Chip-based transcriptome analysis showed that α-Syn overexpression doesn't affect the expression of N-type calcium channel subunits in LUHMES cells. (**b**) qRT-PCR illustrating a mild reduction in the mRNA level of N-type calcium channels in α-Syn overexpressing cells. For comparison of the means, two-tailed unpaired t-test was used. *P < 0.05. Data are shown as means ± SEM.

3.3.3 IHC demonstrates that α-Syn transduction in LUHMES cells does not affect the total N-type calcium channel abundance

In addition to the WB result, we also performed an immunofluorescent experiment to investigate the overall distribution of N-type calcium channels in response to α-Syn overexpression. There was no difference in both mean intensity and the number of puncta between GFP or α-Syn transduced cells (**Figure 33**).

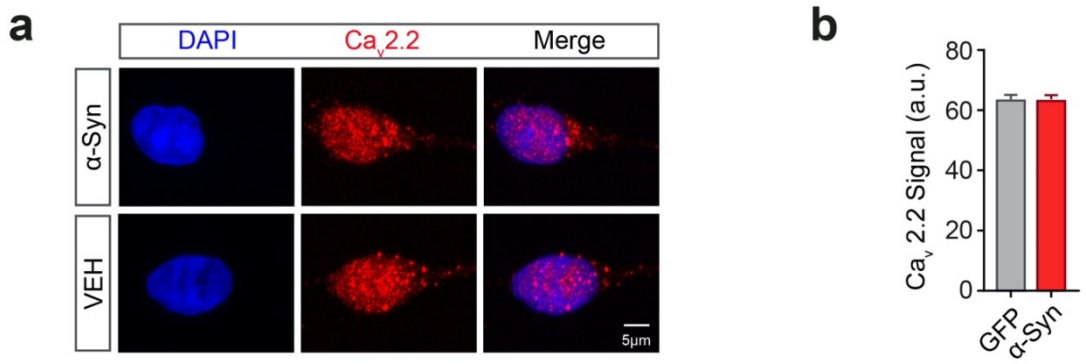

Figure 33 GFP or α-Syn transduced cells exhibited no difference in N-type calcium channel intensity. (**a**) Immunofluorescent staining showing that the total N-type calcium channel intensity in α-Syn transduced cells is similar to cells transduced with GFP. (**b**) The average number of N-type calcium channel punctate in each Triton X 100-permeabilized α-Syn or GFP transduced LUHMES cells was also similar (n = 72). Data are shown as means ± SEM.

3.3.4 FMRP knockdown increases membrane N-type calcium channel and induces inward calcium currents in LUHMES cells

To demonstrate the regulation of N-type calcium channels by FMRP in LUHMES cells, we measured the membrane proportion and calcium channel activity under the condition of FMRP silencing. FMRP silencing did not additionally affect cell viability (**Figure 34**). From **Figure 35**, it can be seen that cells treated with *FMR1* siRNAs exhibited a dramatic increase in the level of membrane N-type calcium channels as well as an increased inward currents under voltage clamp.

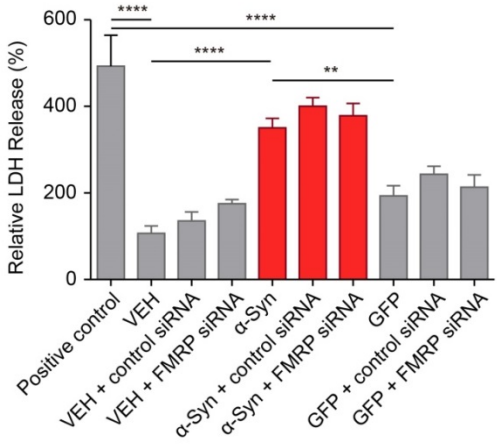

Figure 34 Co-application of FMRP siRNA does not induce further cell death in LUHMES cells. FMRP silencing did not further affect the LDH release (n = 6). For comparison of the means, one-way ANOVA with Tukey's post hoc test was used. ****P < 0.0001, **P < 0.01. Data are shown as means ± SEM.

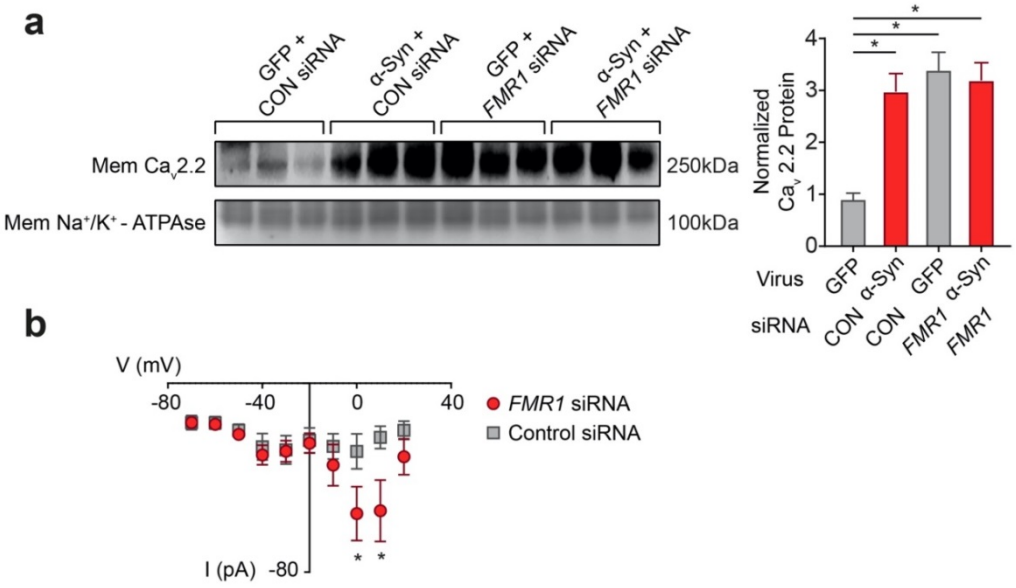

Figure 35 FMRP silencing activated calcium channel and increased membrane abundance of N-type calcium channel. (**a**) WB and quantification of the membrane N-type calcium channel intensity in response to *FMR1* silencing in both GFP and α-Syn transduced LUHMES, suggesting that both *FMR1* silencing and α-Syn overexpression led to an increased membrane N-type calcium channel intensity. Co-transfection of *FMR1* siRNA in α-Syn transduced cells didn't further increase the membrane N-type calcium channel (n=3). (b) I-V graph illustrating that *FMR1* siRNA treatment could induce inward currents in LUHMES cells (n=12). For comparison of the means, one-way ANOVA with Tukey's post hoc test was used in (**a**), and two-way ANOVA with Bonferroni post hoc test was used in (b). *P < 0.05. Data are shown as means ± SEM.

Drawing upon all the data from this chapter, these studies provided reasonably evidence that α-Syn regulates N-type calcium channel by manipulating FMRP.

3.4 Co-expression of FMRP in α-Syn overexpressing LUHMES cells normalizes deregulation of protein synthesis

FMRP is associated with intrinsic synaptic neuronal excitability by regulating the translation of synapse-related proteins (Davis & Broadie, 2017; Ferron, 2016). In FXS, the translation of FMRP-controlled synaptic proteins is greatly elevated due to the absence of direct FMRP-mRNA binding (Ferder et al., 2013; Liu et al., 2018; Tsang et al., 2019). Normally, FMRP interacts with it's target mRNA and thereby inhibits eIF4E initiation complex-mediated translation (Gantois et al., 2017; Napoli et al., 2008). Since our present data support the downregulation of FMRP in α-Syn transduced cells, we further investigated the protein synthesis rate as well as dysregulated translation-related proteins in FXS.

3.4.1 α-Syn overexpression increases the protein synthesis rate in LUHMES

Much of the available literature on FMRP reveal an exaggerated overall protein synthesis rate in *FMR1* KO mice (Richter et al., 2015; Zeng, Adamson, Curry, & Tarbell, 2014). In accordance with previous results, our study also demonstrated an elevated puromycin content, incorporated during peptide elongation, in α-Syn transduced cells (**Figure 36** and **Figure 37**). Cycloheximide treatment served as positive control (**Figure 37**).

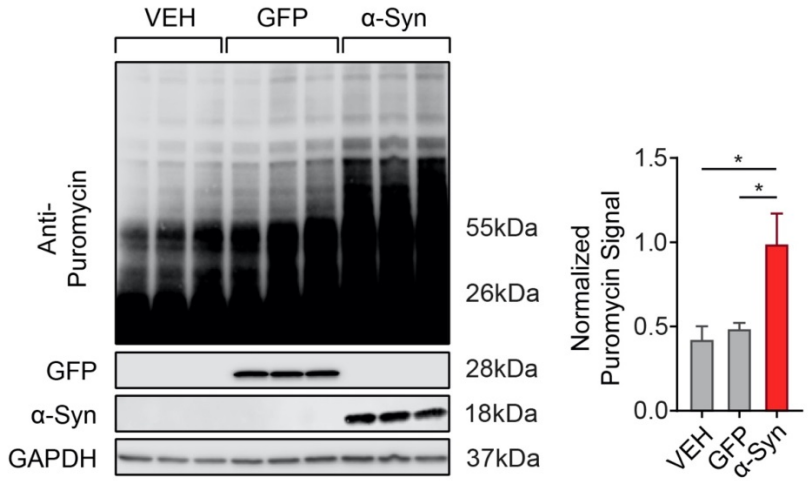

Figure 36 α-Syn overexpression LUHMES cells display elevated protein synthesis rate. As assessed by puromycin incorporation, α-Syn transduced LUHMES cells exhibited an increased overall protein synthesis compared to vehicle (VEH) and GFP transduced cells (n = 6). For comparison of the means, one-way ANOVA with Tukey's post hoc test was used. *P < 0.05. Data are shown as means ± SEM.

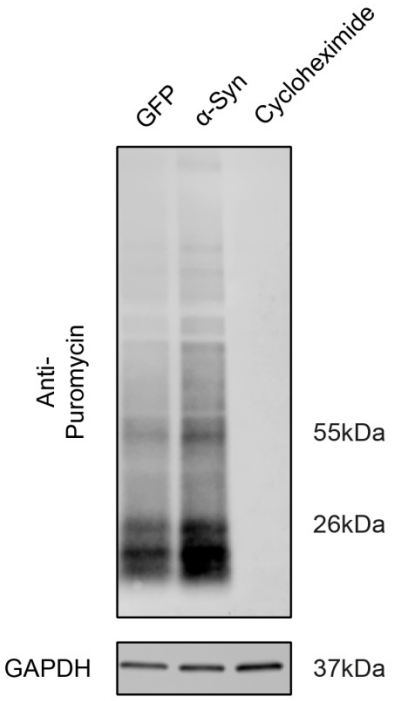

Figure 37 Application of cycloheximide entirely blocks the incorporation of puromycin. WB result demonstrating that α-Syn overexpression lead to an increased puromycin incorporation, whereas cycloheximide (10 uM) blocked the incorporation of puromycin (right lane).

3.4.2 Co-expression of FMRP normalizes the increased phosphorylation of eIF4E, S6 and Erk.

Results from previous studies demonstrate that FMRP is associated with the mTORC1 and Erk-mediated translation pathway (Gross et al., 2018; Osterweil et al., 2010). Hence, it's conceivable to examine the key proteins involved in both pathways. In line with previous FXS studies, the phosphorylation of eIF4E, Erk and S6 was significantly raised in α-Syn transduced cells (**Figure 38**). MMP9, another protein regulated by FMRP, was also dramatically increased in response to α-Syn overexpression. In summary, co-expression of FMRP in α-Syn transduced cells reversed the dysregulated proteins, thus indicated an important role of FMRP in α-Syn related disease.

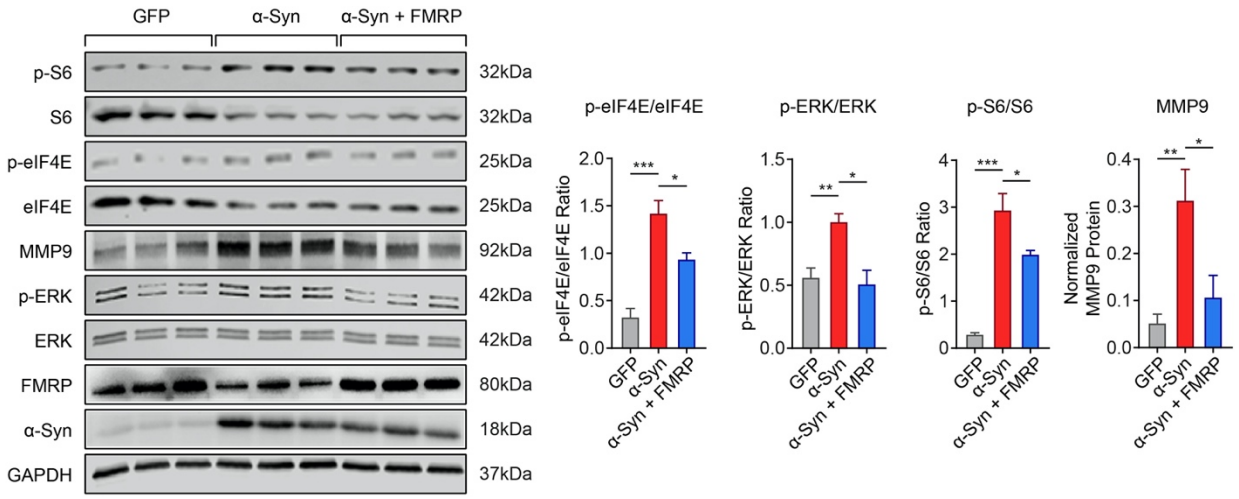

Figure 38 α-Syn overexpression induces upregulation of FXS related proteins expression, which can be also reversed by FMRP co-expression. WB and quantification demonstrating α-Syn transduction to increase the phosphorylation of S6, eIF4E, Erk and the MMP9 expression in LUHMES cells. The upregulation of these proteins was normalized by co-overexpression of FMRP in α-Syn transduced cells (n = 6). For comparison of the means, one-way ANOVA with Tukey's post hoc test was used. ***P < 0.001, **P < 0.01, *P < 0.05. Data are shown as means ± SEM.

These studies evaluated for the first time the role of observed downregulated FMRP as a vital protein in regulating disordered proteins, in agreement with FXS, in α-Syn transduced cells, further support the idea that FMRP may play an important role in pathological events during the progression of PD.

3.5 α-Syn regulates FMRP, not through hypermethylation, but rather potentially through PKC -CREB pathway

Causal factors leading to FMRP loss remain speculative in α-Syn transduced cells. A search of the literature revealed few studies on FMRP protein regulation. Hypermethylation of the FMRP promoter, the pathogenic mechanism involved in FXS, is reported as one of the factors that could induce FMRP loss (Kazdoba et al., 2014; Salat, Bardoni, Wohrle, & Steinbach, 2000). In addition, Wang et al. analyzed the promoter region of FMRP and assumed a regulation of FMRP by phosphorylation of cAMP response element-binding protein (CREB) due to the existence of the CRE sequence in the promoter (H. Wang et al., 2012). Data from different sources have conclusively shown that the phosphorylation of CREB can be regulated by protein kinase C (PKC) (Mao, Tang, & Wang, 2007). Moreover, a direct interaction exists between different isoforms of PKC and α-Syn as identified by Ostrerova et al. (Ostrerova et al., 1999). In view of these results, we speculated that α-Syn might regulate FMRP through either direct binding, hypermethylation of the FMRP promoter or alternatively through the PKC-CREB pathway.

3.5.1 Co-Immunoprecipitation indicates no direct binding between α-Syn and FMRP

A previous proteomic analysis reported a weak interaction between α-Syn and Fragile X mental retardation syndrome-related protein 1/2, which are autosomal homologs of FMRP (Hein et al., 2015). Even though the proteomic analysis implies a potential interaction between FMRP and α-Syn, our co-Immunoprecipitation data, however, rules out the possibility that α-Syn has a direct physical interaction with FMRP (**Figure 39**).

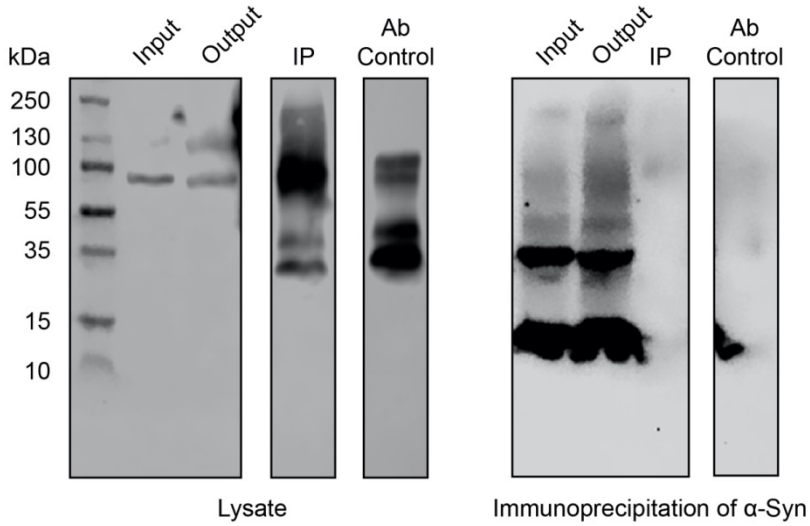

Figure 39 Co-Immunoprecipitation detect no physical interaction between α-Syn and FMRP. As compared to the antibody control (Ab control, left panel), FMRP protein in the cell lysate of LUHMES cells was precipitated in the IP. Right panels illustrating that the pulled-down FMRP band wasn't able to blot the α-Syn antibody, thus indicating the absence of a physical interaction between FMRP and α-Syn. Input and output in the figure was the cell lysate samples before and after FMRP precipitation, respectively.

3.5.2 α-Syn overexpression decreases the mRNA level of FMRP

After excluding a direct interaction, we next aimed to investigate whether the mRNA level of FMRP has a consistent phenotype with FMRP the protein level. **Figure 40** illustrates that *FMR1* mRNA, after normalizing with the housekeeping gene, indeed decreased in α-Syn transduced cells as assessed by using qRT-PCR.

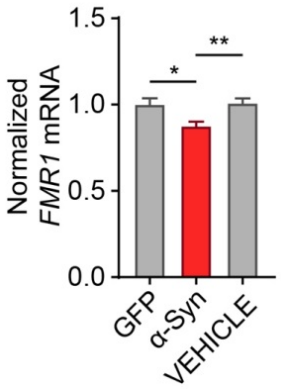

Figure 40 α-Syn overexpression lead to decreased *FMR1* mRNA in LUHMES cells. The qRT-PCR result showing that the mRNA level of *FMR1* in α-Syn transduced LUHMES cells was decreased as compared to GFP transduced cells (n = 6). For comparison of the means, one-way ANOVA with Tukey's post hoc test was used. **P < 0.01, *P < 0.05. Data are shown as means ± SEM.

3.5.3 α-Syn overexpression doesn't affect methylation status of *FMR1* promotor

α-Syn has been found to interact with histones and therefore to induce methylation of promoter regions (Burre et al., 2010), like SNAP25. The methylation status of *FMR1* promoter, in general, determines the transcription of *FMR1*. Hence, current literature provides strong incentive to investigate whether α-Syn overexpression has an effect on the methylation status of the *FMR1* promoter to induce FMRP loss. A comparison of the methylation status of the *FMR1* promoter in GFP or α-Syn transduced cells, however, revealed no difference in the number of CpG islands (**Table 8**, **Figure 41**).

Position on X Chromosome	Mean Methylation GFP	Mean Methylation α-Syn	△ GFP-α-Syn	p-Value
146992908	0.692654837	0.723143076	-0.030488239	0.162
146993010	0.336611029	0.335952806	0.000658222	0.556
146993092	0.082477587	0.097698101	-0.015220515	0.999
146993125	0.450827358	0.448164193	0.002663165	0.2855
146993175	0.516109728	0.563232918	-0.04712319	0.0818
146993420	0.942363374	0.947145719	-0.004782345	0.2382
146993433	0.462917019	0.448689399	0.01422762	0.5845
146993447	0.820288404	0.821642625	-0.001354221	0.6526
146993485	0.931255804	0.94600782	-0.014752016	0.4242
146993722	0.440806175	0.46723549	-0.026429315	0.1311
146993778	0.158826463	0.158217166	0.000609297	0.9151
146994128	0.457139053	0.502463983	-0.04532493	0.002
146994166	0.447973669	0.437237579	0.010736091	0.9021
146994369	0.214187838	0.23952351	-0.025335672	0.5058
146996911	0.407077213	0.414794256	-0.007717043	0.8719
146999718	0.506541132	0.542851083	-0.03630995	0.1759
147004697	0.984888615	0.978570061	0.006318554	0.0953
147011671	0.640345118	0.650572584	-0.010227466	0.6298
147011710	0.587193457	0.626438143	-0.039244685	0.0113
147021905	0.527907972	0.536883186	-0.008975214	0.6199
147023809	0.266867406	0.2545677	0.012299706	0.4443
147024735	0.929010587	0.930883618	-0.001873031	0.8034

Table 8 α-Syn overexpression doesn't affect *FMR1* promotor methylation. *FMR1* mean methylation at individual CpG sites of both α-Syn and GFP transduced LUHMES cells.

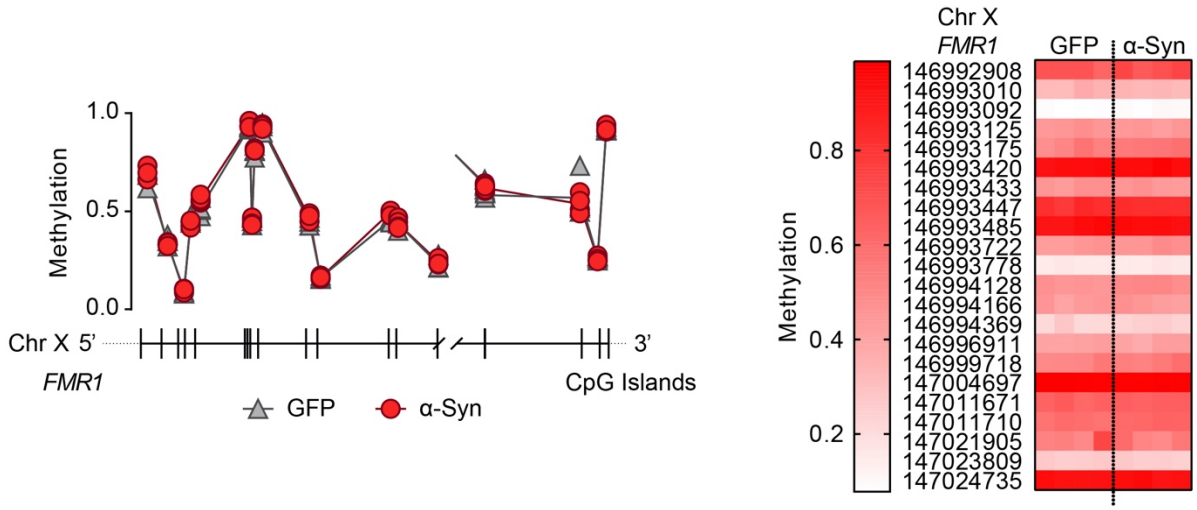

Figure 41 Methylation status of *FMR1* promoter doesn't show any significant differences between GFP and α-Syn transduced cells. No significant difference was observed in the relative *FMR1* methylation status at all CpG loci between α-Syn and GFP transfected LUHMES cells.

3.5.4 α-Syn overexpression leads to inhibition of CREB phosphorylation

We next sought to investigate whether α-Syn regulates FMRP through the PKC-CREB pathway. We first examined the phosphorylation status of CREB in response to α-Syn overexpression. As shown in **Figure 42**, α-Syn transduced cells indeed exhibited a significantly suppressed CREB phosphorylation at Ser133.

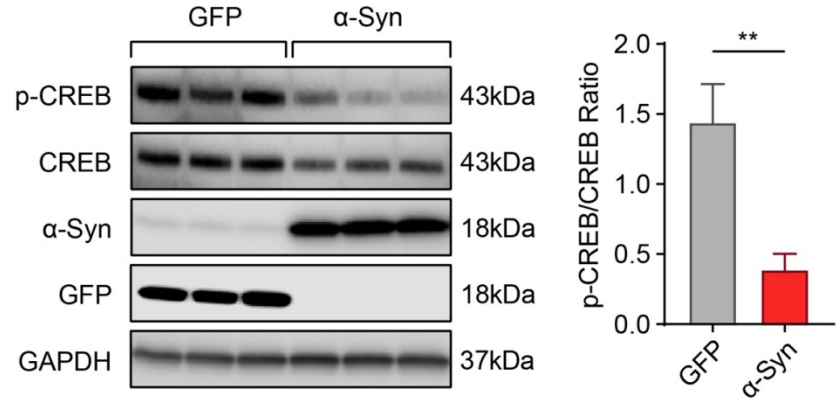

Figure 42 α-Syn overexpression suppresses phosphorylation of CREB. WB and quantification illustrating a reduced phosphorylation of CREB in α-Syn transduced LUHMES cells (n = 6). For comparison of the means, two-tailed unpaired t-test was used. **P < 0.01. Data are shown as means ± SEM.

3.5.5 PKC inhibitor treatment downregulates FMRP in LUHMES

As was pointed out in the introduction of this chapter, phosphorylation of CREB can be modulated by PKC. Since the inhibition of phosphorylation of CREB was identified in α-Syn transduced cells, it went on to suggest that PKC inhibition, similar to an effect of α-Syn overexpression, could induce FMRP loss through regulating CREB phosphorylation. With this intention, we investigated FMRP levels after treatment with PKC inhibitor. The result below (**Figure 43**) demonstrates that PKC inhibition by the PKC inhibitor C1 downregulated FMRP protein and therefore further supports the novel idea that α-Syn regulates FMRP through the PKC-CREB pathway in dopaminergic neurons.

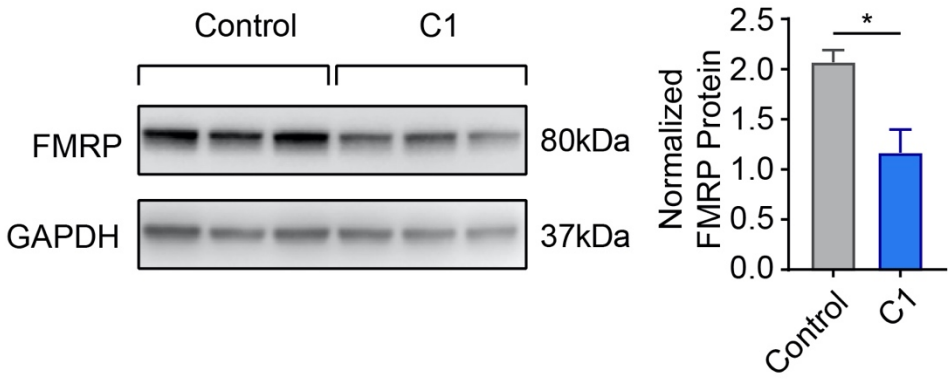

Figure 43 Inhibition of PKC induces FMRP loss. WB and quantification showing that incubation of PKC-inhibitor C1 in LUHMES cells decreased the FMRP expression (n=3). For comparison of the means, two-tailed unpaired t-test was used. *P < 0.05. Data are shown as means ± SEM.

3.5.6 PKC inhibitors treatment increases membrane abundance of N-type calcium channel and induce inward calcium currents in LUHMES

As demonstrated above, PKC appears to regulate FMRP, raising the question whether FMRP-related functions, like N-type calcium channel activity, is equally modulated by PKC activity. Corroborating evidence below in two aspects, both membrane protein concentration,

and electrophysiology demonstrate that N-type calcium channel activity can be truly activated by inhibiting PKC with PKC inhibitors C1 or Go6983 (**Figure 44**).

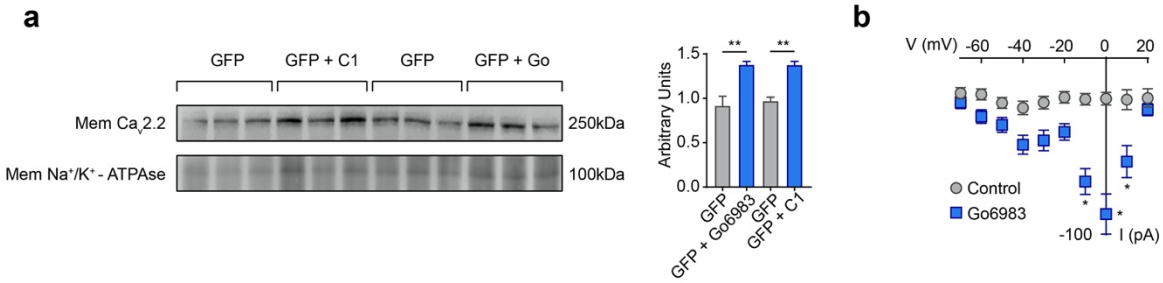

Figure 44 PKC inhibition induce activated N-type calcium channel. (**a**) WB and quantification illustrating that both PKC inhibitors, C1 and Go6983, significantly enhanced the membrane N-type calcium channel intensity in LUHMES cells (n=6). (**b**) I-V graph illustrating that blocking PKC by Go6983 induced an inward current in LUHMES cells (n=16). For comparison of the means, one-way ANOVA with Tukey's post hoc test was used in (**a**), and two-way ANOVA with Bonferroni post hoc test was used in (**b**). **P < 0.01, *P < 0.05. Data are shown as means ± SEM.

In brief, our results in this chapter consolidated the hypothesis that the regulation of FMRP by α-Syn is independent from direct protein-protein interaction or the methylation of *FMR1*, but occurs rather through a PKC-CREB pathway in dopaminergic cells.

3.6 Loss of FMRP in α-Syn overexpression tyrosine hydroxylase-positive cells in a PD mouse model preserves DA release in the striatum

Studies on our immortalized cell model were limited by the absence of a physiological CNS environment, where a variety of cells may interact with each other (Scholz et al., 2011). Therefore, we attempted to evaluate the response of mouse dopaminergic neurons under the condition of viral-induced α-Syn overexpression. It has been demonstrated that the α-Syn overexpression mouse model displays a PD-like progressive dopaminergic neuronal degeneration and an impaired nigrostriatal DA system (Oliveras-Salva et al., 2013; Tonges et al., 2014). In PD patients, reduced dopaminergic neurons lead to a significant reduction of DA release, thus causing typical PD symptoms (Elkouzi, Vedam-Mai, Eisinger, & Okun, 2019; Veys et al., 2019). Since our observations suggest a link between α-Syn and FMRP and because the loss of FMRP precedes cell death, it would be interesting to investigate whether FMRP has an effect on TH^+ cell death, striatal TH fiber density and DA release.

3.6.1 α-Syn overexpression induces FMRP immunofluorescent intensity reduction in tyrosine hydroxylase-positive in the mouse model

In an attempt to study the FMRP intensity in response to α-Syn overexpression in the above-mentioned mouse model, C57BL/6N mice were stereotactically injected with AAV5-α-Syn or AAV5-Luciferase respectively into the SNc. Three weeks after surgery, mice were sacrificed and brains were coronally sliced for FMRP staining. In line with our *in vitro* studies, SNc neurons overexpressing α-Syn also exhibited significant FMRP loss in vivo (**Figure 45**).

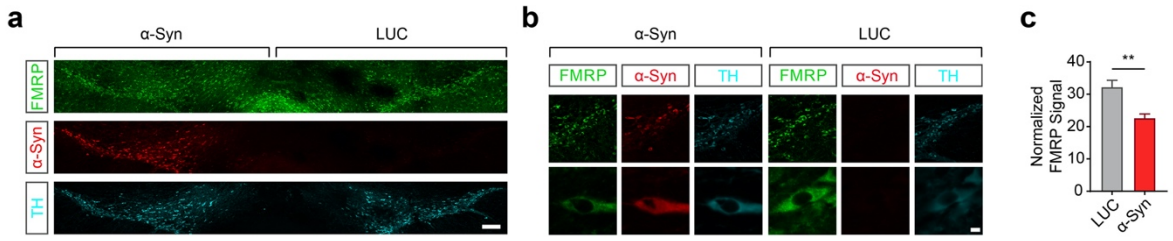

Figure 45 Overexpression of α-Syn decreases FMRP intensity in SNc neurons in mice. (**a, b**) Immunofluorescent result showing a reduced FMRP intensity in mouse SNc TH⁺ neurons overexpressing α-Syn, as compared to Luciferase (LUC) overexpression neurons. Scale bars 150 μm in (**a**) and 5 μm in (**b**). (**c**) Quantification of FMRP mean intensity in both LUC and α-Syn overexpression neurons (n=360, 6 animals per condition). For comparison of the means, two-tailed unpaired t-test was used. **P < 0.01. Data are shown as means ± SEM.

3.6.2 Regression analysis between FMRP and α-Syn

Regression analysis was used to determine the relationship between FMRP and α-Syn. The FMRP and α-Syn mean intensity of each cell was unbiasedly acquired by an ImageJ macro (Section 2.4.1.2). The result of the regression analysis in **Figure 46** indicates a negative non-linear correlation between these two proteins in α-Syn overexpressing mouse SNc neurons.

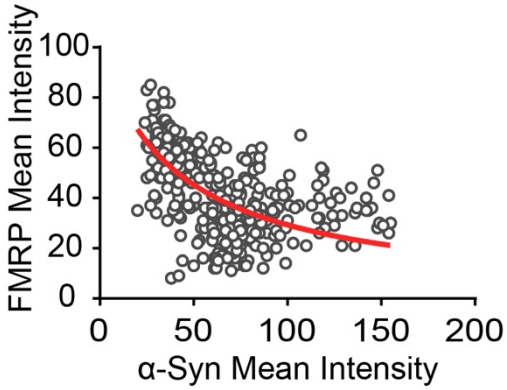

Figure 46 Regression analysis shows negative non-linear correlations between FMRP and α-Syn in mouse model. Increased α-Syn expression induced a reduction of FMRP mean intensity in SNc dopaminergic neurons (n = 360). Non-linear regression was analyzed via Prism 7.

3.6.3 Stereological cell counting of tyrosine hydroxylase-positive cells of *FMR1* KO mice or wildtype control in response to α-Syn overexpression.

To assess the role of FMRP in PD pathology, we first examined the TH^+ cell number in both *FMR1* KO and wildtype (WT) littermate control mice in response to α-Syn overexpression. No significant differences were detected 3 weeks after surgery (**Figure 47**).

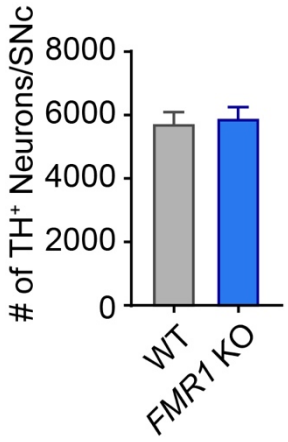

Figure 47 There are no observed differences of TH^+ cells number between WT or *FMR1* KO mice after viral α-Syn overexpression for three weeks. The number of α-Syn overexpressed SNc TH^+ neurons from both WT and *FMR1* KO mice was similar. Data are shown as means ± SEM.

3.6.4 Striatal Tyrosine hydroxylase fibres intensity displays no difference between of *FMR1* KO mice and wildtype control mice in response to α-Syn overexpression

We next investigated striatum TH fiber intensity under the same condition. TH DAB staining suggested the similar mean intensity of TH fiber in both mice three weeks after α-Syn virus injection (**Figure 48**).

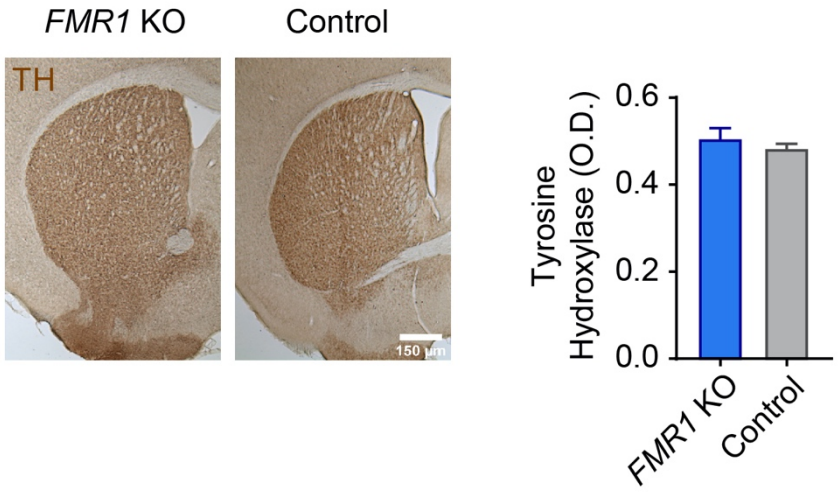

Figure 48 No observed differences of mean tyrosine hydroxylase fibrils intensity are found between wildtype and *FMR1* KO mice after viral α-Syn overexpression for three weeks. DAB staining of TH and quantification demonstrating a similar striatal fiber density between *FMR1* KO and WT animals after α-Syn virus injection for 3 weeks. Data are shown as means ± SEM.

3.6.5 Fast-cycling voltammetry reveals preserved DA release in α-Syn virus injected *FMR1* KO mice

Finally, we examined the effect of FMRP on DA release. By cooperating with Dr. Carmelo Sgobio from Prof. Jochen Herms' lab, we were able to measure striatal DA release ex vivo by using fast-cycling voltammetry (Sgobio et al., 2014) in slices from luciferase or α-Syn virus injected mice. As expected, t-tests revealed a significant reduction of striatal DA release in WT mice after α-Syn virus injection (**Figure 49**). We next injected the *FMR1* KO mice with the same viral conditions. Surprisingly, there was no statistical significant difference between luciferase and α-Syn virus injected mice in regard to the striatal DA release.

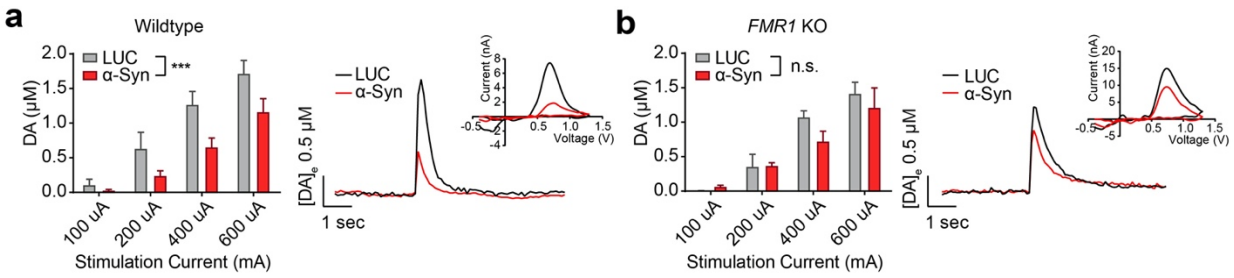

Figure 49 DA release in *FMR1* KO mice is more resistant after α-Syn virus injection. (**a**) Fast-cycling voltammetry demonstrating that, after α-Syn virus injection, WT mice hemispheres exhibit a reduced DA release in the dorsolateral striatum as compared to luciferase (LUC) injected hemispheres (left) (ANOVA Genotype Main Effect: $F(1,40) = 14.02$, $P < 0.001$, $n = 6$). Input/output curve and representative DA traces demonstrate a decreased release of DA in α-Syn injected hemispheres independently from the applied stimulus intensities (right) ($n = 6$). (**b**) DA release in *FMR1* KO mice showed no difference between α-Syn injected hemisphere and luciferase injected hemisphere (ANOVA Genotype Main Effect: $F(1,24) = 1.55$, $P > 0.05$, $n = 4$). For comparison of the means, two-way ANOVA with Bonferroni post hoc test was used in (**a**), (**b**). ***$P < 0.001$; N.S., not significant. Data are shown as means ± SEM.

Together these results provide further support for our previous hypothesis in vivo. Although FMRP had no effect on the numbers of TH^+ cells, fast-cycling voltammetry results indicated a protective role of FMRP loss in preserving DA release after α-Syn overexpression.

3.7 Loss of FMRP occurs in all Braak stages of human SN samples

Last of all, we investigated the role of FMRP under α-Syn related pathological conditions. In the human brain, misfolded α-Syn mainly exists in LBs. Therefore, we evaluated the FMRP intensity of SN dopaminergic neurons from non-LBP cases and LBP cases from Braak stage 1 to 6 (**Table 6**).

3.7.1 H&E staining demonstrating a reduced number of DA neurons in the SNc of PD cases

Previous studies demonstrated a reduced number of DA neurons in PD (Rietdijk, Perez-Pardo, Garssen, van Wezel, & Kraneveld, 2017). In accord, **Figure 50** consistently indicates a significant reduction of neuromelanin-positive, pigmented neurons in the SNc of PD cases at Braak stage 6.

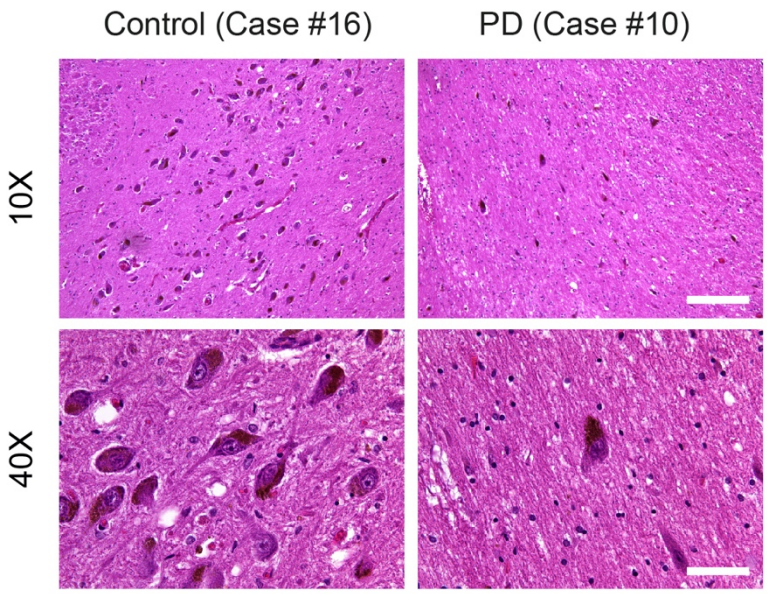

Figure 50 Reduced SN dopaminergic neurons are observed in Braak stage 6 samples. Representative H&E staining of post-mortem SNc sections demonstrating a significant decreased number of neuromelanin-positive DA neurons in PD, as compared to a control case. Scale bars 150 μm for lower magnification and 40 μm for higher magnification.

3.7.2 Immunofluorescence and VIP staining results reveal a reduced FMRP intensity in neuromelanin-positive cells of human SN samples with LBP.

In the follow-up phase of the study, we compared the abundance of FMRP in all the cases, including control cases without LBP as well as other neurological diseases, iLBD cases at Braak stages 1 and 2,, where LBs were constrained to the medulla oblongata and locus coeruleus (Castellani, Smith, Richey, & Perry, 1996; Ulusoy et al., 2016), and PD cases from Braak stage 3 to 6. Interestingly, a clearly reduced FMRP immunofluorescent intensity was observed in all the cases with LBP, whereas all the control cases displayed a clear and strong cytoplasmic FMRP signal (**Figure 51**, **52**, and **53**). An enzymatic VIP staining also exhibited the same trend (**Figure 54**).

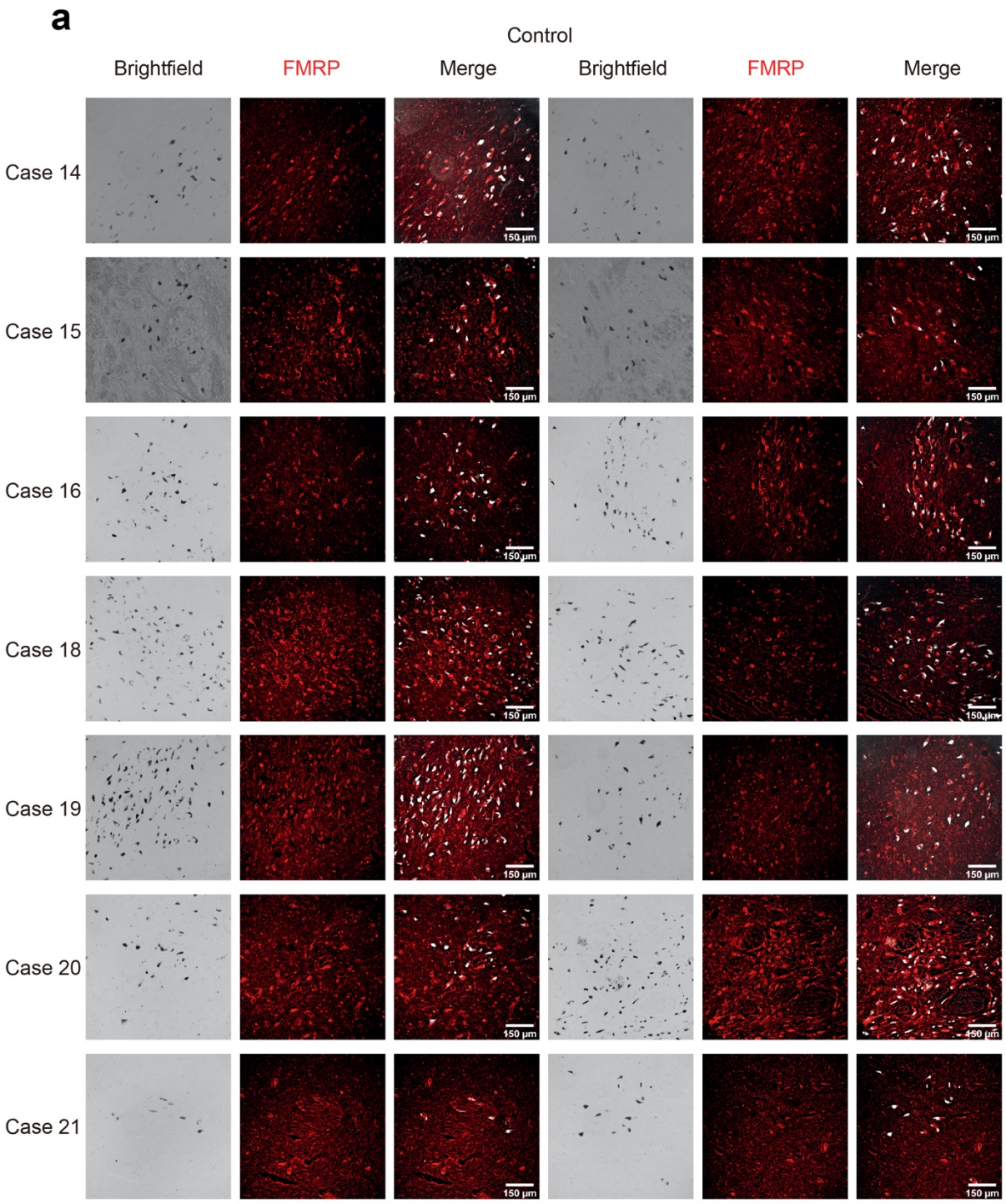
a
Control
Brightfield
FMRP
Merge
Brightfield
FMRP
Merge
Case 14
Case 15
Case 16
Case 18
Case 19
Case 20
Case 21
150 µm

b

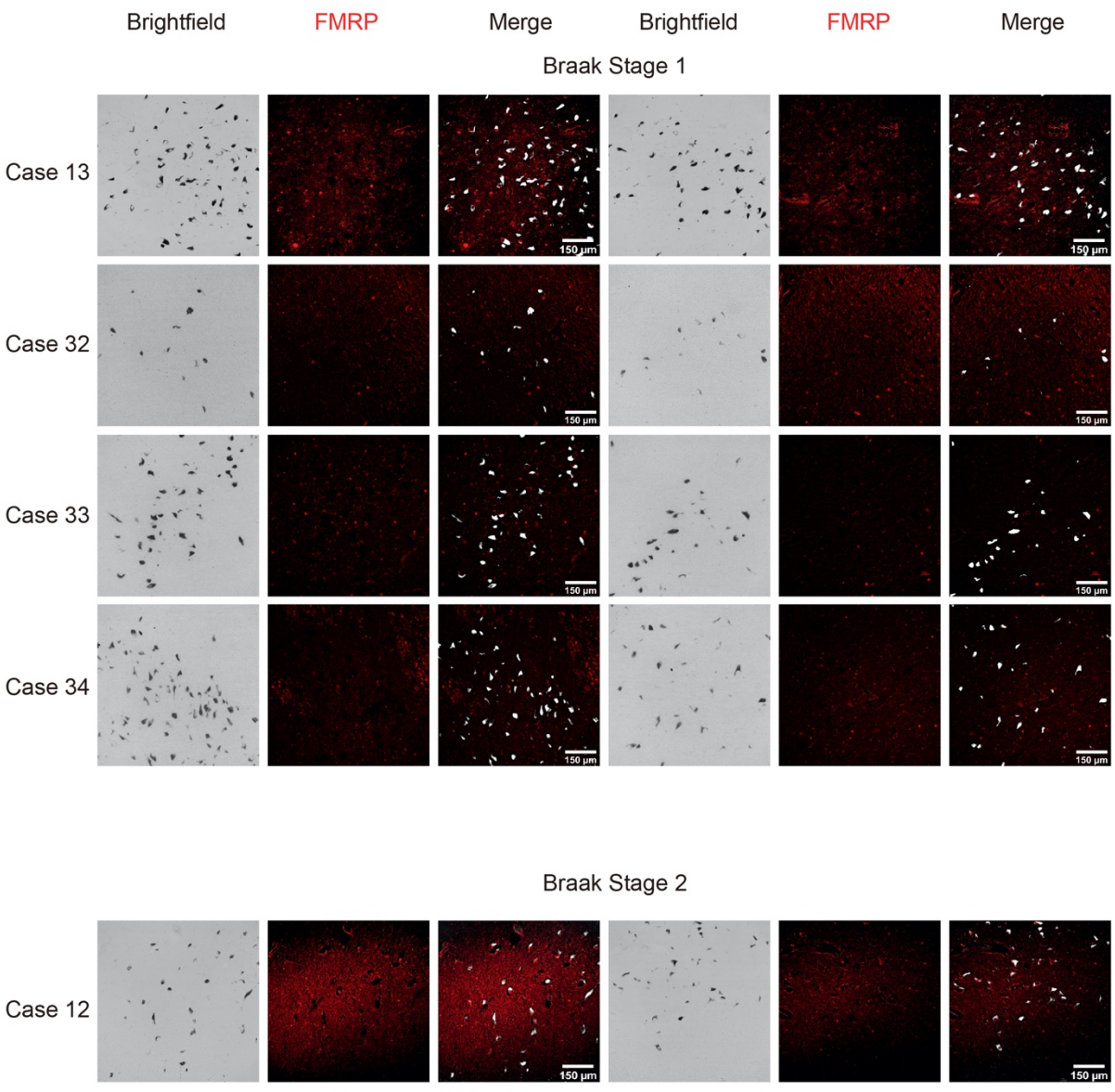
Brightfield
FMRP
Merge
Brightfield
FMRP
Merge
Braak Stage 1
Case 13
Case 32
Case 33
Case 34
Braak Stage 2
Case 12
150 µm

b

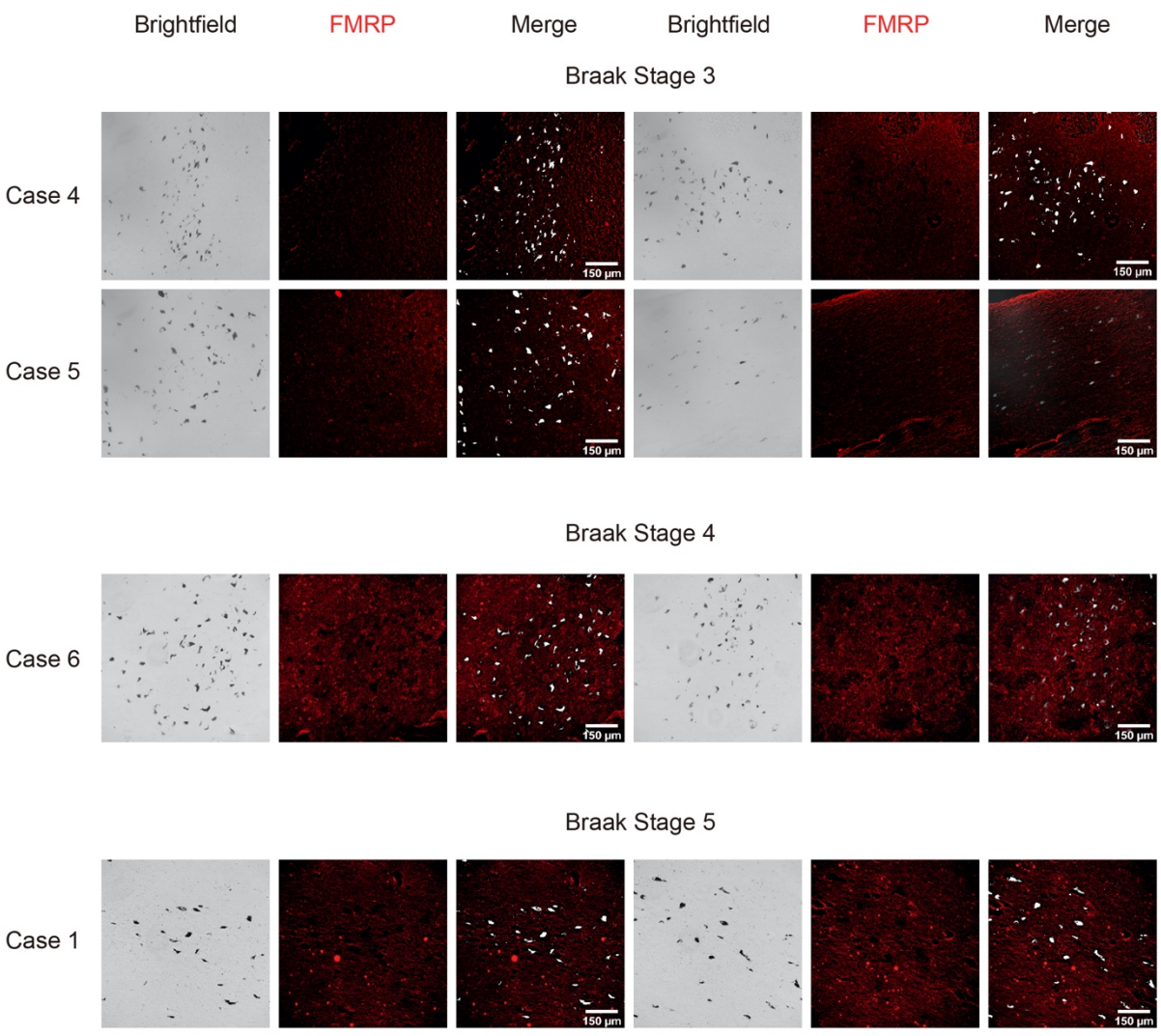
Brightfield
FMRP
Merge
Brightfield
FMRP
Merge
Braak Stage 3
Case 4
Case 5
Braak Stage 4
Case 6
Braak Stage 5
Case 1
150 µm

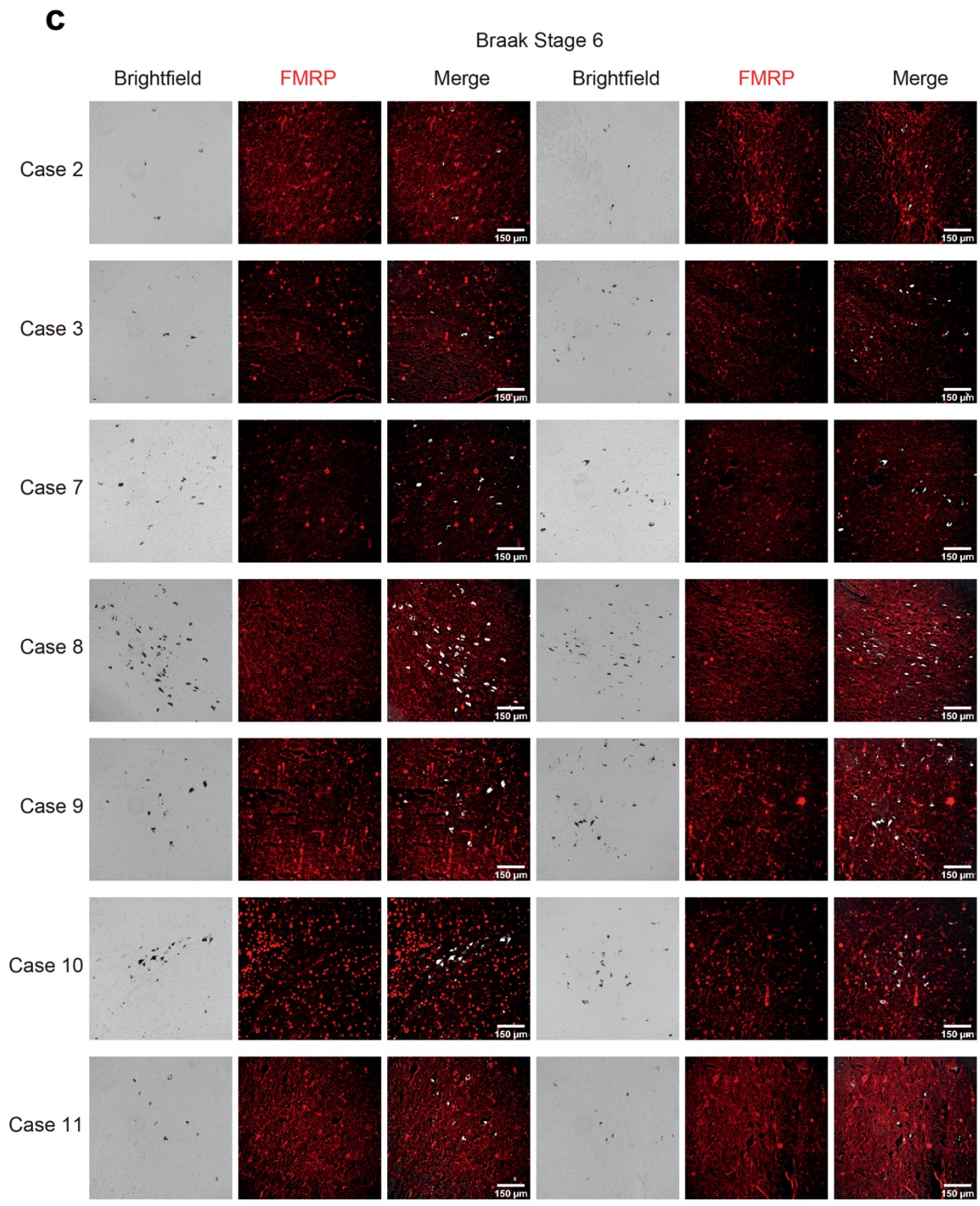

Figure 51 Cases with LBP display reduced FMRP intensity. (**a-c**) Immunofluorescent staining of FMRP combined with bright field photomicrographs of neuromelanin-containing neurons in SNc demonstrating a dramatic reduction of FMRP intensity in iLBD cases at different Braak stages, as compared to the control cases.

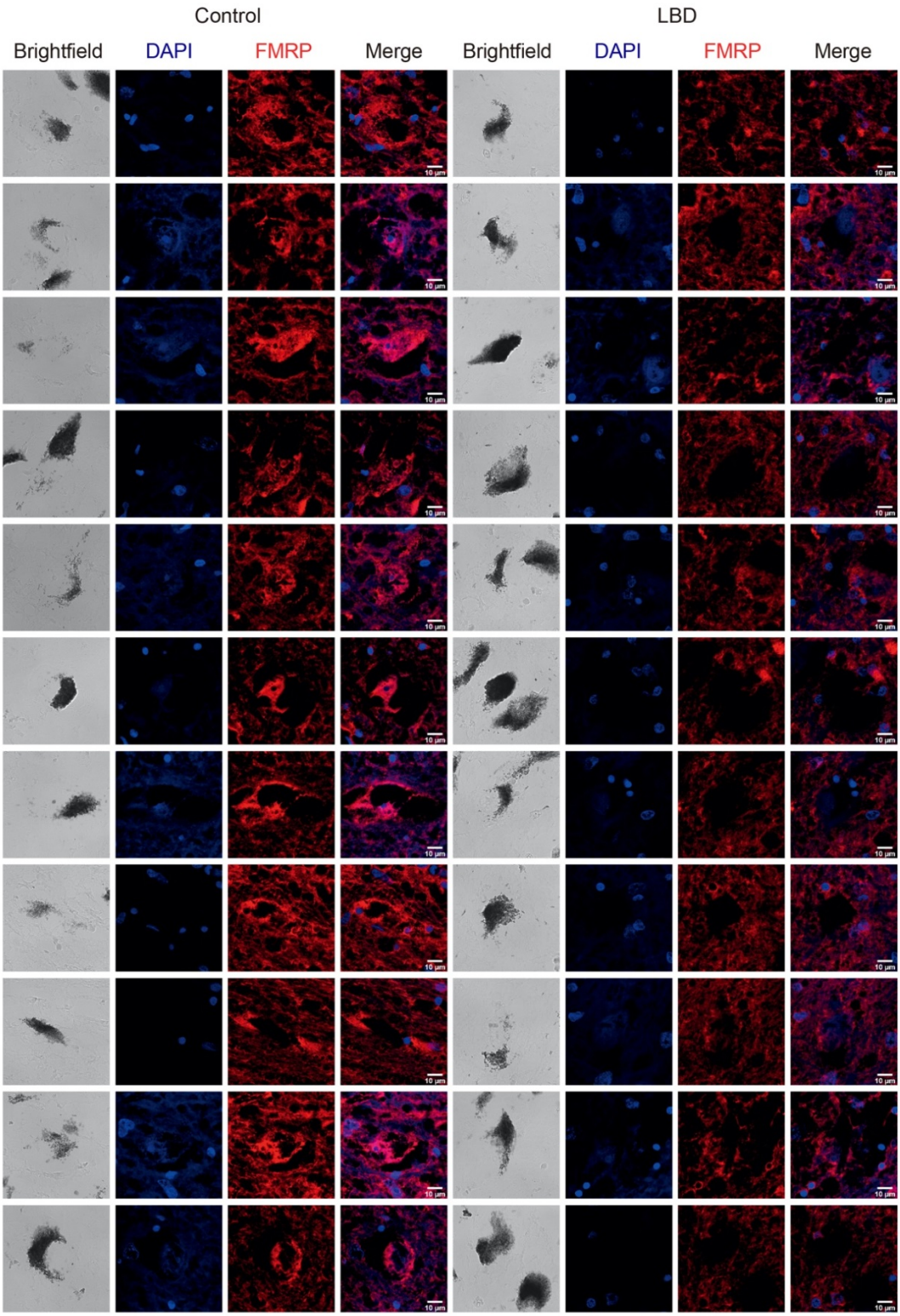

Figure 52 Zoomed in pictures of FMRP in both control cases and cases with LBP. High magnification (63x) micrographs demonstrating a reduced FMRP immunostaining intensity in LBD cases, as compared to control cases.

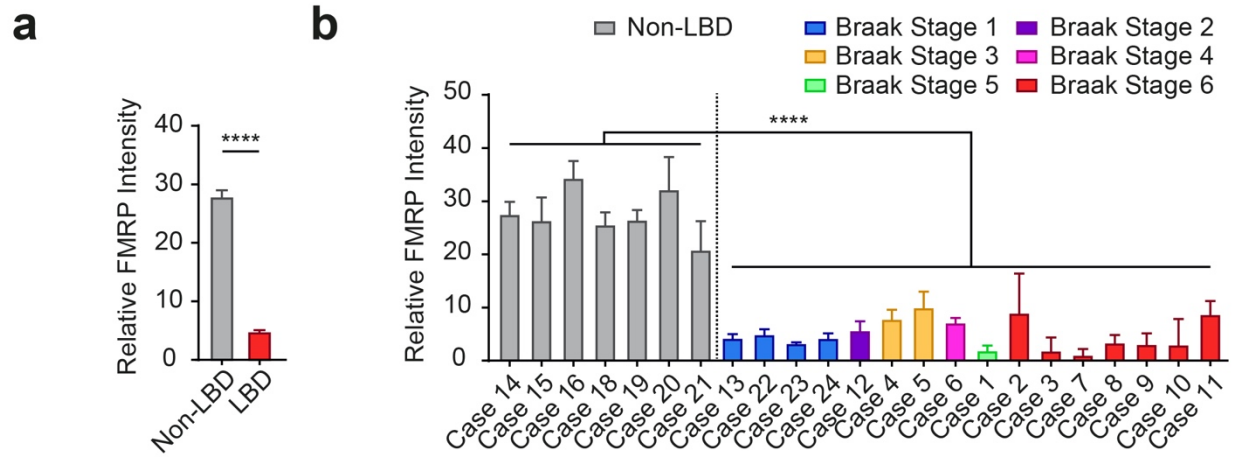

Figure 53 Significant reduced FMRP intensity are identified in LBP cases, and quantification of FMRP signal for all cases. (**a**) Quantification of FMRP mean intensity of all cells from both LBP cases (cases/neurons = 16/1169) and non-LBP control cases (cases/neurons = 7/670) demonstrating a loss of FMRP in LBP cases. (**b**) Bar graph shows the abundance of FMRP mean intensity in each non-LBD cases and iLBD cases at different Braak stages. All the iLBD cases show a reduced FMRP abundance irrespective of the Braak stage. For comparison of the means, two-tailed unpaired t-test was used in (**a, b**). ****P < 0.0001. Data are shown as means ± SEM.

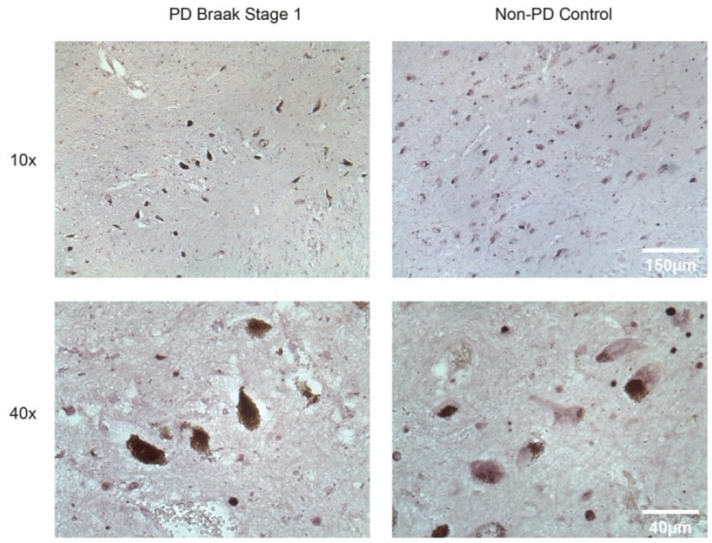

Figure 54 VIP staining of FMRP for control case and Braak stage 1 case. Representative chromogenic VIP staining shows a reduced cytoplasmatic FMRP signal in iLBD as compared to a non-PD control case.

3.7.3 FMRP is decreased in neuromelanin-positive cells with LBP, but retained in neurons in locus coeruleus, raphe nuclei and nucleus basalis of Meynert

To investigate the expression of FMRP in SNc neurons, we stained FMRP in conjugation with a TH antibody in human SNc sections (**Figure 55**). Besides the SNc DA neurons, TH-positive noradrenergic cells in the locus coeruleus (lc), tryptophan hydroxylase 2 (TH2) -positive serotonergic cells in the raphe nuclei (rn) and choline acetyltransferase (ChAT)-positive cholinergic neurons in the nucleus basalis of Meynert (nbM) have been reported to exhibit LBP (Bohnen & Albin, 2011; Braak et al., 2003; Giguere, Burke Nanni, & Trudeau, 2018; G. M. Halliday, Blumbergs, Cotton, Blessing, & Geffen, 1990; Schulz, Pagano, Fernandez Bonfante, Wilson, & Politis, 2018). Therefore, we also investigated the expression of FMRP in these cells in conjunction with corresponding marker proteins (**Figure 56**). Immunostaining data confirmed a consistent downregulation of FMRP in TH-positive SNc DA cells in PD cases. However, the expression of FMRP was found to be retained in neurons from lc, rn and nbM in PD cases.

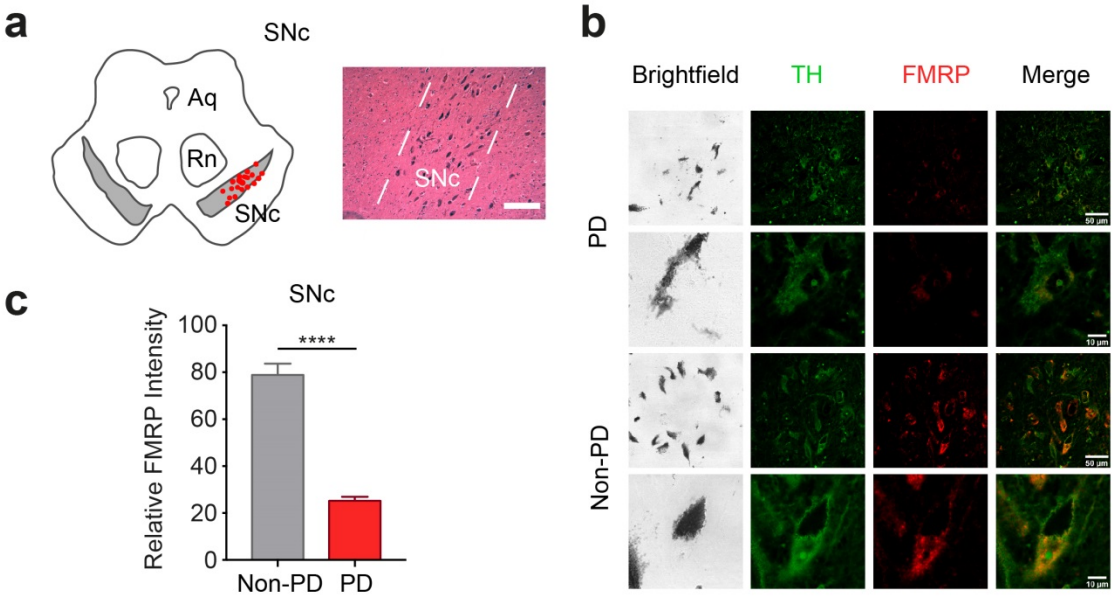

Figure 55 Loss of FMRP present in the TH-positive cells of LBP cases. FMRP is decreased in neuromelanin- and TH double-positive neurons. (**a**) Schematic and corresponding H&E staining depict the anatomical and histological presence of neurons in the SN. (**b-c**) TH and FMRP double Immunohistochemically staining and quantification of FMRP intensity in both PD (n cases/neurons = 11/78) and Non-PD cases (n cases/neurons = 4/46). For comparison of the

means, the two-tailed unpaired t-test was used in (**c**). ****P < 0.0001. Data are shown as means ± SEM. Aq: aquaeduct; SNc: substantia nigra pars compacta; Rn: red nucleus.

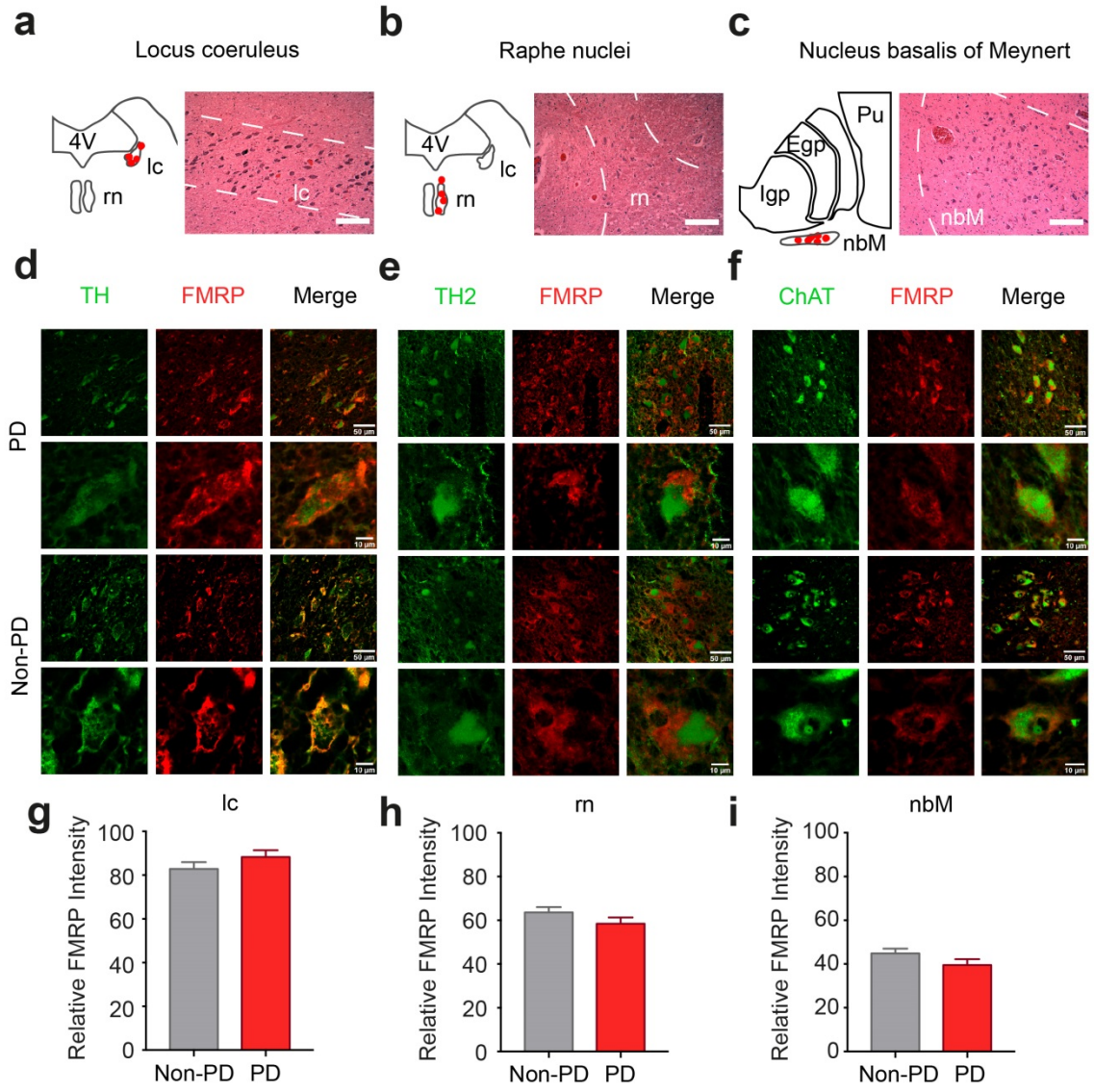

Figure 56 FMRP is retained in neurons in the region of locus coeruleus (lc), raphe nuclei (rn) and nucleus basalis of Meynert (nbM) in PD cases. (**a-c**) Schematic and corresponding H&E staining depict the anatomical and histological presence of neurons in the locus coeruleus (lc) (**a**), the dorsal raphe nuclei (rn) (**b**) and the nucleus basalis of Meynert (nbM) (**c**). (d-f) Double immunohistochemically staining for both PD and control cases from the corresponding regions as shown in (**a-c**). The sections were double-stained with FMRP in conjunction with either TH (**d**), tryptophan hydroxylase 2 (TH2) (**e**) or choline acetyltransferase (ChAT) (**f**). (g-i) Bar graphs demonstrate the FMRP expression to be retained in neurons from lc (PD: n cases/neurons = 4/93 vs. control: n cases/neurons = 5/119), rn (PD: n cases/neurons = 5/60 vs. control: n cases/neurons = 4/123), and nbM (PD: n cases/neurons = 9/65 vs. control: n cases/neurons = 5/105). For comparison of the means, the two-tailed unpaired t-test was used in (**g-i**). Data are

shown as means ± SEM. 4V: fourth ventricle; rn: raphe nuclei; lc: locus coeruleus; lgp: internal globus pallidus; Egp: external globus pallidus; Pu: putamen (Pu); nbM: nucleus basalis of Meynert.

3.7.4 Immunofluorescent staining results reveal FMRP to be decreased in DA SNc neurons in PSP and MSA cases

To further investigate the expression of FMRP in other neurodegenerative conditions, we also stained FMRP in SNc DA neurons from Progressive Supranuclear Palsy (PSP) cases (**Table 7**, **Figure 57**) and Multiple System Atrophy (MSA) cases (**Table 7**, **Figure 58**). Likewise, FMRP also decreased in SNc neurons in both conditions thus indicating an important role of FMRP during neurodegenerative process in different neurodegenerative conditions.

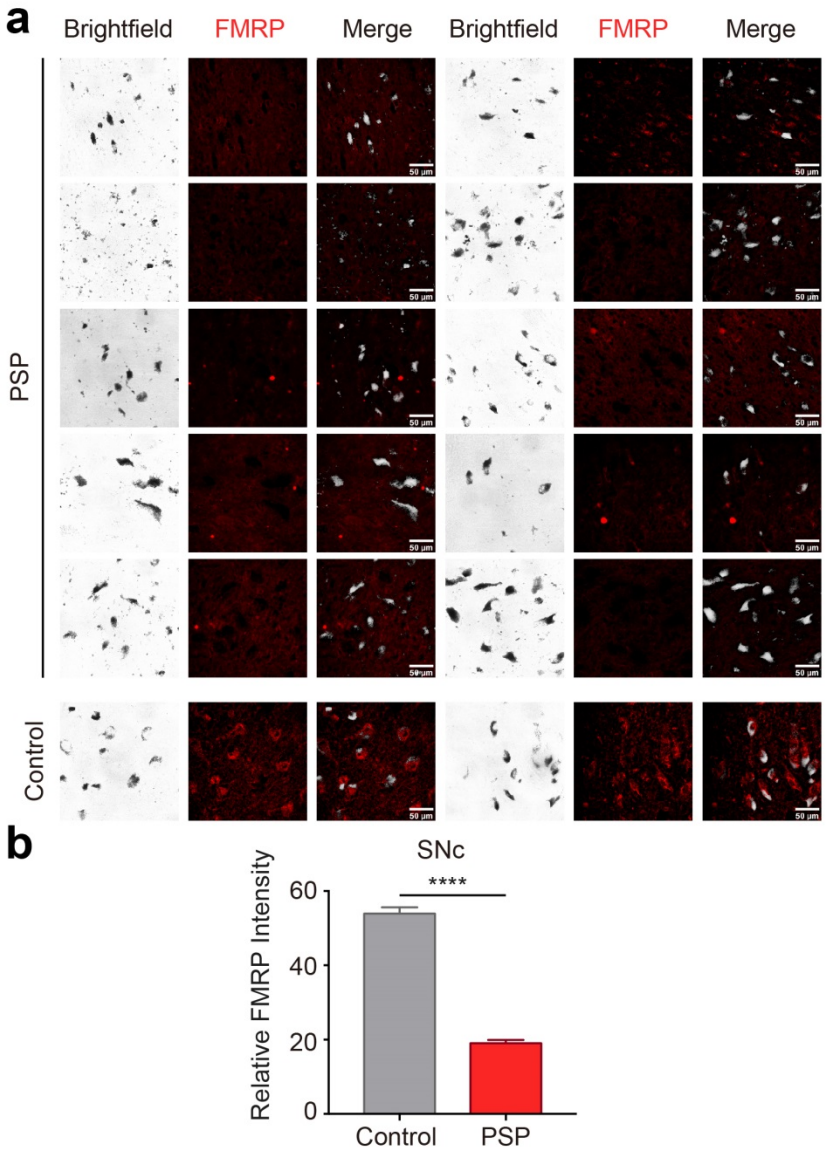

Figure 57 loss of FMRP also present in dopaminergic SNc neurons of PSP. (**a,b**) Photomicrographs and bar graphs demonstrating FMRP to be decreased in SNc neurons in Progressive Supranuclear Palsy (PSP) cases (n cases/neurons = 10/88), as compared to control cases (n cases/neurons = 4/54). For comparison of the means, two-tailed unpaired t-test was used ****P < 0.0001. Data are shown as means ± SEM.

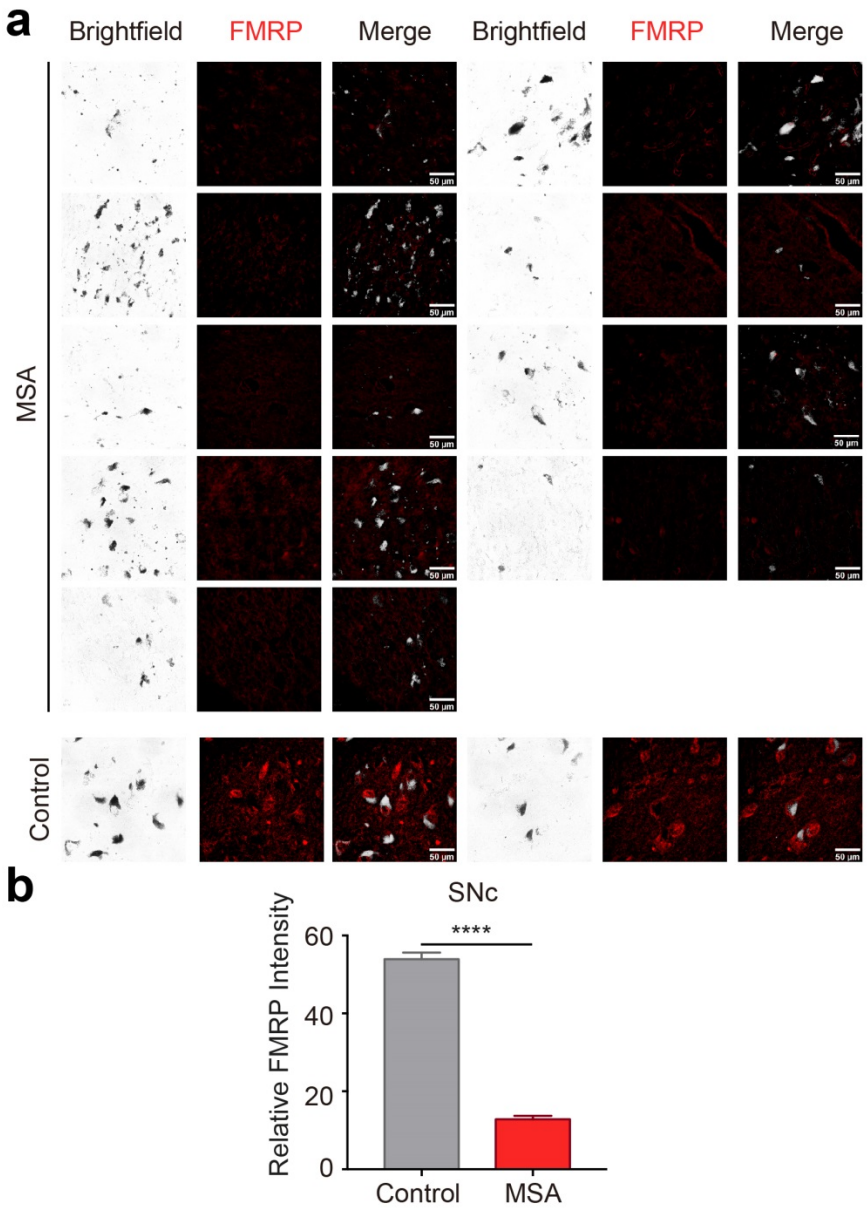

Figure 58 loss of FMRP also present in dopaminergic SNc neurons of MSA. (**a,b**) Photomicrographs and bar graphs demonstrating FMRP to be decreased in SNc neurons in Multiple System Atrophy (MSA) cases (n cases/neurons = 9/77), as compared to control cases (n cases/neurons = 4/54). For comparison of the means, two-tailed unpaired t-test was used ****P < 0.0001. Data are shown as means ± SEM.

In summary, our study on human samples suggests an overall reduction of FMRP among all the tested LBP cases. It is, therefore, demonstrated that FMRP has a strong connection with

α-Syn related pathology. In general, the whole study indicates an important role of FMRP during PD progression, the early stage in particular.

4 Discussion

4.1 α-Syn overexpression results in a loss of FMRP in vitro

The present research was designed to study the effect of α-Syn overexpression on human DA neurons. The most compelling finding in our study is a decreased abundance of FMRP in these cells in response to α-Syn (**Figure 21**) as well as in the SNc of mice injected with α-Syn overexpressing virus (**Figure 45**).

FMRP contains a nuclear localization and export sequence (Bhattacharya et al., 2012), and although its expression is largely cytoplasmic, FMRP can be found shuttling in and out of the nucleus (Carbone, Costa, Provensi, Mannaioni, & Masi, 2017; Ceman et al., 2003; Ferron et al., 2014). In the nucleus, FMRP binds to newly synthesized pre-mRNAs while being transcribed (Contractor et al., 2015) and transporting them from the soma to the dendrites and axons while inhibiting the translation of the encased mRNA (Aryee et al., 2014; Ashley, Wilkinson, Reines, & Warren, 1993; Berg et al., 2014; V. Brown et al., 2001). Once arrived at the synapse, mRNAs are released from these RNA granules and subsequently translated in response to stimuli (Damier, Hirsch, Agid, & Graybiel, 1999). FMRP thus presumably also acts as an mRNA binding and transport protein. In cultured DA neurons, we found the abundance of FMRP to be decreased in the cytoplasm, where it segregates with ER-associated membranes (**Figure 23**). Our data thus demonstrate a decrease of FMRP in the cytoplasm of α-Syn transduced neurons.

FMRP related protein translation activity is regulated by phosphoinositide 3-kinase (PI3K) and mTORC1 that phosphorylate 4E-BPs and thus lead to a de-repression of protein translation. The mTOR also phosphorylates and activates p70 S6K1, which phosphorylates ribosomal protein S6 to promote cap-dependent translation. Loss of FMRP in FXS and *FMR1* KO mice leads to elevated phosphorylation of ERK, eIF4E, S6 and protein level of MMP9 (**Figure 59**). In accordance with previous researches, α-Syn overexpressed LUHMES cells display the same core phenotypes (**Figure 38**). Thus, our study provides an additional perspective with respect to α-Syn-mediated PD pathology.

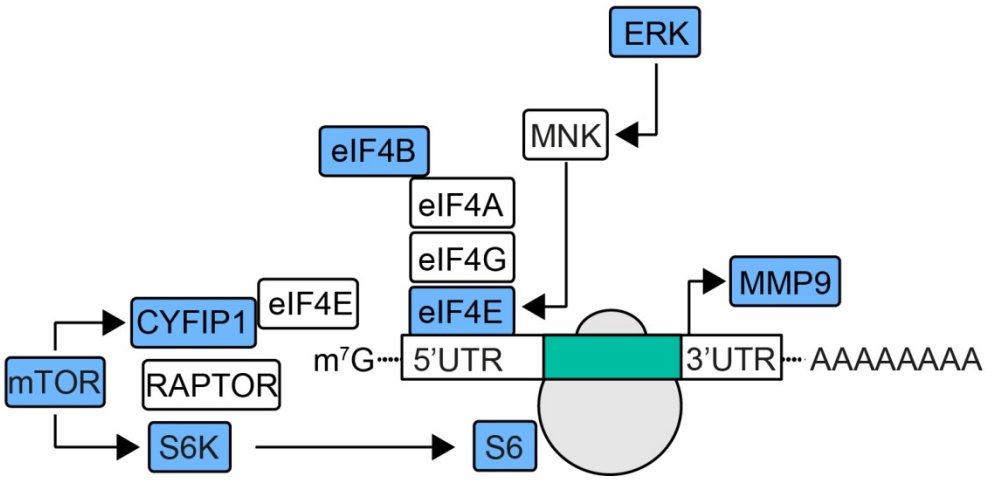

Figure 59 Schematic illustrate the affected translation pathway involved in FXS. The expressions of MMP9 are increased and the phosphorylation of other blue labelled proteins are elevated in FXS.

4.2 α-Syn regulates neuronal proteins through modulating FMRP

Most neuronal cell types vulnerable to PD-associated cell death including DA neurons in the SNc have long and highly branched axons, requiring a high amount of energy supply and oxidative phosphorylation (Dijkstra et al., 2014). For instance, neurons in the ventral tegmental area (VTA), which are considerably less vulnerable than SNc DA neurons, have less L-type-mediated calcium currents (Brager, Akhavan, & Johnston, 2012; M. C. Chartier-Harlin et al., 2011; Cilia et al., 2009) and increased hyperpolarization-activated and cyclic nucleotide-gated (HCN) currents upon treatment with the complex I inhibitor MPTP, ultimately leading to attenuated somatic calcium currents (Braak, Ghebremedhin, Rub, Bratzke, & Del Tredici, 2004). Another example is the selective activation of Kir6.2-containing ATP-sensitive potassium channels (K-ATP) and tonic hyperpolarization in SNc DA neurons in response to mitochondrial stress (De Pablo-Fernandez et al., 2015). These DA neurons have broad APs, large oscillations in intracellular Ca^{2+} and are autonomous pacemakers (Guzman et al., 2009; Nedergaard et al., 1993) further increasing their vulnerability to age or cellular stress factors. These physiological traits distinguish SNc DA cells from neurons that are less vulnerable in PD (Braak et al., 2004). The differential expression or function of particular neuronal genes may be the basis for the selective vulnerability in PD.

FMRP is predominantly expressed in neurons in the brain including DA cells of the SNc. In accord with previous reports, we found a strong FMRP expression in mouse SNc DA cells (**Figure 45**). As FMRP regulates a number of DA associated neuronal genes, α-Syn-mediated FMRP regulation in these cells may thus contribute to PD pathology. For instance, big potassium (BK) channels modulate AP duration and the afterhyperpolarization. Because a loss of FMRP reduces BK channel activity, *FMR1* KO mice have an excessive AP broadening leading to elevated presynaptic Ca^{2+} influx during repetitive activity in both hippocampal and cortical pyramidal neurons (Deng et al., 2013). Future research needs to deceiver the specific effect of α-Syn on these conductances. Another good example of a cell-type and region-specific

effect of FMRP are HCN channels. Their expression is increased (and input resistance reduced) in dendrites of hippocampal neurons of *FMR1* KO mice (Brager et al., 2012), which is opposite to what is observed in the dendrites of cortical L5 neurons (Zhang et al., 2014). These findings emphasize the non-uniformity of excitability changes caused by FMRP loss, which affects intrinsic membrane excitability in a brain region- and cell type-specific manner.

4.3 The potential role of FMRP in α-Syn related disease

FXS is the most common inherited form of human intellectual disability including low IQ, learning disabilities, perseverative behaviors, hyperactivity, impulsivity, and disrupted sleep (Del Tredici & Braak, 2016). The majority of these signs and symptoms may be explained by circuit hyper-excitability (Brichta & Greengard, 2014) further reflected by hypersensitivity to sensory stimuli and hyper-arousal to seizures. In FXS, the dysregulated protein translation is proposed to perturb neuronal function by disrupting synaptic maturation and plasticity and eventually altering network activity throughout the brain in a cell-type (Bhakar et al., 2012; M. R. Brown et al., 2010) and the compartment-specific way (Froula et al., 2018). In our study, FMRP was found to be decreased in α-Syn overexpressed cultured dopaminergic neurons (**Figure 21**), which leads to an increased membrane abundance of N-type calcium channel and subsequent increased N-type-mediated calcium current (**Figure 14** and **Figure 31**). The consequence of calcium overloading through N-type calcium channel and loss of FMRP in SNc DA neurons (**Figure 60**) are confounding factors inducing cell hyperexcitability (Surmeier, Obeso, & Halliday, 2017). Further research should be undertaken to investigate these channels in helping us to better understand the pathology of PD.

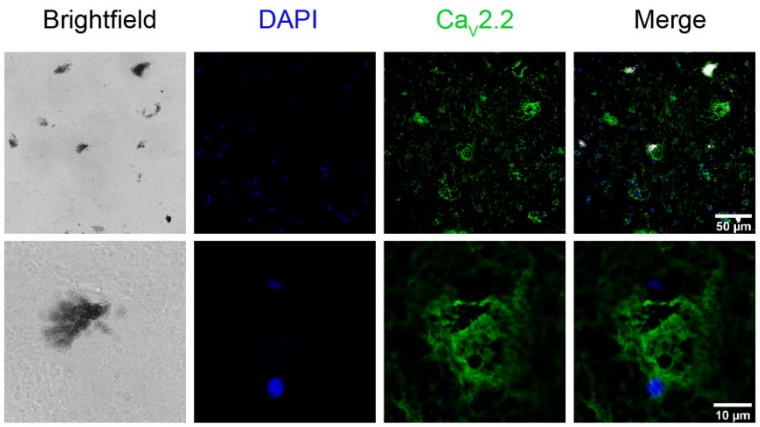

Figure 60 Human neuromelanin-positive SNc neurons contain N-type calcium channel. Immunofluorescent staining demonstrating the existence of N-type calcium channel subunits ($Ca_V2.2$) (green) in SNc neurons of post-mortem human brain tissue.

According to the metabotropic glutamate receptor (mGluR) theory, the loss of FMRP in FXS induces an exaggerated translation of synaptic plasticity-related mRNAs downstream group I mGluRs (Boivin et al., 2018). Besides, FMRP can also regulate some proteins through direct binding. For example, the carboxyl-terminal domain of FMRP has been recently shown to interact with the N-type calcium channel α1 subunit $Ca_V2.2$ to promote its proteasome-mediated destruction. Decreasing FMRP levels, therefore, reduced $Ca_V2.2$ degradation and led to an increased $Ca_V2.2$ membrane abundance and increased N-type-mediated calcium currents in dorsal root neurons. Other examples include the K^+ channels BK and Slack (Braak et al., 2003; Bruch et al., 2014; Ferron et al., 2014) that are regulated by FMRP independent from protein translation.

Different from FXS, *FMR1* did not exhibit hyper-methylation-induced transcriptional silencing in cultured neurons overexpressing α-Syn but appeared to be regulated through a mechanism involving PKC and CREB-driven transcription (**Figure 42-44**). *FMR1* KO mice were protected from reduced striatal DA release when injected with an α-Syn-overexpressing adeno-associated virus into the SNc (**Figure 49**), suggesting a protective effect of FMRP loss.

In addition to DA cell death in the SNc, an α-Syn associated neuronal malfunction has been also demonstrated in extra-striatal neuronal circuits, where it may contribute to the cognitive demise in PD or DLB (Ferreira et al., 2017; Froula et al., 2018; Nguyen & Krainc, 2018). Thus investigating FMRP in these circuits will also contribute to the understanding of the molecular events that account for neuronal dysfunction outside the basal ganglia in PD.

4.4 FMRP as an early biomarker for PD and a potential target for PD therapy

Based upon the neuropathological examination of iLBD and PD cases, Braak et al. proposed that in preclinical stages of PD, LBs appear first in either the olfactory bulb (OB) or the dorsal motor nucleus of the vagus (DMV) in the caudal medulla - two brain regions that have axons extending to the body surface. It is assumed that axons at these sites were exposed to a pathogens or infectious agents to cause LP and that this pathology then retrogradely spreads to neighboring neurons by passing from the infected cell to the next cell through synaptic connections, ultimately reaching the SNc where it is assumed to initiate the loss of neurons and thus symptom onset, before ultimately spreading to the forebrain by the end-stage (Bolam & Pissadaki, 2012; Ceravolo et al., 2005). The Braak staging is divided into 6 different stages that reflect a progression of LP from the DMV (Braak stage 1) and LC (Braak stage 2) to the SNc and amygdala (Braak stage 3) and ultimately reaching cortical areas (Braak stage 4-6) (Braak et al., 2003; Del Tredici & Braak, 2016). The Braak stages are correlated with the type and degree of clinical symptoms with disease progression. Whereas early stages are characterized by non-motor symptoms, the typical PD motor signs appear once the SNc is affected at Braak stages 4, and cognitive symptoms arise only as LP affects the cortex in Braak stages 5 and 6 (Jellinger, 2009).

In line with a prion-like spreading of LP, transplanted fetal DA neurons exhibited proteinaceous inclusions after years that strongly resembled LP (Costa et al., 2011; Darnell et al., 2011), which were interpreted as spread of LP from the host to the graft. In mice, synthetic, preformed α-Syn fibrils propagate from the site of stereotaxic injection to synaptically connected, neighboring structures, creating Lewy-like pathology (DelleDonne et al., 2008; Dragicevic, Schiemann, & Liss, 2015; Feng et al., 1997). Similarly, proteins extracted from human brains with LP and injected into the striatum of monkeys can retrograde propagate (Dury et al., 2013). In accord with a spread through anatomical defined connections, LP appears gradually in

defined anatomical structures during PD disease progression (Bloch et al., 2006; Bruch et al., 2017).

On the other hand, previous studies demonstrated that cell death and LP do not entirely correlate. For instance, there is neuronal death in the supraoptic nucleus, even though LP is not present there. By contrast, there is no discernible neuron loss in the neighboring, LP-laden tuberomammillary nucleus of the hypothalamus (Alisch et al., 2013). In patients who do not manifest dementia, the only cortical region that shows substantial neuronal death is the pre-supplementary motor cortex, where small intra-telencephalic pyramidal neurons degenerate in the absence of LP (Deng et al., 2013; Dolen et al., 2007). Furthermore, only about 50% of all PD patients have a distribution of LP in the brain that is consistent with the Braak staging model (M.-C. Chartier-Harlin et al., 2004). In conclusion, it is apparent that the cellular context is important for DA cell death and that the spreading of LP does not necessarily overlap with PD-associated pathology or disease progression.

Moreover, in patients with PD with genetic mutation-associated disease risk, the pattern of LP can be quite distinct from that of idiopathic PD. For instance, only a part of PD patients with a G2019S mutation in the LRRK2 gene manifest LP and most patients with other LRRK2 mutations even do not have LP (Chen, Wu, Mesri, & Chen, 2016). Another example are PD patients harbouring PARK2 mutations that have only sparsely distributed LP in older patients with a pattern that is distinct from that found in non-genetic PD cases (Budimirovic & Kaufmann, 2011).

The known disease phenotypes associated with *FMR1* are related to the expansion of CGG repeats and hypermethylation of *FMR1*. Conversely, *FMR1* is not subjected to epigenetic modifications in response to α-Syn because the methylation status of the *FMR1* promoter region remained unaffected by α-Syn overexpression in cultured neurons (**Figure 41**). In accordance with these results, FMRP was also lost in most neuromelanin-positive neurons of the SNc in

human post-mortem brain tissue from PD patients (**Figure 55**). Surprisingly, we found a similar reduction of FMRP in cases that had no history of clinical PD and that had LBP restricted to the brain stem.

FMRP loss precedes LP and DA cell death, thus demonstrating a specific molecular event preceding LP in PD. In summary, these results suggest a new role for FMRP in the disease progression of LP-associated pathological conditions. A screening study in 56 FXTAS patients, in fact, revealed PD was the most frequent initial diagnosis (D. A. Hall et al., 2005). Based on our findings, future studies need to examine the usefulness of FMRP as a molecular biomarker for disease progression in PD. This is particularly important as only the characterization of early molecular changes will permit the development of disease-modifying therapies, that otherwise come too late, once the diseases progressed towards DA cell death.

5 Summary

Returning to the aims posed at the beginning of this dissertation, we investigated the role of FMRP, which has a pivotal role in regulating neuronal gene expression through mRNA binding in FXS, in different models of PD including PD patients' brain tissue. The most significant finding to emerge from this study is that the expression of FMRP is decreased in response to α-Syn overexpression in vitro and in mouse model. The loss of FMRP also present in all Braak stages of PD cases. As the consequence of FMRP loss, dopaminergic LUHMES cells show hyper-activation of mTOR and ERK pathway which reminiscent of FXS (**Figure 61**). Meanwhile, FMRP also activate N-type calcium channel, suggesting a disrupted ion homeostasis in DA neurons in the early stage of PD. In summary, our work highlights the important role of FMRP in the development of PD pathology and other α-Syn associated diseases.

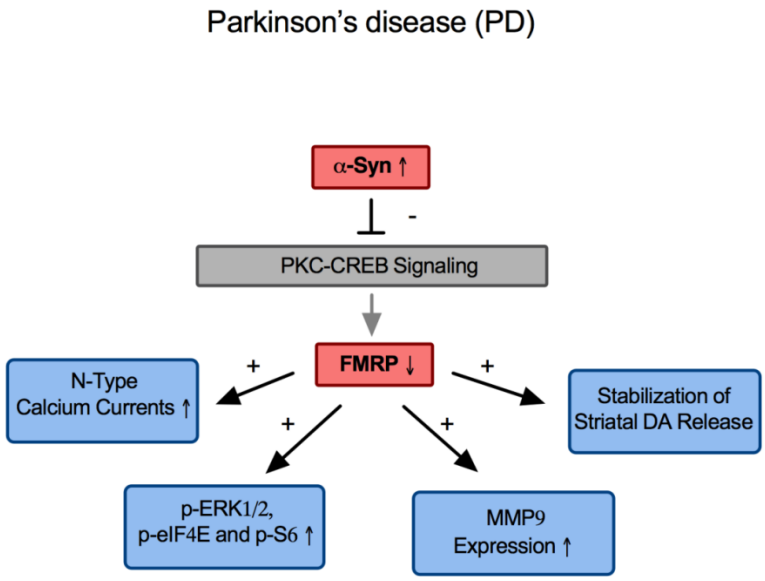

Figure 61 Schematic depict how α-Syn regulate indicated proteins through modulating FRMP. α-Syn overexpression decreases the expression of FMRP through inhibiting PKC-CREB pathway. Reduced FMRP results in an increased calcium influx through modulating N-type calcium channel, an activated eIF4E and ERK pathway, increased overall protein synthesis, and an increased MMP9 expression.

6 Bibliography

Adamczyk, A., & Strosznajder, J. B. (2006). Alpha-synuclein potentiates Ca2+ influx through voltage-dependent Ca2+ channels. *Neuroreport, 17*(18), 1883-1886. doi: 10.1097/WNR.0b013e3280115185

Adamowicz, D. H., Roy, S., Salmon, D. P., Galasko, D. R., Hansen, L. A., Masliah, E., & Gage, F. H. (2017). Hippocampal alpha-Synuclein in Dementia with Lewy Bodies Contributes to Memory Impairment and Is Consistent with Spread of Pathology. *J Neurosci, 37*(7), 1675-1684. doi: 10.1523/JNEUROSCI.3047-16.2016

Alegre-Abarrategui, J., Brimblecombe, K. R., Roberts, R. F., Velentza-Almpani, E., Tilley, B. S., Bengoa-Vergniory, N., & Proukakis, C. (2019). Selective vulnerability in alpha-synucleinopathies. *Acta Neuropathol*. doi: 10.1007/s00401-019-02010-2

Alisch, R. S., Wang, T., Chopra, P., Visootsak, J., Conneely, K. N., & Warren, S. T. (2013). Genome-wide analysis validates aberrant methylation in fragile X syndrome is specific to the FMR1 locus. *BMC Med Genet, 14*, 18. doi: 10.1186/1471-2350-14-18

Arawaka, S., Wada, M., Goto, S., Karube, H., Sakamoto, M., Ren, C. H., . . . Kato, T. (2006). The role of G-protein-coupled receptor kinase 5 in pathogenesis of sporadic Parkinson's disease. *J Neurosci, 26*(36), 9227-9238. doi: 10.1523/JNEUROSCI.0341-06.2006

Arsenault, J., Gholizadeh, S., Niibori, Y., Pacey, L. K., Halder, S. K., Koxhioni, E., . . . Hampson, D. R. (2016). FMRP Expression Levels in Mouse Central Nervous System Neurons Determine Behavioral Phenotype. *Hum Gene Ther, 27*(12), 982-996. doi: 10.1089/hum.2016.090

Aryee, M. J., Jaffe, A. E., Corrada-Bravo, H., Ladd-Acosta, C., Feinberg, A. P., Hansen, K. D., & Irizarry, R. A. (2014). Minfi: a flexible and comprehensive Bioconductor package for the analysis of Infinium DNA methylation microarrays. *Bioinformatics, 30*(10), 1363-1369. doi: 10.1093/bioinformatics/btu049

Ashley, C. T., Jr., Wilkinson, K. D., Reines, D., & Warren, S. T. (1993). FMR1 protein: conserved RNP family domains and selective RNA binding. *Science, 262*(5133), 563-566.

Auluck, P. K., Caraveo, G., & Lindquist, S. (2010). alpha-Synuclein: membrane interactions and toxicity in Parkinson's disease. *Annu Rev Cell Dev Biol, 26*, 211-233. doi: 10.1146/annurev.cellbio.042308.113313

Bagni, C., Tassone, F., Neri, G., & Hagerman, R. (2012). Fragile X syndrome: causes, diagnosis, mechanisms, and therapeutics. *J Clin Invest, 122*(12), 4314-4322. doi: 10.1172/JCI63141

Bartels, T., Choi, J. G., & Selkoe, D. J. (2011). alpha-Synuclein occurs physiologically as a helically folded tetramer that resists aggregation. *Nature, 477*(7362), 107-110. doi: 10.1038/nature10324

Berg, D., Postuma, R. B., Bloem, B., Chan, P., Dubois, B., Gasser, T., . . . Deuschl, G. (2014). Time to redefine PD? Introductory statement of the MDS Task Force on the definition of Parkinson's disease. *Mov Disord, 29*(4), 454-462. doi: 10.1002/mds.25844

Beyer, K., Domingo-Sabat, M., & Ariza, A. (2009). Molecular pathology of Lewy body diseases. *Int J Mol Sci, 10*(3), 724-745. doi: 10.3390/ijms10030724

Bhakar, A. L., Dolen, G., & Bear, M. F. (2012). The pathophysiology of fragile X (and what it teaches us about synapses). *Annu Rev Neurosci, 35*, 417-443. doi: 10.1146/annurev-neuro-060909-153138

Bhattacharya, A., Kaphzan, H., Alvarez-Dieppa, A. C., Murphy, J. P., Pierre, P., & Klann, E. (2012). Genetic removal of p70 S6 kinase 1 corrects molecular, synaptic, and behavioral phenotypes in fragile X syndrome mice. *Neuron, 76*(2), 325-337. doi: 10.1016/j.neuron.2012.07.022

Bloch, A., Probst, A., Bissig, H., Adams, H., & Tolnay, M. (2006). Alpha-synuclein pathology of the spinal and peripheral autonomic nervous system in neurologically unimpaired elderly subjects. *Neuropathol Appl Neurobiol, 32*(3), 284-295. doi: 10.1111/j.1365-2990.2006.00727.x

Bohnen, N. I., & Albin, R. L. (2011). The cholinergic system and Parkinson disease. *Behav Brain Res, 221*(2), 564-573. doi: 10.1016/j.bbr.2009.12.048

Boivin, M., Willemsen, R., Hukema, R. K., & Sellier, C. (2018). Potential pathogenic mechanisms underlying Fragile X Tremor Ataxia Syndrome: RAN translation and/or RNA gain-of-function? *Eur J Med Genet, 61*(11), 674-679. doi: 10.1016/j.ejmg.2017.11.001

Bolam, J. P., & Pissadaki, E. K. (2012). Living on the edge with too many mouths to feed: why dopamine neurons die. *Mov Disord, 27*(12), 1478-1483. doi: 10.1002/mds.25135

Braak, H., Del Tredici, K., Rub, U., de Vos, R. A., Jansen Steur, E. N., & Braak, E. (2003). Staging of brain pathology related to sporadic Parkinson's disease. *Neurobiol Aging, 24*(2), 197-211.

Braak, H., Ghebremedhin, E., Rub, U., Bratzke, H., & Del Tredici, K. (2004). Stages in the development of Parkinson's disease-related pathology. *Cell Tissue Res, 318*(1), 121-134. doi: 10.1007/s00441-004-0956-9

Brager, D. H., Akhavan, A. R., & Johnston, D. (2012). Impaired dendritic expression and plasticity of h-channels in the fmr1(-/y) mouse model of fragile X syndrome. *Cell Rep, 1*(3), 225-233. doi: 10.1016/j.celrep.2012.02.002

Brichta, L., & Greengard, P. (2014). Molecular determinants of selective dopaminergic vulnerability in Parkinson's disease: an update. *Front Neuroanat, 8*, 152. doi: 10.3389/fnana.2014.00152

Brown, M. R., Kronengold, J., Gazula, V. R., Chen, Y., Strumbos, J. G., Sigworth, F. J., . . . Kaczmarek, L. K. (2010). Fragile X mental retardation protein controls gating of the sodium-activated potassium channel Slack. *Nat Neurosci, 13*(7), 819-821. doi: 10.1038/nn.2563

Brown, V., Jin, P., Ceman, S., Darnell, J. C., O'Donnell, W. T., Tenenbaum, S. A., . . . Warren, S. T. (2001). Microarray identification of FMRP-associated brain mRNAs and altered mRNA translational profiles in fragile X syndrome. *Cell, 107*(4), 477-487.

Bruch, J., Xu, H., De Andrade, A., & Hoglinger, G. (2014). Mitochondrial complex 1 inhibition increases 4-repeat isoform tau by SRSF2 upregulation. *PLoS One, 9*(11), e113070. doi: 10.1371/journal.pone.0113070

Bruch, J., Xu, H., Rosler, T. W., De Andrade, A., Kuhn, P. H., Lichtenthaler, S. F., . . . Hoglinger, G. U. (2017). PERK activation mitigates tau pathology in vitro and in vivo. *EMBO Mol Med*. doi: 10.15252/emmm.201606664

Brys, I., Nunes, J., & Fuentes, R. (2017). Motor deficits and beta oscillations are dissociable in an alpha-synuclein model of Parkinson's disease. *Eur J Neurosci*. doi: 10.1111/ejn.13568

Budimirovic, D. B., & Kaufmann, W. E. (2011). What can we learn about autism from studying fragile X syndrome? *Dev Neurosci, 33*(5), 379-394. doi: 10.1159/000330213

Buraei, Z., & Yang, J. (2013). Structure and function of the beta subunit of voltage-gated Ca(2)(+) channels. *Biochim Biophys Acta, 1828*(7), 1530-1540. doi: 10.1016/j.bbamem.2012.08.028

Burre, J., Sharma, M., Tsetsenis, T., Buchman, V., Etherton, M. R., & Sudhof, T. C. (2010). Alpha-synuclein promotes SNARE-complex assembly in vivo and in vitro. *Science, 329*(5999), 1663-1667. doi: 10.1126/science.1195227

Caku, A., Pellerin, D., Bouvier, P., Riou, E., & Corbin, F. (2014). Effect of lovastatin on behavior in children and adults with fragile X syndrome: an open-label study. *Am J Med Genet A, 164A*(11), 2834-2842. doi: 10.1002/ajmg.a.36750

Calabresi, P., Picconi, B., Tozzi, A., Ghiglieri, V., & Di Filippo, M. (2014). Direct and indirect pathways of basal ganglia: a critical reappraisal. *Nat Neurosci, 17*(8), 1022-1030. doi: 10.1038/nn.3743

Campelo, C., & Silva, R. H. (2017). Genetic Variants in SNCA and the Risk of Sporadic Parkinson's Disease and Clinical Outcomes: A Review. *Parkinsons Dis, 2017*, 4318416. doi: 10.1155/2017/4318416

Candelise, N., Schmitz, M., Llorens, F., Villar-Pique, A., Cramm, M., Thom, T., . . . Zerr, I. (2019). Seeding variability of different alpha synuclein strains in synucleinopathies. *Ann Neurol, 85*(5), 691-703. doi: 10.1002/ana.25446

Carbone, C., Costa, A., Provensi, G., Mannaioni, G., & Masi, A. (2017). The Hyperpolarization-Activated Current Determines Synaptic Excitability, Calcium Activity and Specific Viability of Substantia Nigra Dopaminergic Neurons. *Front Cell Neurosci, 11*, 187. doi: 10.3389/fncel.2017.00187

Castagnola, S., Delhaye, S., Folci, A., Paquet, A., Brau, F., Duprat, F., . . . Maurin, T. (2018). New Insights Into the Role of Cav2 Protein Family in Calcium Flux Deregulation in Fmr1-KO Neurons. *Front Mol Neurosci, 11*, 342. doi: 10.3389/fnmol.2018.00342

Castellani, R., Smith, M. A., Richey, P. L., & Perry, G. (1996). Glycoxidation and oxidative stress in Parkinson disease and diffuse Lewy body disease. *Brain Res, 737*(1-2), 195-200.

Ceman, S., O'Donnell, W. T., Reed, M., Patton, S., Pohl, J., & Warren, S. T. (2003). Phosphorylation influences the translation state of FMRP-associated polyribosomes. *Hum Mol Genet, 12*(24), 3295-3305. doi: 10.1093/hmg/ddg350

Ceravolo, R., Antonini, A., Volterrani, D., Rossi, C., Goldwurm, S., Di Maria, E., . . . Murri, L. (2005). Dopamine transporter imaging study in parkinsonism occurring in fragile X premutation carriers. *Neurology, 65*(12), 1971-1973. doi: 10.1212/01.wnl.0000188821.51055.52

Chan, C. S., Guzman, J. N., Ilijic, E., Mercer, J. N., Rick, C., Tkatch, T., . . . Surmeier, D. J. (2007). 'Rejuvenation' protects neurons in mouse models of Parkinson's disease. *Nature, 447*(7148), 1081-1086. doi: 10.1038/nature05865

Chartier-Harlin, M.-C., Kachergus, J., Roumier, C., Mouroux, V., Douay, X., Lincoln, S., . . . Destée, A. (2004). α-Synuclein locus duplication as a cause of familial Parkinson's disease. *The Lancet, 364*(9440), 1167-1169. doi: 10.1016/s0140-6736(04)17103-1

Chartier-Harlin, M. C., Dachsel, J. C., Vilarino-Guell, C., Lincoln, S. J., Lepretre, F., Hulihan, M. M., . . . Farrer, M. J. (2011). Translation initiator EIF4G1 mutations in familial Parkinson disease. *Am J Hum Genet, 89*(3), 398-406. doi: 10.1016/j.ajhg.2011.08.009

Chen, Y. C., Wu, Y. R., Mesri, M., & Chen, C. M. (2016). Associations of Matrix Metalloproteinase-9 and Tissue Inhibitory Factor-1 Polymorphisms With Parkinson Disease in Taiwan. *Medicine (Baltimore), 95*(5), e2672. doi: 10.1097/MD.0000000000002672

Cilia, R., Kraff, J., Canesi, M., Pezzoli, G., Goldwurm, S., Amiri, K., . . . Tassone, F. (2009). Screening for the presence of FMR1 premutation alleles in women with parkinsonism. *Arch Neurol, 66*(2), 244-249. doi: 10.1001/archneurol.2008.548

Contractor, A., Klyachko, V. A., & Portera-Cailliau, C. (2015). Altered Neuronal and Circuit Excitability in Fragile X Syndrome. *Neuron, 87*(4), 699-715. doi: 10.1016/j.neuron.2015.06.017

Costa, A., Gao, L., Carrillo, F., Caceres-Redondo, M. T., Carballo, M., Diaz-Martin, J., . . . Pintado, E. (2011). Intermediate alleles at the FRAXA and FRAXE loci in Parkinson's disease. *Parkinsonism Relat Disord, 17*(4), 281-284. doi: 10.1016/j.parkreldis.2010.12.013

Covell, D. J., Robinson, J. L., Akhtar, R. S., Grossman, M., Weintraub, D., Bucklin, H. M., . . . Lee, V. M. (2017). Novel conformation-selective alpha-synuclein antibodies raised against different in vitro fibril forms show distinct patterns of Lewy pathology in Parkinson's disease. *Neuropathol Appl Neurobiol*. doi: 10.1111/nan.12402

Cuervo, A. M., Stefanis, L., Fredenburg, R., Lansbury, P. T., & Sulzer, D. (2004). Impaired degradation of mutant alpha-synuclein by chaperone-mediated autophagy. *Science, 305*(5688), 1292-1295. doi: 10.1126/science.1101738

Dai, S., Hall, D. D., & Hell, J. W. (2009). Supramolecular assemblies and localized regulation of voltage-gated ion channels. *Physiol Rev, 89*(2), 411-452. doi: 10.1152/physrev.00029.2007

Damier, P., Hirsch, E. C., Agid, Y., & Graybiel, A. M. (1999). The substantia nigra of the human brain. II. Patterns of loss of dopamine-containing neurons in Parkinson's disease. *Brain, 122 (Pt 8)*, 1437-1448. doi: 10.1093/brain/122.8.1437

Danesi, C., Achuta, V. S., Corcoran, P., Peteri, U. K., Turconi, G., Matsui, N., . . . Castren, M. L. (2018). Increased Calcium Influx through L-type Calcium Channels in Human and Mouse Neural Progenitors Lacking Fragile X Mental Retardation Protein. *Stem Cell Reports*. doi: 10.1016/j.stemcr.2018.11.003

Danzer, K. M., Haasen, D., Karow, A. R., Moussaud, S., Habeck, M., Giese, A., . . . Kostka, M. (2007). Different species of alpha-synuclein oligomers induce calcium influx and seeding. *J Neurosci, 27*(34), 9220-9232. doi: 10.1523/JNEUROSCI.2617-07.2007

Darnell, J. C., Van Driesche, S. J., Zhang, C., Hung, K. Y., Mele, A., Fraser, C. E., . . . Darnell, R. B. (2011). FMRP stalls ribosomal translocation on mRNAs linked to synaptic function and autism. *Cell, 146*(2), 247-261. doi: 10.1016/j.cell.2011.06.013

Dauer, W., & Przedborski, S. (2003). Parkinson's disease: mechanisms and models. *Neuron, 39*(6), 889-909.

Davis, J. K., & Broadie, K. (2017). Multifarious Functions of the Fragile X Mental Retardation Protein. *Trends Genet, 33*(10), 703-714. doi: 10.1016/j.tig.2017.07.008

De Pablo-Fernandez, E., Doherty, K. M., Holton, J. L., Revesz, T., Djamshidian, A., Limousin, P., . . . Ling, H. (2015). Concomitant fragile X-associated tremor ataxia syndrome and Parkinson's disease: a clinicopathological report of two cases. *J Neurol Neurosurg Psychiatry, 86*(8), 934-936. doi: 10.1136/jnnp-2014-309460

De Pablo-Fernandez, E., Lees, A. J., Holton, J. L., & Warner, T. T. (2019). Prognosis and Neuropathologic Correlation of Clinical Subtypes of Parkinson Disease. *JAMA Neurol*. doi: 10.1001/jamaneurol.2018.4377

De Rubeis, S., & Bagni, C. (2011). Regulation of molecular pathways in the Fragile X Syndrome: insights into Autism Spectrum Disorders. *J Neurodev Disord, 3*(3), 257-269. doi: 10.1007/s11689-011-9087-2

Del Rey, N. L., Quiroga-Varela, A., Garbayo, E., Carballo-Carbajal, I., Fernandez-Santiago, R., Monje, M. H. G., . . . Blesa, J. (2018). Advances in Parkinson's Disease: 200 Years Later. *Front Neuroanat, 12*, 113. doi: 10.3389/fnana.2018.00113

Del Tredici, K., & Braak, H. (2016). Review: Sporadic Parkinson's disease: development and distribution of alpha-synuclein pathology. *Neuropathol Appl Neurobiol, 42*(1), 33-50. doi: 10.1111/nan.12298

Delic, V., Chandra, S., Abdelmotilib, H., Maltbie, T., Wang, S., Kem, D., . . . West, A. B. (2018). Sensitivity and specificity of phospho-Ser129 alpha-synuclein monoclonal antibodies. *J Comp Neurol, 526*(12), 1978-1990. doi: 10.1002/cne.24468

DelleDonne, A., Klos, K. J., Fujishiro, H., Ahmed, Z., Parisi, J. E., Josephs, K. A., . . . Dickson, D. W. (2008). Incidental Lewy body disease and preclinical Parkinson disease. *Arch Neurol, 65*(8), 1074-1080. doi: 10.1001/archneur.65.8.1074

Deng, P. Y., Rotman, Z., Blundon, J. A., Cho, Y., Cui, J., Cavalli, V., . . . Klyachko, V. A. (2013). FMRP regulates neurotransmitter release and synaptic information transmission by modulating action potential duration via BK channels. *Neuron, 77*(4), 696-711. doi: 10.1016/j.neuron.2012.12.018

Dictenberg, J. B., Swanger, S. A., Antar, L. N., Singer, R. H., & Bassell, G. J. (2008). A direct role for FMRP in activity-dependent dendritic mRNA transport links filopodial-spine morphogenesis to fragile X syndrome. *Dev Cell, 14*(6), 926-939. doi: 10.1016/j.devcel.2008.04.003

Dijkstra, A. A., Voorn, P., Berendse, H. W., Groenewegen, H. J., Netherlands Brain, B., Rozemuller, A. J., & van de Berg, W. D. (2014). Stage-dependent nigral neuronal loss in incidental Lewy body and Parkinson's disease. *Mov Disord, 29*(10), 1244-1251. doi: 10.1002/mds.25952

Dolen, G., Osterweil, E., Rao, B. S., Smith, G. B., Auerbach, B. D., Chattarji, S., & Bear, M. F. (2007). Correction of fragile X syndrome in mice. *Neuron, 56*(6), 955-962. doi: 10.1016/j.neuron.2007.12.001

Dolphin, A. C. (2009). Calcium channel diversity: multiple roles of calcium channel subunits. *Curr Opin Neurobiol, 19*(3), 237-244. doi: 10.1016/j.conb.2009.06.006

Doria, M., Maugest, L., Moreau, T., Lizard, G., & Vejux, A. (2016). Contribution of cholesterol and oxysterols to the pathophysiology of Parkinson's disease. *Free Radic Biol Med, 101*, 393-400. doi: 10.1016/j.freeradbiomed.2016.10.008

Doty, R. L. (2012). Olfactory dysfunction in Parkinson disease. *Nat Rev Neurol, 8*(6), 329-339. doi: 10.1038/nrneurol.2012.80

Dragicevic, E., Schiemann, J., & Liss, B. (2015). Dopamine midbrain neurons in health and Parkinson's disease: emerging roles of voltage-gated calcium channels and ATP-sensitive potassium channels. *Neuroscience, 284*, 798-814. doi: 10.1016/j.neuroscience.2014.10.037

Duda, J., Potschke, C., & Liss, B. (2016). Converging roles of ion channels, calcium, metabolic stress, and activity pattern of Substantia nigra dopaminergic neurons in health and Parkinson's disease. *J Neurochem, 139 Suppl 1*, 156-178. doi: 10.1111/jnc.13572

Dury, A. Y., El Fatimy, R., Tremblay, S., Rose, T. M., Cote, J., De Koninck, P., & Khandjian, E. W. (2013). Nuclear Fragile X Mental Retardation Protein is localized to Cajal bodies. *PLoS Genet, 9*(10), e1003890. doi: 10.1371/journal.pgen.1003890

Ebrahimi, S. S., Oryan, S., Izadpanah, E., & Hassanzadeh, K. (2017). Thymoquinone exerts neuroprotective effect in animal model of Parkinson's disease. *Toxicol Lett, 276*, 108-114. doi: 10.1016/j.toxlet.2017.05.018

El-Agnaf, O., Overk, C., Rockenstein, E., Mante, M., Florio, J., Adame, A., . . . Rissman, R. A. (2017). Differential effects of immunotherapy with antibodies targeting alpha-synuclein oligomers and fibrils in a transgenic model of synucleinopathy. *Neurobiol Dis, 104*, 85-96. doi: 10.1016/j.nbd.2017.05.002

Elkouzi, A., Vedam-Mai, V., Eisinger, R. S., & Okun, M. S. (2019). Emerging therapies in Parkinson disease - repurposed drugs and new approaches. *Nat Rev Neurol, 15*(4), 204-223. doi: 10.1038/s41582-019-0155-7

Fay-Karmon, T., & Hassin-Baer, S. (2019). The spectrum of tremor among carriers of the FMR1 premutation with or without the fragile X-associated tremor/ataxia syndrome (FXTAS). *Parkinsonism Relat Disord*. doi: 10.1016/j.parkreldis.2019.05.010

Feng, Y., Gutekunst, C. A., Eberhart, D. E., Yi, H., Warren, S. T., & Hersch, S. M. (1997). Fragile X mental retardation protein: nucleocytoplasmic shuttling and association with somatodendritic ribosomes. *J Neurosci, 17*(5), 1539-1547.

Ferder, I., Parborell, F., Sundblad, V., Chiauzzi, V., Gomez, K., Charreau, E. H., . . . Dain, L. (2013). Expression of fragile X mental retardation protein and Fmr1 mRNA during folliculogenesis in the rat. *Reproduction, 145*(4), 335-343. doi: 10.1530/REP-12-0305

Ferreira, D. G., Temido-Ferreira, M., Vicente Miranda, H., Batalha, V. L., Coelho, J. E., Szego, E. M., . . . Outeiro, T. F. (2017). alpha-synuclein interacts with PrP(C) to induce cognitive impairment through mGluR5 and NMDAR2B. *Nat Neurosci, 20*(11), 1569-1579. doi: 10.1038/nn.4648

Ferron, L. (2016). Fragile X mental retardation protein controls ion channel expression and activity. *J Physiol*. doi: 10.1113/JP270675

Ferron, L., Nieto-Rostro, M., Cassidy, J. S., & Dolphin, A. C. (2014). Fragile X mental retardation protein controls synaptic vesicle exocytosis by modulating N-type calcium channel density. *Nat Commun, 5*, 3628. doi: 10.1038/ncomms4628

Follett, J., Darlow, B., Wong, M. B., Goodwin, J., & Pountney, D. L. (2013). Potassium depolarization and raised calcium induces alpha-synuclein aggregates. *Neurotox Res, 23*(4), 378-392. doi: 10.1007/s12640-012-9366-z

Froula, J. M., Henderson, B. W., Gonzalez, J. C., Vaden, J. H., McLean, J. W., Wu, Y., . . . Volpicelli-Daley, L. A. (2018). alpha-Synuclein fibril-induced paradoxical structural and functional defects in hippocampal neurons. *Acta Neuropathol Commun, 6*(1), 35. doi: 10.1186/s40478-018-0537-x

Fussi, N., Hollerhage, M., Chakroun, T., Nykanen, N. P., Rosler, T. W., Koeglsperger, T., . . . Hoglinger, G. U. (2018). Exosomal secretion of alpha-synuclein as protective mechanism after upstream blockage of macroautophagy. *Cell Death Dis, 9*(7), 757. doi: 10.1038/s41419-018-0816-2

Fyfe, I. (2017). Movement disorders: Comparison of cognitive impairment in Parkinson disease and essential tremor. *Nat Rev Neurol*. doi: 10.1038/nrneurol.2017.40

Gantois, I., Khoutorsky, A., Popic, J., Aguilar-Valles, A., Freemantle, E., Cao, R., . . . Sonenberg, N. (2017). Metformin ameliorates core deficits in a mouse model of fragile X syndrome. *Nat Med*. doi: 10.1038/nm.4335

Garber, K., Smith, K. T., Reines, D., & Warren, S. T. (2006). Transcription, translation and fragile X syndrome. *Curr Opin Genet Dev, 16*(3), 270-275. doi: 10.1016/j.gde.2006.04.010

Giasson, B. I., Murray, I. V., Trojanowski, J. Q., & Lee, V. M. (2001). A hydrophobic stretch of 12 amino acid residues in the middle of alpha-synuclein is essential for filament assembly. *J Biol Chem, 276*(4), 2380-2386. doi: 10.1074/jbc.M008919200

Gibb, W. R., & Lees, A. J. (1988). The relevance of the Lewy body to the pathogenesis of idiopathic Parkinson's disease. *J Neurol Neurosurg Psychiatry, 51*(6), 745-752. doi: 10.1136/jnnp.51.6.745

Giguere, N., Burke Nanni, S., & Trudeau, L. E. (2018). On Cell Loss and Selective Vulnerability of Neuronal Populations in Parkinson's Disease. *Front Neurol, 9*, 455. doi: 10.3389/fneur.2018.00455

Giri, A., Mok, K. Y., Jansen, I., Sharma, M., Tesson, C., Mangone, G., . . . Simon-Sanchez, J. (2017). Lack of evidence for a role of genetic variation in TMEM230 in the risk for Parkinson's disease in the Caucasian population. *Neurobiol Aging, 50*, 167 e111-167 e113. doi: 10.1016/j.neurobiolaging.2016.10.004

Goedert, M., Spillantini, M. G., Del Tredici, K., & Braak, H. (2013). 100 years of Lewy pathology. *Nat Rev Neurol, 9*(1), 13-24. doi: 10.1038/nrneurol.2012.242

Grassi, D., Howard, S., Zhou, M., Diaz-Perez, N., Urban, N. T., Guerrero-Given, D., . . . Lasmezas, C. I. (2018). Identification of a highly neurotoxic alpha-synuclein species inducing mitochondrial damage and mitophagy in Parkinson's disease. *Proc Natl Acad Sci U S A, 115*(11), E2634-E2643. doi: 10.1073/pnas.1713849115

Greco, C. M., Hagerman, R. J., Tassone, F., Chudley, A. E., Del Bigio, M. R., Jacquemont, S., . . . Hagerman, P. J. (2002). Neuronal intranuclear inclusions in a new cerebellar tremor/ataxia syndrome among fragile X carriers. *Brain, 125*(Pt 8), 1760-1771.

Gross, C., Banerjee, A., Tiwari, D., Longo, F., White, A. R., Allen, A. G., . . . Bassell, G. J. (2018). Isoform-selective phosphoinositide 3-kinase inhibition ameliorates a broad range

of fragile X syndrome-associated deficits in a mouse model. *Neuropsychopharmacology*. doi: 10.1038/s41386-018-0150-5

Guzman, J. N., Ilijic, E., Yang, B., Sanchez-Padilla, J., Wokosin, D., Galtieri, D., . . . Surmeier, D. J. (2018). Systemic isradipine treatment diminishes calcium-dependent mitochondrial oxidant stress. *J Clin Invest, 128*(6), 2266-2280. doi: 10.1172/JCI95898

Hafner, A. S., Donlin-Asp, P. G., Leitch, B., Herzog, E., & Schuman, E. M. (2019). Local protein synthesis is a ubiquitous feature of neuronal pre- and postsynaptic compartments. *Science, 364*(6441). doi: 10.1126/science.aau3644

Hagerman, P. J., & Hagerman, R. J. (2015). Fragile X-associated tremor/ataxia syndrome. *Ann N Y Acad Sci, 1338*, 58-70. doi: 10.1111/nyas.12693

Hagerman, R. J., & Hagerman, P. (2016). Fragile X-associated tremor/ataxia syndrome - features, mechanisms and management. *Nat Rev Neurol, 12*(7), 403-412. doi: 10.1038/nrneurol.2016.82

Hall, D., Pickler, L., Riley, K., Tassone, F., & Hagerman, R. (2010). Parkinsonism and cognitive decline in a fragile X mosaic male. *Mov Disord, 25*(10), 1523-1524. doi: 10.1002/mds.23150

Hall, D. A., Berry-Kravis, E., Jacquemont, S., Rice, C. D., Cogswell, J., Zhang, L., . . . Leehey, M. A. (2005). Initial diagnoses given to persons with the fragile X associated tremor/ataxia syndrome (FXTAS). *Neurology, 65*(2), 299-301. doi: 10.1212/01.wnl.0000168900.86323.9c

Hall, D. A., Howard, K., Hagerman, R., & Leehey, M. A. (2009). Parkinsonism in FMR1 premutation carriers may be indistinguishable from Parkinson disease. *Parkinsonism Relat Disord, 15*(2), 156-159. doi: 10.1016/j.parkreldis.2008.04.037

Hall, D. A., Jennings, D., Seibyl, J., Tassone, F., & Marek, K. (2010). FMR1 gene expansion and scans without evidence of dopaminergic deficits in parkinsonism patients. *Parkinsonism Relat Disord, 16*(9), 608-611. doi: 10.1016/j.parkreldis.2010.07.006

Halliday, G., Herrero, M. T., Murphy, K., McCann, H., Ros-Bernal, F., Barcia, C., . . . Obeso, J. A. (2009). No Lewy pathology in monkeys with over 10 years of severe MPTP Parkinsonism. *Mov Disord, 24*(10), 1519-1523. doi: 10.1002/mds.22481

Halliday, G. M., Blumbergs, P. C., Cotton, R. G., Blessing, W. W., & Geffen, L. B. (1990). Loss of brainstem serotonin- and substance P-containing neurons in Parkinson's disease. *Brain Res, 510*(1), 104-107. doi: 10.1016/0006-8993(90)90733-r

Halliday, G. M., McRitchie, D. A., Cartwright, H., Pamphlett, R., Hely, M. A., & Morris, J. G. (1996). Midbrain neuropathology in idiopathic Parkinson's disease and diffuse Lewy body disease. *J Clin Neurosci, 3*(1), 52-60.

Hasegawa, M., Nonaka, T., & Masuda-Suzukake, M. (2016). Prion-like mechanisms and potential therapeutic targets in neurodegenerative disorders. *Pharmacol Ther*. doi: 10.1016/j.pharmthera.2016.11.010

Hashimoto, M., Hsu, L. J., Xia, Y., Takeda, A., Sisk, A., Sundsmo, M., & Masliah, E. (1999). Oxidative stress induces amyloid-like aggregate formation of NACP/alpha-synuclein in vitro. *Neuroreport, 10*(4), 717-721.

Hashimoto, M., Takeda, A., Hsu, L. J., Takenouchi, T., & Masliah, E. (1999). Role of cytochrome c as a stimulator of alpha-synuclein aggregation in Lewy body disease. *J Biol Chem, 274*(41), 28849-28852. doi: 10.1074/jbc.274.41.28849

Hawkes, C. H., Del Tredici, K., & Braak, H. (2010). A timeline for Parkinson's disease. *Parkinsonism Relat Disord, 16*(2), 79-84. doi: 10.1016/j.parkreldis.2009.08.007

Hein, M. Y., Hubner, N. C., Poser, I., Cox, J., Nagaraj, N., Toyoda, Y., . . . Mann, M. (2015). A human interactome in three quantitative dimensions organized by stoichiometries and abundances. *Cell, 163*(3), 712-723. doi: 10.1016/j.cell.2015.09.053

Higashimori, H., Morel, L., Huth, J., Lindemann, L., Dulla, C., Taylor, A., . . . Yang, Y. (2013). Astroglial FMRP-dependent translational down-regulation of mGluR5 underlies glutamate transporter GLT1 dysregulation in the fragile X mouse. *Hum Mol Genet, 22*(10), 2041-2054. doi: 10.1093/hmg/ddt055

Hollerhage, M., Goebel, J. N., de Andrade, A., Hildebrandt, T., Dolga, A., Culmsee, C., . . . Hoglinger, G. U. (2014). Trifluoperazine rescues human dopaminergic cells from wild-type alpha-synuclein-induced toxicity. *Neurobiol Aging, 35*(7), 1700-1711. doi: 10.1016/j.neurobiolaging.2014.01.027

Hurley, M. J., & Dexter, D. T. (2012). Voltage-gated calcium channels and Parkinson's disease. *Pharmacol Ther, 133*(3), 324-333. doi: 10.1016/j.pharmthera.2011.11.006

Jalnapurkar, I., Cochran, D. M., & Frazier, J. A. (2019). New Therapeutic Options for Fragile X Syndrome. *Curr Treat Options Neurol, 21*(3), 12. doi: 10.1007/s11940-019-0551-8

Jellinger, K. A. (2009). A critical evaluation of current staging of alpha-synuclein pathology in Lewy body disorders. *Biochim Biophys Acta, 1792*(7), 730-740. doi: 10.1016/j.bbadis.2008.07.006

Jellinger, K. A., & Lantos, P. L. (2010). Papp-Lantos inclusions and the pathogenesis of multiple system atrophy: an update. *Acta Neuropathol, 119*(6), 657-667. doi: 10.1007/s00401-010-0672-3

Jeon, S. J., Han, S. H., Yang, S. I., Choi, J. W., Kwon, K. J., Park, S. H., . . . Shin, C. Y. (2012). Positive feedback regulation of Akt-FMRP pathway protects neurons from cell death. *J Neurochem, 123*(2), 226-238. doi: 10.1111/j.1471-4159.2012.07886.x

Jiang, P., & Dickson, D. W. (2018). Parkinson's disease: experimental models and reality. *Acta Neuropathol, 135*(1), 13-32. doi: 10.1007/s00401-017-1788-5

Kalia, L. V., & Lang, A. E. (2015). Parkinson's disease. *The Lancet, 386*(9996), 896-912. doi: 10.1016/s0140-6736(14)61393-3

Karampetsou, M., Ardah, M. T., Semitekolou, M., Polissidis, A., Samiotaki, M., Kalomoiri, M., . . . Vekrellis, K. (2017). Phosphorylated exogenous alpha-synuclein fibrils exacerbate pathology and induce neuronal dysfunction in mice. *Sci Rep, 7*(1), 16533. doi: 10.1038/s41598-017-15813-8

Kazdoba, T. M., Leach, P. T., Silverman, J. L., & Crawley, J. N. (2014). Modeling fragile X syndrome in the Fmr1 knockout mouse. *Intractable Rare Dis Res, 3*(4), 118-133. doi: 10.5582/irdr.2014.01024

Kim, M., Bellini, M., & Ceman, S. (2009). Fragile X mental retardation protein FMRP binds mRNAs in the nucleus. *Mol Cell Biol, 29*(1), 214-228. doi: 10.1128/MCB.01377-08

Kones, R. (2010). Parkinson's disease: mitochondrial molecular pathology, inflammation, statins, and therapeutic neuroprotective nutrition. *Nutr Clin Pract, 25*(4), 371-389. doi: 10.1177/0884533610373932

Kordower, J. H., Chu, Y., Hauser, R. A., Freeman, T. B., & Olanow, C. W. (2008). Lewy body-like pathology in long-term embryonic nigral transplants in Parkinson's disease. *Nat Med, 14*(5), 504-506. doi: 10.1038/nm1747

Kurtis, M. M., Rajah, T., Delgado, L. F., & Dafsari, H. S. (2017). The effect of deep brain stimulation on the non-motor symptoms of Parkinson's disease: a critical review of the current evidence. *NPJ Parkinsons Dis, 3*, 16024. doi: 10.1038/npjparkd.2016.24

Kuusisto, E., Parkkinen, L., & Alafuzoff, I. (2003). Morphogenesis of Lewy bodies: dissimilar incorporation of alpha-synuclein, ubiquitin, and p62. *J Neuropathol Exp Neurol, 62*(12), 1241-1253. doi: 10.1093/jnen/62.12.1241

Lai, D., Sakkas, D., & Huang, Y. (2006). The fragile X mental retardation protein interacts with a distinct mRNA nuclear export factor NXF2. *RNA, 12*(8), 1446-1449. doi: 10.1261/rna.94306

Lashuel, H. A., Overk, C. R., Oueslati, A., & Masliah, E. (2013). The many faces of alpha-synuclein: from structure and toxicity to therapeutic target. *Nat Rev Neurosci, 14*(1), 38-48. doi: 10.1038/nrn3406

Lazaro, D. F., Dias, M. C., Carija, A., Navarro, S., Madaleno, C. S., Tenreiro, S., . . . Outeiro, T. F. (2016). The effects of the novel A53E alpha-synuclein mutation on its oligomerization and aggregation. *Acta Neuropathol Commun, 4*(1), 128. doi: 10.1186/s40478-016-0402-8

Lee, B., Lee, K., Panda, S., Gonzales-Rojas, R., Chong, A., Bugay, V., . . . Lee, H. Y. (2018). Nanoparticle delivery of CRISPR into the brain rescues a mouse model of fragile X syndrome from exaggerated repetitive behaviours. *Nat Biomed Eng, 2*(7), 497-507. doi: 10.1038/s41551-018-0252-8

Lee, H. Y., Ge, W. P., Huang, W., He, Y., Wang, G. X., Rowson-Baldwin, A., . . . Jan, L. Y. (2011). Bidirectional regulation of dendritic voltage-gated potassium channels by the fragile X mental retardation protein. *Neuron, 72*(4), 630-642. doi: 10.1016/j.neuron.2011.09.033

Lemkau, L. R., Comellas, G., Kloepper, K. D., Woods, W. S., George, J. M., & Rienstra, C. M. (2012). Mutant protein A30P alpha-synuclein adopts wild-type fibril structure, despite slower fibrillation kinetics. *J Biol Chem, 287*(14), 11526-11532. doi: 10.1074/jbc.M111.306902

Li, J., Uversky, V. N., & Fink, A. L. (2001). Effect of familial Parkinson's disease point mutations A30P and A53T on the structural properties, aggregation, and fibrillation of human alpha-synuclein. *Biochemistry, 40*(38), 11604-11613. doi: 10.1021/bi010616g

Li, J. Y., Englund, E., Holton, J. L., Soulet, D., Hagell, P., Lees, A. J., . . . Brundin, P. (2008). Lewy bodies in grafted neurons in subjects with Parkinson's disease suggest host-to-graft disease propagation. *Nat Med, 14*(5), 501-503. doi: 10.1038/nm1746

Li, Y., Xu, M., Ding, X., Yan, C., Song, Z., Chen, L., . . . Yang, C. (2016). Protein kinase C controls lysosome biogenesis independently of mTORC1. *Nat Cell Biol, 18*(10), 1065-1077. doi: 10.1038/ncb3407

Lill, C. M. (2016). Genetics of Parkinson's disease. *Mol Cell Probes, 30*(6), 386-396. doi: 10.1016/j.mcp.2016.11.001

Liss, B., & Striessnig, J. (2019). The Potential of L-Type Calcium Channels as a Drug Target for Neuroprotective Therapy in Parkinson's Disease. *Annu Rev Pharmacol Toxicol, 59*, 263-289. doi: 10.1146/annurev-pharmtox-010818-021214

Liu, B., Li, Y., Stackpole, E. E., Novak, A., Gao, Y., Zhao, Y., . . . Richter, J. D. (2018). Regulatory discrimination of mRNAs by FMRP controls mouse adult neural stem cell differentiation. *Proc Natl Acad Sci U S A, 115*(48), E11397-E11405. doi: 10.1073/pnas.1809588115

Lubs, H. A. (1969). A marker X chromosome. *Am J Hum Genet, 21*(3), 231-244.

Mao, L. M., Tang, Q., & Wang, J. Q. (2007). Protein kinase C-regulated cAMP response element-binding protein phosphorylation in cultured rat striatal neurons. *Brain Res Bull, 72*(4-6), 302-308. doi: 10.1016/j.brainresbull.2007.01.009

Marat, A. L., Wallroth, A., Lo, W. T., Muller, R., Norata, G. D., Falasca, M., . . . Haucke, V. (2017). mTORC1 activity repression by late endosomal phosphatidylinositol 3,4-bisphosphate. *Science, 356*(6341), 968-972. doi: 10.1126/science.aaf8310

Marin, R., Fabelo, N., Martin, V., Garcia-Esparcia, P., Ferrer, I., Quinto-Alemany, D., & Diaz, M. (2017). Anomalies occurring in lipid profiles and protein distribution in frontal cortex lipid rafts in dementia with Lewy bodies disclose neurochemical traits partially shared by Alzheimer's and Parkinson's diseases. *Neurobiol Aging, 49*, 52-59. doi: 10.1016/j.neurobiolaging.2016.08.027

Maroteaux, L., Campanelli, J. T., & Scheller, R. H. (1988). Synuclein: a neuron-specific protein localized to the nucleus and presynaptic nerve terminal. *J Neurosci, 8*(8), 2804-2815.

Melo, T. Q., Copray, S., & Ferrari, M. F. R. (2018). Alpha-Synuclein Toxicity on Protein Quality Control, Mitochondria and Endoplasmic Reticulum. *Neurochem Res, 43*(12), 2212-2223. doi: 10.1007/s11064-018-2673-x

Miyashiro, K. Y., Beckel-Mitchener, A., Purk, T. P., Becker, K. G., Barret, T., Liu, L., . . . Eberwine, J. (2003). RNA cargoes associating with FMRP reveal deficits in cellular functioning in Fmr1 null mice. *Neuron, 37*(3), 417-431.

Moors, T. E., Hoozemans, J. J., Ingrassia, A., Beccari, T., Parnetti, L., Chartier-Harlin, M. C., & van de Berg, W. D. (2017). Therapeutic potential of autophagy-enhancing agents in Parkinson's disease. *Mol Neurodegener, 12*(1), 11. doi: 10.1186/s13024-017-0154-3

Morris, T. J., Butcher, L. M., Feber, A., Teschendorff, A. E., Chakravarthy, A. R., Wojdacz, T. K., & Beck, S. (2014). ChAMP: 450k Chip Analysis Methylation Pipeline. *Bioinformatics, 30*(3), 428-430. doi: 10.1093/bioinformatics/btt684

Napoli, I., Mercaldo, V., Boyl, P. P., Eleuteri, B., Zalfa, F., De Rubeis, S., . . . Bagni, C. (2008). The fragile X syndrome protein represses activity-dependent translation through CYFIP1, a new 4E-BP. *Cell, 134*(6), 1042-1054. doi: 10.1016/j.cell.2008.07.031

Narkiewicz, J., Giachin, G., & Legname, G. (2014). In vitro aggregation assays for the characterization of alpha-synuclein prion-like properties. *Prion, 8*(1), 19-32. doi: 10.4161/pri.28125

Nath, S., Goodwin, J., Engelborghs, Y., & Pountney, D. L. (2011). Raised calcium promotes alpha-synuclein aggregate formation. *Mol Cell Neurosci, 46*(2), 516-526. doi: 10.1016/j.mcn.2010.12.004

Nguyen, M., & Krainc, D. (2018). LRRK2 phosphorylation of auxilin mediates synaptic defects in dopaminergic neurons from patients with Parkinson's disease. *Proc Natl Acad Sci U S A, 115*(21), 5576-5581. doi: 10.1073/pnas.1717590115

Niere, F., & Raab-Graham, K. F. (2017). mTORC1 Is a Local, Postsynaptic Voltage Sensor Regulated by Positive and Negative Feedback Pathways. *Front Cell Neurosci, 11*, 152. doi: 10.3389/fncel.2017.00152

Niu, Y. Q., Yang, J. C., Hall, D. A., Leehey, M. A., Tassone, F., Olichney, J. M., . . . Zhang, L. (2014). Parkinsonism in fragile X-associated tremor/ataxia syndrome (FXTAS): revisited. *Parkinsonism Relat Disord, 20*(4), 456-459. doi: 10.1016/j.parkreldis.2014.01.006

Nordlund, J., Backlin, C. L., Wahlberg, P., Busche, S., Berglund, E. C., Eloranta, M. L., . . . Syvanen, A. C. (2013). Genome-wide signatures of differential DNA methylation in pediatric acute lymphoblastic leukemia. *Genome Biol, 14*(9), r105. doi: 10.1186/gb-2013-14-9-r105

Nuber, S., Rajsombath, M., Minakaki, G., Winkler, J., Muller, C. P., Ericsson, M., . . . Selkoe, D. J. (2018). Abrogating Native alpha-Synuclein Tetramers in Mice Causes a L-DOPA-Responsive Motor Syndrome Closely Resembling Parkinson's Disease. *Neuron, 100*(1), 75-90 e75. doi: 10.1016/j.neuron.2018.09.014

Oliveira, L. M., Falomir-Lockhart, L. J., Botelho, M. G., Lin, K. H., Wales, P., Koch, J. C., . . . Jovin, T. M. (2015). Elevated alpha-synuclein caused by SNCA gene triplication impairs neuronal differentiation and maturation in Parkinson's patient-derived induced pluripotent stem cells. *Cell Death Dis, 6*, e1994. doi: 10.1038/cddis.2015.318

Oliveras-Salva, M., Van der Perren, A., Casadei, N., Stroobants, S., Nuber, S., D'Hooge, R., . . . Baekelandt, V. (2013). rAAV2/7 vector-mediated overexpression of alpha-synuclein in mouse substantia nigra induces protein aggregation and progressive dose-dependent neurodegeneration. *Mol Neurodegener, 8*, 44. doi: 10.1186/1750-1326-8-44

Oostra, B. A., & Willemsen, R. (2003). A fragile balance: FMR1 expression levels. *Hum Mol Genet, 12 Spec No 2*, R249-257. doi: 10.1093/hmg/ddg298

Orr, A. A., Wordehoff, M. M., Hoyer, W., & Tamamis, P. (2016). Uncovering the Binding and Specificity of beta-Wrapins for Amyloid-beta and alpha-Synuclein. *J Phys Chem B, 120*(50), 12781-12794. doi: 10.1021/acs.jpcb.6b08485

Osterweil, E. K., Chuang, S. C., Chubykin, A. A., Sidorov, M., Bianchi, R., Wong, R. K., & Bear, M. F. (2013). Lovastatin corrects excess protein synthesis and prevents epileptogenesis in a mouse model of fragile X syndrome. *Neuron, 77*(2), 243-250. doi: 10.1016/j.neuron.2012.01.034

Osterweil, E. K., Krueger, D. D., Reinhold, K., & Bear, M. F. (2010). Hypersensitivity to mGluR5 and ERK1/2 leads to excessive protein synthesis in the hippocampus of a mouse model of fragile X syndrome. *J Neurosci, 30*(46), 15616-15627. doi: 10.1523/JNEUROSCI.3888-10.2010

Ostrerova, N., Petrucelli, L., Farrer, M., Mehta, N., Choi, P., Hardy, J., & Wolozin, B. (1999). alpha-Synuclein shares physical and functional homology with 14-3-3 proteins. *J Neurosci, 19*(14), 5782-5791.

Pacelli, C., Giguere, N., Bourque, M. J., Levesque, M., Slack, R. S., & Trudeau, L. E. (2015). Elevated Mitochondrial Bioenergetics and Axonal Arborization Size Are Key Contributors to the Vulnerability of Dopamine Neurons. *Curr Biol, 25*(18), 2349-2360. doi: 10.1016/j.cub.2015.07.050

Pan-Montojo, F., Schwarz, M., Winkler, C., Arnhold, M., O'Sullivan, G. A., Pal, A., . . . Reichmann, H. (2012). Environmental toxins trigger PD-like progression via increased alpha-synuclein release from enteric neurons in mice. *Sci Rep, 2*, 898. doi: 10.1038/srep00898

Parkinson, J. (1817). An essay on the shaking palsy.

Patil, S. P., Jain, P. D., Ghumatkar, P. J., Tambe, R., & Sathaye, S. (2014). Neuroprotective effect of metformin in MPTP-induced Parkinson's disease in mice. *Neuroscience, 277*, 747-754. doi: 10.1016/j.neuroscience.2014.07.046

Peelaerts, W., Bousset, L., Baekelandt, V., & Melki, R. (2018). a-Synuclein strains and seeding in Parkinson's disease, incidental Lewy body disease, dementia with Lewy bodies and multiple system atrophy: similarities and differences. *Cell Tissue Res, 373*(1), 195-212. doi: 10.1007/s00441-018-2839-5

Peelaerts, W., Bousset, L., Van der Perren, A., Moskalyuk, A., Pulizzi, R., Giugliano, M., . . . Baekelandt, V. (2015). alpha-Synuclein strains cause distinct synucleinopathies after local and systemic administration. *Nature, 522*(7556), 340-344. doi: 10.1038/nature14547

Peng, C., Gathagan, R. J., Covell, D. J., Medellin, C., Stieber, A., Robinson, J. L., . . . Lee, V. M. (2018). Cellular milieu imparts distinct pathological alpha-synuclein strains in alpha-synucleinopathies. *Nature, 557*(7706), 558-563. doi: 10.1038/s41586-018-0104-4

Perez-Villalba, A., Sirerol-Piquer, M. S., Belenguer, G., Soriano-Canton, R., Munoz-Manchado, A. B., Villadiego, J., . . . Farinas, I. (2018). Synaptic Regulator alpha-Synuclein in Dopaminergic Fibers Is Essentially Required for the Maintenance of Subependymal Neural Stem Cells. *J Neurosci, 38*(4), 814-825. doi: 10.1523/JNEUROSCI.2276-17.2017

Phillipson, O. T. (2017). Alpha-synuclein, epigenetics, mitochondria, metabolism, calcium traffic, & circadian dysfunction in Parkinson's disease. An integrated strategy for management. *Ageing Res Rev, 40*, 149-167. doi: 10.1016/j.arr.2017.09.006

Poewe, W., Seppi, K., Tanner, C. M., Halliday, G. M., Brundin, P., Volkmann, J., . . . Lang, A. E. (2017). Parkinson disease. *Nat Rev Dis Primers, 3*, 17013. doi: 10.1038/nrdp.2017.13

Ponzini, E., De Palma, A., Cerboni, L., Natalello, A., Rossi, R., Moons, R., . . . Grandori, R. (2019). Methionine oxidation in alpha-synuclein inhibits its propensity for ordered secondary structure. *J Biol Chem, 294*(14), 5657-5665. doi: 10.1074/jbc.RA118.001907

Postuma, R. B., & Berg, D. (2016). Advances in markers of prodromal Parkinson disease. *Nat Rev Neurol, 12*(11), 622-634. doi: 10.1038/nrneurol.2016.152

Prymaczok, N. C., Riek, R., & Gerez, J. (2016). More than a Rumor Spreads in Parkinson's Disease. *Front Hum Neurosci, 10*, 608. doi: 10.3389/fnhum.2016.00608

Puschmann, A., Ross, O. A., Vilarino-Guell, C., Lincoln, S. J., Kachergus, J. M., Cobb, S. A., . . . Nilsson, C. (2009). A Swedish family with de novo alpha-synuclein A53T mutation: evidence for early cortical dysfunction. *Parkinsonism Relat Disord, 15*(9), 627-632. doi: 10.1016/j.parkreldis.2009.06.007

Ray Chaudhuri, K., Qamar, M. A., Rajah, T., Loehrer, P., Sauerbier, A., Odin, P., & Jenner, P. (2016). Non-oral dopaminergic therapies for Parkinson's disease: current treatments and the future. *NPJ Parkinsons Dis, 2*, 16023. doi: 10.1038/npjparkd.2016.23

Rcom-H'cheo-Gauthier, A., Goodwin, J., & Pountney, D. L. (2014). Interactions between calcium and alpha-synuclein in neurodegeneration. *Biomolecules, 4*(3), 795-811. doi: 10.3390/biom4030795

Richter, J. D., Bassell, G. J., & Klann, E. (2015). Dysregulation and restoration of translational homeostasis in fragile X syndrome. *Nat Rev Neurosci, 16*(10), 595-605. doi: 10.1038/nrn4001

Rietdijk, C. D., Perez-Pardo, P., Garssen, J., van Wezel, R. J., & Kraneveld, A. D. (2017). Exploring Braak's Hypothesis of Parkinson's Disease. *Front Neurol, 8*, 37. doi: 10.3389/fneur.2017.00037

Rodriguez-Sabate, C., Sabate, M., Llanos, C., Morales, I., Sanchez, A., & Rodriguez, M. (2017). The functional connectivity in the motor loop of human basal ganglia. *Brain Imaging Behav, 11*(2), 417-429. doi: 10.1007/s11682-016-9512-y

Rodriguez, J. A., Ivanova, M. I., Sawaya, M. R., Cascio, D., Reyes, F. E., Shi, D., . . . Eisenberg, D. S. (2015). Structure of the toxic core of alpha-synuclein from invisible crystals. *Nature, 525*(7570), 486-490. doi: 10.1038/nature15368

Salat, U., Bardoni, B., Wohrle, D., & Steinbach, P. (2000). Increase of FMRP expression, raised levels of FMR1 mRNA, and clonal selection in proliferating cells with unmethylated fragile X repeat expansions: a clue to the sex bias in the transmission of full mutations? *J Med Genet, 37*(11), 842-850.

Schmidt, E. K., Clavarino, G., Ceppi, M., & Pierre, P. (2009). SUnSET, a nonradioactive method to monitor protein synthesis. *Nat Methods, 6*(4), 275-277. doi: 10.1038/nmeth.1314

Scholz, D., Poltl, D., Genewsky, A., Weng, M., Waldmann, T., Schildknecht, S., & Leist, M. (2011). Rapid, complete and large-scale generation of post-mitotic neurons from the human LUHMES cell line. *J Neurochem, 119*(5), 957-971. doi: 10.1111/j.1471-4159.2011.07255.x

Schrag, A., Sheikh, S., Quinn, N. P., Lees, A. J., Selai, C., Mathias, C., . . . Jahanshahi, M. (2010). A comparison of depression, anxiety, and health status in patients with progressive supranuclear palsy and multiple system atrophy. *Mov Disord, 25*(8), 1077-1081. doi: 10.1002/mds.22794

Schulz, J., Pagano, G., Fernandez Bonfante, J. A., Wilson, H., & Politis, M. (2018). Nucleus basalis of Meynert degeneration precedes and predicts cognitive impairment in Parkinson's disease. *Brain, 141*(5), 1501-1516. doi: 10.1093/brain/awy072

Sellier, C., Buijsen, R. A. M., He, F., Natla, S., Jung, L., Tropel, P., . . . Charlet-Berguerand, N. (2017). Translation of Expanded CGG Repeats into FMRpolyG Is Pathogenic and May Contribute to Fragile X Tremor Ataxia Syndrome. *Neuron, 93*(2), 331-347. doi: 10.1016/j.neuron.2016.12.016

Sgobio, C., Kupferschmidt, D. A., Cui, G., Sun, L., Li, Z., Cai, H., & Lovinger, D. M. (2014). Optogenetic measurement of presynaptic calcium transients using conditional genetically encoded calcium indicator expression in dopaminergic neurons. *PLoS One, 9*(10), e111749. doi: 10.1371/journal.pone.0111749

Sharma, A., Hoeffer, C. A., Takayasu, Y., Miyawaki, T., McBride, S. M., Klann, E., & Zukin, R. S. (2010). Dysregulation of mTOR signaling in fragile X syndrome. *J Neurosci, 30*(2), 694-702. doi: 10.1523/JNEUROSCI.3696-09.2010

Shen, M., Wang, F., Li, M., Sah, N., Stockton, M. E., Tidei, J. J., . . . Zhao, X. (2019). Reduced mitochondrial fusion and Huntingtin levels contribute to impaired dendritic maturation and behavioral deficits in Fmr1-mutant mice. *Nat Neurosci, 22*(3), 386-400. doi: 10.1038/s41593-019-0338-y

Sidhu, H., Dansie, L. E., Hickmott, P. W., Ethell, D. W., & Ethell, I. M. (2014). Genetic removal of matrix metalloproteinase 9 rescues the symptoms of fragile X syndrome in a mouse model. *J Neurosci, 34*(30), 9867-9879. doi: 10.1523/JNEUROSCI.1162-14.2014

Smyth, G. K. (2004). Linear models and empirical bayes methods for assessing differential expression in microarray experiments. *Stat Appl Genet Mol Biol, 3*, Article3. doi: 10.2202/1544-6115.1027

Soldner, F., Stelzer, Y., Shivalila, C. S., Abraham, B. J., Latourelle, J. C., Barrasa, M. I., . . . Jaenisch, R. (2016). Parkinson-associated risk variant in distal enhancer of alpha-synuclein modulates target gene expression. *Nature, 533*(7601), 95-99. doi: 10.1038/nature17939

Sorrentino, Z. A., Brooks, M. M. T., Hudson, V., 3rd, Rutherford, N. J., Golde, T. E., Giasson, B. I., & Chakrabarty, P. (2017). Intrastriatal injection of alpha-synuclein can lead to widespread synucleinopathy independent of neuroanatomic connectivity. *Mol Neurodegener, 12*(1), 40. doi: 10.1186/s13024-017-0182-z

Spillantini, M. G., Schmidt, M. L., Lee, V. M., Trojanowski, J. Q., Jakes, R., & Goedert, M. (1997). Alpha-synuclein in Lewy bodies. *Nature, 388*(6645), 839-840. doi: 10.1038/42166

Stacy, M. (2011). Nonmotor symptoms in Parkinson's disease. *Int J Neurosci, 121 Suppl 2*, 9-17. doi: 10.3109/00207454.2011.620196

Stefani, G., Fraser, C. E., Darnell, J. C., & Darnell, R. B. (2004). Fragile X mental retardation protein is associated with translating polyribosomes in neuronal cells. *J Neurosci, 24*(33), 7272-7276. doi: 10.1523/JNEUROSCI.2306-04.2004

Sunamura, N., Iwashita, S., Enomoto, K., Kadoshima, T., & Isono, F. (2018). Loss of the fragile X mental retardation protein causes aberrant differentiation in human neural progenitor cells. *Sci Rep, 8*(1), 11585. doi: 10.1038/s41598-018-30025-4

Surmeier, D. J., Obeso, J. A., & Halliday, G. M. (2017). Selective neuronal vulnerability in Parkinson disease. *Nat Rev Neurosci, 18*(2), 101-113. doi: 10.1038/nrn.2016.178

Tan, Y., Sgobio, C., Arzberger, T., Machleid, F., Tang, Q., Findeis, E., . . . Koeglsperger, T. (2019). Loss of fragile X mental retardation protein precedes Lewy pathology in Parkinson's disease. *Acta Neuropathol*. doi: 10.1007/s00401-019-02099-5

Teschendorff, A. E., Marabita, F., Lechner, M., Bartlett, T., Tegner, J., Gomez-Cabrero, D., & Beck, S. (2013). A beta-mixture quantile normalization method for correcting probe

design bias in Illumina Infinium 450 k DNA methylation data. *Bioinformatics, 29*(2), 189-196. doi: 10.1093/bioinformatics/bts680

Tian, Y., Morris, T. J., Webster, A. P., Yang, Z., Beck, S., Feber, A., & Teschendorff, A. E. (2017). ChAMP: updated methylation analysis pipeline for Illumina BeadChips. *Bioinformatics, 33*(24), 3982-3984. doi: 10.1093/bioinformatics/btx513

Tibar, H., El Bayad, K., Bouhouche, A., Ait Ben Haddou, E. H., Benomar, A., Yahyaoui, M., . . . Regragui, W. (2018). Non-Motor Symptoms of Parkinson's Disease and Their Impact on Quality of Life in a Cohort of Moroccan Patients. *Front Neurol, 9*, 170. doi: 10.3389/fneur.2018.00170

Tonges, L., Szego, E. M., Hause, P., Saal, K. A., Tatenhorst, L., Koch, J. C., . . . Lingor, P. (2014). Alpha-synuclein mutations impair axonal regeneration in models of Parkinson's disease. *Front Aging Neurosci, 6*, 239. doi: 10.3389/fnagi.2014.00239

Tranfaglia, M. R. (2011). The psychiatric presentation of fragile x: evolution of the diagnosis and treatment of the psychiatric comorbidities of fragile X syndrome. *Dev Neurosci, 33*(5), 337-348. doi: 10.1159/000329421

Tsang, B., Arsenault, J., Vernon, R. M., Lin, H., Sonenberg, N., Wang, L. Y., . . . Forman-Kay, J. D. (2019). Phosphoregulated FMRP phase separation models activity-dependent translation through bidirectional control of mRNA granule formation. *Proc Natl Acad Sci U S A*. doi: 10.1073/pnas.1814385116

Ulusoy, A., Phillips, R. J., Helwig, M., Klinkenberg, M., Powley, T. L., & Di Monte, D. A. (2016). Brain-to-stomach transfer of alpha-synuclein via vagal preganglionic projections. *Acta Neuropathol*. doi: 10.1007/s00401-016-1661-y

Veys, L., Vandenabeele, M., Ortuno-Lizaran, I., Baekelandt, V., Cuenca, N., Moons, L., & De Groef, L. (2019). Retinal alpha-synuclein deposits in Parkinson's disease patients and animal models. *Acta Neuropathol, 137*(3), 379-395. doi: 10.1007/s00401-018-01956-z

Visanji, N. P., Brotchie, J. M., Kalia, L. V., Koprich, J. B., Tandon, A., Watts, J. C., & Lang, A. E. (2016). alpha-Synuclein-Based Animal Models of Parkinson's Disease: Challenges and Opportunities in a New Era. *Trends Neurosci, 39*(11), 750-762. doi: 10.1016/j.tins.2016.09.003

Volpicelli-Daley, L. A., Kirik, D., Stoyka, L. E., Standaert, D. G., & Harms, A. S. (2016). How can rAAV-alpha-synuclein and the fibril alpha-synuclein models advance our understanding of Parkinson's disease? *J Neurochem, 139 Suppl 1*, 131-155. doi: 10.1111/jnc.13627

Volpicelli-Daley, L. A., Luk, K. C., & Lee, V. M. (2014). Addition of exogenous alpha-synuclein preformed fibrils to primary neuronal cultures to seed recruitment of endogenous alpha-synuclein to Lewy body and Lewy neurite-like aggregates. *Nat Protoc, 9*(9), 2135-2146. doi: 10.1038/nprot.2014.143

Wang, C. Y., Lai, M. D., Phan, N. N., Sun, Z., & Lin, Y. C. (2015). Meta-Analysis of Public Microarray Datasets Reveals Voltage-Gated Calcium Gene Signatures in Clinical Cancer Patients. *PLoS One, 10*(7), e0125766. doi: 10.1371/journal.pone.0125766

Wang, G., Achim, C. L., Hamilton, R. L., Wiley, C. A., & Soontornniyomkij, V. (1999). Tyramide signal amplification method in multiple-label immunofluorescence confocal microscopy. *Methods, 18*(4), 459-464. doi: 10.1006/meth.1999.0813

Wang, H., Morishita, Y., Miura, D., Naranjo, J. R., Kida, S., & Zhuo, M. (2012). Roles of CREB in the regulation of FMRP by group I metabotropic glutamate receptors in cingulate cortex. *Mol Brain, 5*, 27. doi: 10.1186/1756-6606-5-27

Wang, H., Pati, S., Pozzo-Miller, L., & Doering, L. C. (2015). Targeted pharmacological treatment of autism spectrum disorders: fragile X and Rett syndromes. *Front Cell Neurosci, 9*, 55. doi: 10.3389/fncel.2015.00055

Wang, H., Wu, L. J., Kim, S. S., Lee, F. J., Gong, B., Toyoda, H., . . . Zhuo, M. (2008). FMRP acts as a key messenger for dopamine modulation in the forebrain. *Neuron, 59*(4), 634-647. doi: 10.1016/j.neuron.2008.06.027

Wang, W., Nguyen, L. T., Burlak, C., Chegini, F., Guo, F., Chataway, T., . . . Hoang, Q. Q. (2016). Caspase-1 causes truncation and aggregation of the Parkinson's disease-associated protein alpha-synuclein. *Proc Natl Acad Sci U S A*. doi: 10.1073/pnas.1610099113

Wang, W., Perovic, I., Chittuluru, J., Kaganovich, A., Nguyen, L. T., Liao, J., . . . Hoang, Q. Q. (2011). A soluble alpha-synuclein construct forms a dynamic tetramer. *Proc Natl Acad Sci U S A, 108*(43), 17797-17802. doi: 10.1073/pnas.1113260108

Waskiewicz, A. J., Flynn, A., Proud, C. G., & Cooper, J. A. (1997). Mitogen-activated protein kinases activate the serine/threonine kinases Mnk1 and Mnk2. *EMBO J, 16*(8), 1909-1920. doi: 10.1093/emboj/16.8.1909

Waskiewicz, A. J., Johnson, J. C., Penn, B., Mahalingam, M., Kimball, S. R., & Cooper, J. A. (1999). Phosphorylation of the cap-binding protein eukaryotic translation initiation factor 4E by protein kinase Mnk1 in vivo. *Mol Cell Biol, 19*(3), 1871-1880. doi: 10.1128/mcb.19.3.1871

Winslow, A. R., Chen, C. W., Corrochano, S., Acevedo-Arozena, A., Gordon, D. E., Peden, A. A., . . . Rubinsztein, D. C. (2010). alpha-Synuclein impairs macroautophagy: implications for Parkinson's disease. *J Cell Biol, 190*(6), 1023-1037. doi: 10.1083/jcb.201003122

Yorgason, J. T., Espana, R. A., & Jones, S. R. (2011). Demon voltammetry and analysis software: analysis of cocaine-induced alterations in dopamine signaling using multiple kinetic measures. *J Neurosci Methods, 202*(2), 158-164. doi: 10.1016/j.jneumeth.2011.03.001

Zaichick, S. V., McGrath, K. M., & Caraveo, G. (2017). The role of Ca(2+) signaling in Parkinson's disease. *Dis Model Mech, 10*(5), 519-535. doi: 10.1242/dmm.028738

Zeng, Y., Adamson, R. H., Curry, F. R., & Tarbell, J. M. (2014). Sphingosine-1-phosphate protects endothelial glycocalyx by inhibiting syndecan-1 shedding. *Am J Physiol Heart Circ Physiol, 306*(3), H363-372. doi: 10.1152/ajpheart.00687.2013

Zhang, K., Li, Y. J., Guo, Y., Zheng, K. Y., Yang, Q., Yang, L., . . . Zhao, M. G. (2017). Elevated progranulin contributes to synaptic and learning deficit due to loss of fragile X mental retardation protein. *Brain, 140*(12), 3215-3232. doi: 10.1093/brain/awx265

Zhang, M., Mu, H., Shang, Z., Kang, K., Lv, H., Duan, L., . . . Zhang, R. (2017). Genome-wide pathway-based association analysis identifies risk pathways associated with Parkinson's disease. *Neuroscience, 340*, 398-410. doi: 10.1016/j.neuroscience.2016.11.004

Zhang, W., Xu, C., Tu, H., Wang, Y., Sun, Q., Hu, P., . . . Liu, J. (2015). GABAB receptor upregulates fragile X mental retardation protein expression in neurons. *Sci Rep, 5*, 10468. doi: 10.1038/srep10468

Zhao, W., Chuang, S. C., Bianchi, R., & Wong, R. K. (2011). Dual regulation of fragile X mental retardation protein by group I metabotropic glutamate receptors controls translation-dependent epileptogenesis in the hippocampus. *J Neurosci, 31*(2), 725-734. doi: 10.1523/JNEUROSCI.2915-10.2011

Zhou, W., Laird, P. W., & Shen, H. (2017). Comprehensive characterization, annotation and innovative use of Infinium DNA methylation BeadChip probes. *Nucleic Acids Res, 45*(4), e22. doi: 10.1093/nar/gkw967

Zhu, P. J., Chen, C. J., Mays, J., Stoica, L., & Costa-Mattioli, M. (2018). mTORC2, but not mTORC1, is required for hippocampal mGluR-LTD and associated behaviors. *Nat Neurosci, 21*(6), 799-802. doi: 10.1038/s41593-018-0156-7

7 Publication

Tan, Y., Sgobio, C., Arzberger, T., Machleid, F., Tang, Q., Findeis, E., . . . Koeglsperger, T. (2019). Loss of fragile X mental retardation protein precedes Lewy pathology in Parkinson's disease. Acta Neuropathol. doi: 10.1007/s00401-019-02099-5

8 Copyright authorization

Copyright Transfer 12.11.2019

Besuchen Sie uns: springer.com

Copyright Transfer Statement

Lieber Autor, liebe Autorin,

Hinweis: Sie haben dem Copyright Transfer Statement (CTS) zugestimmt und erhalten diese E-Mail für Ihre persönliche Ablage.

1. Publication
The copyright to this article, (including any supplementary information and graphic elements therein (e.g. illustrations, charts, moving images) (the 'Article'), is hereby assigned for good and valuable consideration to Springer-Verlag GmbH Germany, part of Springer Nature (the 'Assignee'). Headings are for convenience only.

2. Grant of Rights
In consideration of the Assignee evaluating the Article for publication, the Author(s) grant the Assignee without limitation the exclusive (except as set out in clauses 3, 4 and 5 a) iv), assignable and sub-licensable right, unlimited in time and territory, to copy-edit, reproduce, publish, distribute, transmit, make available and store the Article, including abstracts thereof, in all forms of media of expression now known or developed in the future, including pre- and reprints, translations, photographic reproductions and extensions. Furthermore, to enable additional publishing services, such as promotion of the Article, the Author(s) grant the Assignee the right to use the Article (including the use of any graphic elements on a stand-alone basis) in whole or in part in electronic form, such as for display in databases or data networks (e.g. the Internet), or for print or download to stationary or portable devices. This includes interactive and multimedia use as well as posting the Article in full or in part or its abstract on social media, and the right to alter the Article to the extent necessary for such use. The Assignee may also let third parties share the Article in full or in part or its abstract on social media and may in this context sub-license the Article and its abstract to social media users. Author(s) grant to Assignee the right to re-license Article metadata without restriction (including but not limited to author name, title, abstract, citation, references, keywords and any additional information as determined by Assignee).

3. Self-Archiving
Author(s) are permitted to self-archive a pre-print and an author's accepted manuscript version of their Article.

a. A pre-print is the author's version of the Article before peer-review has taken place ("Pre-Print"). Prior to acceptance for publication, Author(s) retain the right to make a Pre-Print of their Article available on any of the following: their own personal, self-maintained website; a legally compliant, non-commercial pre-print server such as but

not limited to arXiv and bioRxiv. Once the Article has been published, the Author(s) should update the acknowledgement and provide a link to the definitive version on the publisher's website: "This is a pre-print of an article published in [insert journal title]. The final authenticated version is available online at: https://doi.org/[insert DOI]".

b. An Author's Accepted Manuscript (AAM) is the version accepted for publication in a journal following peer review but prior to copyediting and typesetting that can be made available under the following conditions:
    a. Author(s) retain the right to make an AAM of their Article available on their own personal, self-maintained website immediately on acceptance,
    b. Author(s) retain the right to make an AAM of their Article available for public release on any of the following 12 months after first publication ("Embargo Period"): their employer's internal website; their institutional and/or funder repositories. AAMs may also be deposited in such repositories immediately on acceptance, provided that they are not made publicly available until after the Embargo Period.

An acknowledgement in the following form should be included, together with a link to the published version on the publisher's website: "This is a post-peer-review, pre-copyedit version of an article published in [insert journal title]. The final authenticated version is available online at: http://dx.doi.org/[insert DOI]".

4. Authors' Retained Rights

Author(s) retain the following non-exclusive rights for the published version provided that, when reproducing the Article or extracts from it, the Author(s) acknowledge and reference first publication in the Journal:

a. to reuse graphic elements created by the Author(s) and contained in the Article, in presentations and other works created by them;
b. they and any academic institution where they work at the time may reproduce the Article for the purpose of course teaching (but not for inclusion in course pack material for onward sale by libraries and institutions); and
c. to reproduce, or to allow a third party Assignee to reproduce the Article in whole or in part in any printed volume (book or thesis) written by the Author(s).

5. Warranties

The Author(s) warrant and represent that:

a. (i) the Author(s) are the sole copyright owners or have been authorised by any additional copyright owner(s) to assign the rights defined in clause 2, (ii) the Article does not infringe any intellectual property rights (including without limitation copyright, database rights or trade mark rights) or other third party rights and no licence from or payments to a third party are required to publish the Article, (iii) the Article has not been previously published or licensed, (iv) if the Article contains material from other sources (e.g. illustrations, tables, text quotations), Author(s) have obtained written permissions to the extent necessary from the copyright holder(s), to license to the Assignee the same rights as set out in Clause 2 but on a non-exclusive basis and without the right to use any graphic elements on a stand-alone basis and have cited any such material correctly;
b. all of the facts contained in the Article are according to the current body of science true and accurate;
c. nothing in the Article is obscene, defamatory, violates any right of privacy or publicity, infringes any other human, personal or other rights of any person or entity or is otherwise unlawful and that informed consent to publish has been obtained for all research participants;
d. nothing in the Article infringes any duty of confidentiality which any of the Author(s)

might owe to anyone else or violates any contract, express or implied, of any of the Author(s). All of the institutions in which work recorded in the Article was created or carried out have authorised and approved such research and publication; and

e. the signatory (the Author or the employer) who has signed this agreement has full right, power and authority to enter into this agreement on behalf of all of the Author(s).

6. Cooperation
The Author(s) shall cooperate fully with the Assignee in relation to any legal action that might arise from the publication of the Article, and the Author(s) shall give the Assignee access at reasonable times to any relevant accounts, documents and records within the power or control of the Author(s). The Author(s) agree that the distributing entity is intended to have the benefit of and shall have the right to enforce the terms of this agreement.

7. Author List
After signing, changes of authorship or the order of the authors listed will not be accepted unless formally approved in writing by the Assignee.

8. Edits & Corrections
The Author(s) agree(s) that the Assignee may retract the Article or publish a correction or other notice in relation to the Article if the Assignee considers in its reasonable opinion that such actions are appropriate from a legal, editorial or research integrity perspective.

Diese E-Mail wurde automatisch gesendet; Bitte antworten Sie nicht auf diese Adresse. Falls Sie Fragen haben, besuchen Sie bitte unsere Hilfe-Seiten.

Vielen Dank.

Mit freundlichen Grüßen,

Springer Autorenservice

Details des Artikels

Zeitschrift	Titel des Artikels
Acta Neuropathologica	Loss of Fragile X Mental Retardation Protein Precedes Lewy Pathology in Parkinson's Disease.
DOI	**Korrespondenzautor**
10.1007/s00401-019-02099-5	Thomas Koeglsperger
Übertragung des Urheberrechts an	**Übertragen am**
Springer-Verlag GmbH Germany, part of Springer Nature	Tue Nov 12 10:42:40 CET 2019

Service Contacts

Springer Nature Customer Service Center

Tiergartenstr. 15-17
69121 Heidelberg
Germany
phone: +49 6221 345 0
fax: +49 6221 345 4229
customerservice@springernature.com

Springer New York, LCC

233 Spring Street
New York, NY 10013
USA
phone: +1 212 460 1500 or 800-SPRINGER
(Weekdays 8:30am - 5:30pm ET)
fax: +1 212-460-1700
customerservice@springernature.com

9 Acknowledgment

First of all, I would like to express my sincere gratitude to all my supervisors, Prof. Dr. Günter U. Höglinger, Prof. Dr. Harald Luksch and Dr. Thomas Köglsperger for giving me the opportunity to do my Ph.D. at DZNE and TUM. Both are internationally renowned and I am very proud that I have had a chance to work in such a nice academic environment. Especially, I would like to express my greatest appreciation to Dr. Thomas Köglsperger for all the tireless guidance and constant inspiration throughout my Ph.D. process. Whenever we had a conversation, he supervised me well and always brought versatile ideas for the project. His guidance helped me to broaden my vision of the research field and to think more independently.

I am equally indebted to my present and previous group members: Felix Machleid, Qilin Tang, Pan Gao, Diana Haba-Schneider, Rohit Kumar, Dr. Hong Xu, Dr. Sigrid Schwarz, Dr. Thomas Rösler, Dr. Matthias Höllerhage, Dr. Niko-Petteri Nykänen, Sofia Zampagni, Moritz Kolling, Natasha Fussi, Tasnim Chakroun, Elisabeth Findeiss, Valentin Evsyukov, Tabea Strauß, Amir Tayaranian, Andreas Peukert, Christina Tauber, Charlotte Voigt, Lena Jaschkowitz, Sabine Gallagher, Ruth Götz. Thanks to all of you for providing me a friendly and homely lab environment.

My cordial gratitude goes to my collaborators: Prof. Dr. J. Herms, Dr. Carmelo Sgobio, Dr. Thomas Arzberger, Dr. Joerg Tost, and Prof. Dr. med. Kai Bötzel. All your help and contribution facilitated our publication and I also learned a lot through fruitful conversation.

It would be an injustice not to mention my colleagues from the neighboring research groups: Dr. Farida Hellal, Dr. Chenchen Pan, Shan Zhao, Dr. Marika Ruiyao Cai. You all gave me lots of support and help.

Undoubtedly, I would like to appreciate my beloved Yiyuan Chen for years of waiting and mental support. Likewise, without my parents' unconditional support and love, I could not have fulfilled my academic achievement.

Finally, I would like to acknowledge the China Scholarship Council (CSC) for four-year financial support in Munich and Dr. Thomas Köglsperger for an additional 15 months of funding support.

Thanks again for all of you. You all are the best!